ENERGY EXCHANGE ON A MELTING GLACIER

by

DONALD SCOTT MUNRO, B.Sc., M.Sc.

A Thesis

Submitted to the School of Graduate Studies

in Partial Fulfilment of the Requirements

for the Degree

Doctor of Philosophy

McMaster University

September 1975

ENERGY EXCHANGE ON A MELTING GLACIER

DOCTOR OF PHILOSOPHY (1975)

(Geography)

McMASTER UNIVERSITY

Hamilton, Ontario

TITLE: Energy Exchange on a Melting Glacier

AUTHOR: Donald Scott Munro, B.Sc. (McGILL University)

M.Sc. (McGILL University)

SUPERVISOR: Professor J.A. Davies

NUMBER OF PAGES: 182

ii

ABSTRACT

Although methods of evaluating various energy exchanges between the atmosphere and the earth's surface are available, a need for additional knowledge about the turbulent transfer of sensible and latent heat on a melting glacier is recognized. The micrometeorological investigation described in this study is a response to this need. A measurement programme was conducted during the summer of 1971 on Peyto Glacier, Alberta. Data collected include net radiation, melt energy, and the atmospheric parameters, wind speed, temperature and vapour pressure, at several levels above the ice.

Emphasis is placed upon computing sensible and latent heat exchange from profiles of the atmospheric parameters. This is approached through an examination of boundary layer thickness, stability relationships in the boundary layer, and surface roughness lengths. Since all temperature profiles showed inversions, the results characterize stable conditions, where turbulence is dampened. In addition, katabatic flow results from the slope of the glacier.

Turbulent boundary layers in stable flow are known to be relatively thin, but an unexpectedly thin boundary layer, approximately one metre thick, is found over the glacier. The thinness of this layer is attributed to katabatic control of the flow. Deviation from the adiabatic profile form due to stability is adequately described by a log-linear framework, a finding which agrees with other work. However, it is accompanied by an inequality of transfer coefficients, that for heat exceeding

that for momentum. This has not been reported previously. A tentative hypothesis is advanced to explain this. Contrary to previous glaciological opinion, the wind profile roughness length is found to be smaller than that of the temperature profile. This is explained using results of other work on other surfaces.

A bulk transfer procedure is chosen as the most suitable method of evaluating the turbulent fluxes. The procedure is strengthened by the findings of this study. It is used to obtain half-hourly estimates of sensible and latent heat exchange which appear to be reasonable. Short-term variations in the meltwater hydrograph are found to be closely controlled by the net radiative flux, but daily totals indicate that the sensible heat flux is also an important energy source. Latent heat transfer by the water vapour flux between the atmosphere and the surface is small.

The contribution of this investigation to establishing the link between glacier hydrology and climate is indicated.

ACKNOWLEDGEMENTS

I deeply appreciate the support and guidance of Dr. J.A. Davies, not only for his indispensible supervision of my research, but for constructively influencing my attitude toward academic life in general; the support and advice of Mr. L. Derikx of the Glaciology Division, who has made it possible to conduct this investigation. Special thanks are due to the other members of my supervisory committee, Dr. W.R. Rouse and Mr. F.C. Elder, for their critical review of the manuscript and helpful advice; to Dr. M.K. Woo and Dr. P.D.M. Macdonald, for commenting upon parts of the manuscript; to Mr. D. Chisholm, for his excellent assistance in the field; to Mr. D. Bonham, for his advice on data reduction procedures; to Mr. R. Quirouette, for preparing the photographic illustrations. My gratitude extends to friends and colleagues at McMaster University, the University of Toronto and the Glaciology Division who have freely given me their time and advice upon many occasions.

Final and deepest appreciation goes to my wife, Krystyna, for her assistance during particular phases of the investigation, and for patiently supporting me in the pursuit of my studies.

TABLE OF CONTENTS

viii

LIST OF ILLUSTRATIONS

Figure

LIST OF TABLES

CHAPTER ONE

INTRODUCTION

The relationship between the physics of glacier movement and atmospheric processes is vitally important for two reasons. Firstly, glaciers advance or retreat over time, in response to climatic variations. Secondly, ice masses are stores of fresh water which, subject to climatic control, affect the hydrology of large areas. Much attention has been concentrated on the complex linkages which constitute this relationship (Paterson, 1969). Among these, the interaction between the energy balance of a glacier, and its mass balance is crucial.

. The energy balance comprises all forms of energy exchange at the surface. These involve shortwave and longwave radiation, as well as the transfer of sensible heat between the atmosphere and the surface. Latent heat exchange is associated with the transport of water vapour to and from the glacier. It also occurs through melting or freezing at the surface. The energy used in melting ice is hereinafter referred to as the melt energy. Heat conduction may occur within the ice. In addition, precipitation plays a small and sporadic role in the energy balance. Each term represents either an income or an expenditure of energy. Furthermore, incomes and expenditures balance.

The mass balance comprises all gains and losses of ice over the glacier. In contrast to the energy balance, gains seldom balance

1

losses during periods which may extend over many years. A detailed description of the mass balance is complex (Müller, 1962). In simplified terms it may be divided into two periods, the occurrence of one or the other governed by the position of the zero-degree isotherm. Air temperature below freezing characterizes the accumulation period, during which mass is gained through precipitation, mainly in the form of snow. The energy balance plays a passive role since melt energy is absent. Air temperature is above freezing during the melt period, and melt energy becomes a large expenditure to which the rest of the energy balance contributes. Consequently the energy balance plays an active role in determining the mass balance. It is for this reason that considerable effort has been directed toward studying glacier energy balances during this period (Sverdrup, 1936; Wallén, 1948; LaChapelle, 1959; Havens, Müller and Wilmot, 1965; Wendler and Streten, 1969).

Because direct measurement of the melt is difficult, indirect estimates have been attempted using the energy balance (Müller and Keeler, 1969; Derikx, 1971; Föhn, 1973; Wendler and Ishikawa, 1973). The success of this approach rests upon two conditions: that the theory of transfer for each component of the energy balance is well understood, and that measurements are sufficiently accurate and precise.

The theory of radiative transfer, and heat storage within ice, is known well enough that evaluating the energy which they represent is mainly a measurement problem. It has been shown recently that satisfactory measurements can be obtained over ice, particularly for radiation (Weller, 1967; 1968). By contrast, sensible and latent heat transfer

theory requires further investigation before good estimates can be made, even if suitable measurements are available. It is known that these transfers control the distribution of temperature and humidity in the lower atmosphere. It is also known that the principal transfer mechanism is turbulent mixing. How this mechanism links the exchanges to the vertical distribution of temperature and humidity is incompletely understood. Thermal stratification over melting ice is characterized by strong inversions, and associated stable conditions, which dampen turbulent motion. The smoothness of the surface, and the existence of local drainage winds, reinforce this effect.

Significant steps have been made in understanding the transfer mechanism in unstable conditions, where temperature decreases with height (Swinbank and Dyer, 1967; Dyer and Hicks, 1970; Businger, Wyngaard, Izumi and Bradley, 1971). Some progress has also been made in stable conditions (McVehil, 1964; Webb, 1970; Businger et al., 1971), though this has been hampered by weak wind speeds, which are typical of most stable flows outside of glacial environments. The significant findings have been empirical, and developments in instrumentation have been crucial.
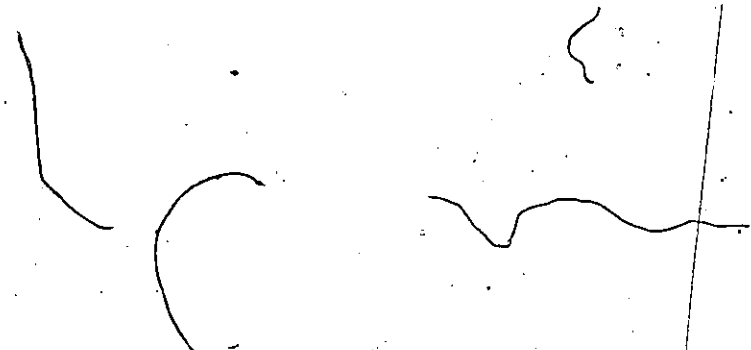
The difficulty of obtaining good measurements may account for the tendency of most glaciologists to ignore the detailed investigation of turbulent transfer. The emphasis has been toward obtaining rough estimates of sensible and latent heat transfer from overly simple models. The outstanding works of Sverdrup (1936), Liljequist (1955) and Hölmgren (1971) are exceptions. Nevertheless, there is a need for additional investigations with more refined measurements. In response to this, detailed micrometeorological measurements were made during the summer of 1971 on Peyto

Glacier. These measurements were directed toward the problem of improving the procedure for estimating sensible and latent heat transfer.

This thesis describes the investigation of the problem. It is organized in three parts:

(1) atmospheric structure close to the surface, and its implications for the use of the turbulent transfer approach,

(2) the influence of thermal stratification on turbulent transfer, and

(3) surface roughness, and its effect on turbulent transfer computations.

The results are incorporated into a transfer model which may be useful in computing sensible and latent heat exchanges over melting ice.

CHAPTER TWO

PHYSICAL BASIS

Turbulence is the principle transporting mechanism for momentum, heat and water vapour in the lower atmosphere. Molecular exchange is significant only within a few millimeters of the surface.

Turbulent transfer theory, which has been derived from fluid mechanics, is empirically based. Its applicability to the computation of atmospheric fluxes can only be assessed by experimental studies. The air layer over melting ice is in special need of investigation because existing data are relatively meagre, and of generally lower quality than those obtained over other surfaces.

This experiment focuses upon the relationship between the observed height distributions (profiles) of wind speed, temperature and vapour pressure, and the surface heat fluxes. Alternatively, fluxes can be measured directly (Bradley, 1968b; Wesely, Thurtell and Tanner, 1970; Pruitt, Morgan and Lourence, 1973), but existing instrumentation for doing this is generally unsuitable for the glacier environment. In contrast to this, evaluations based upon the vertical profiles of wind speed, temperature and vapour pressure offer the following advantages:

(1) Measurements can be obtained with relatively simple, and easily maintained instruments. This increases the likelihood of successful data collection in a difficult field environment.

(2) They are readily applied to even simpler data sources, such as meteorological shelters, or two-level measurement systems.

(3) Information may be obtained about the structure of the air layer near the ground which is useful to the application of direct and profile approaches to heat flux estimation.

The Système Internationale d'Unités (SI) is used throughout. A complete list of symbols and units is given in Appendix One.

A. Transfer in the Boundary Layer Over Melting Ice

Surface fluxes of momentum, τ, sensible heat, Q_H, and latent heat, Q_E, are related to vertical gradients of wind speed, u, temperature, θ, and vapour pressure, e, by

$$\tau = \rho \, K_M \, \frac{\partial u}{\partial z} \qquad (2.1a)$$

$$Q_H = \rho \, c_p \, K_H \, \frac{\partial \theta}{\partial z} \qquad (2.1b)$$

$$\text{and} \quad Q_E = \rho \, \frac{\lambda_v \varepsilon}{p} \, K_E \, \frac{\partial e}{\partial z} \qquad (2.1c)$$

where K is the turbulent transfer coefficient, subscripts E, H and M applying to water vapour, heat and momentum, respectively, c_p the specific heat of air at constant pressure, p the atmospheric pressure, z the height above the surface, ε the ratio of the molecular weights of water and air, λ_v the latent heat of vapourization, and ρ the density of air. Positive flux values indicate transfer toward the surface. Transfer away from the surface is negative. The validity of these equations rests upon two assumptions:

(1) that mean values of atmospheric parameters (u, θ and e) are constant with time, and are horizontally uniform;

(2) that fluxes do not diverge horizontally.

These assumptions are correct within the boundary layer.

The boundary layer is usually defined to be an air layer, in contact with the ground, which is directly influenced by surface processes. A more specific definition is made by requiring that the fluxes in this layer are constant with height. The justification for a constant flux layer can be illustrated with the simplified equation for horizontal transport:

$$\frac{\partial \chi}{\partial t} + u \frac{\partial \chi}{\partial x} = - \frac{K \partial^2 \chi}{\partial x^2} + \frac{K \partial^2 \chi}{\partial z^2} \qquad (2.2)$$

in which t is the time, x the distance along the wind direction, and χ any of the entities, heat ($\rho \, c_p \, \theta$), momentum ($\rho \, u$) and water vapour ($\rho \, \epsilon \, e/p$). From the assumptions, $\partial \chi/\partial t$, $\partial \chi/\partial x$ and $\partial^2 \chi/\partial x^2$ each equal to zero, it follows that $\partial^2 \chi/\partial z^2 = 0$. The assumed absence of vertical flux divergence underlies the estimation procedures used in this thesis. Experimental evidence supports the existence of a constant flux layer, with a depth of at least 30 m, over extensive horizontal sites (Haugen, Kaimal and Bradley, 1971; Dyer and Hicks, 1972).

These assumptions do not necessarily apply to the air layer over a melting glacier, because the surface is usually inclined, and

cold. The overlying warm air is cooled from below, forming a relatively dense surface layer, within which the air is accelerated downslope by gravity. This is the origin of the glacier wind (Defant, 1951), a katabatic flow which has been analytically described by Hölmgren (1971).

Following Hölmgren (1971), the momentum form of Eq. (2.2) can be written to include the katabatic effect so that the horizontal momentum flux divergence becomes a function of the horizontal pressure gradient force, and the katabatic force:

$$\frac{\partial \tau}{\partial x} \cos \psi = -\frac{\partial p}{\partial x} \cos \psi + \frac{\theta'}{\theta_0} \rho g \sin \psi \qquad (2.3)$$

in which g is the acceleration due to gravity, θ_0 the surface temperature, θ' the temperature disturbance $(\theta - \theta_0)$, and ψ the slope angle. The katabatic force is likely to dominate for slopes steeper than 0.2 degrees (Ball, 1960). Therefore, $\partial \tau/\partial x$ will not equal zero and $\partial p/\partial x \neq 0$ (the usual assumption for micrometeorological work). The steady-state assumption, $\partial u/\partial t = 0$, is not strictly correct because katabatic flow is characterized by short-term accelerations (Ball, 1960; Lettau, 1966). Moreover the flow diverges, since it is accelerating downslope, and therefore $\partial u/\partial x$ does not equal zero. These circumstances should result in a change of momentum flux with height.

Height divergence can be postulated for the sensible heat and moisture fluxes, since these entities are advected by the wind. The difference between the glacier surface temperature (0 C), and the temperature of the surrounding land area (> 0 C) can be large. Therefore

$\partial\theta/\partial x \neq 0$, especially near the glacier margin. Similarly, $\partial e/\partial x \neq 0$ when marked vapour pressure contrasts exist. In addition, the steady-state assumption, $\partial\theta/\partial t = 0$, appears to be weak for katabatic flow (Lettau, 1966).

The relationship between sensible heat flux divergence, and horizontal gradients of wind speed and temperature is illustrated in Fig. 2.1. Here, an increase of wind speed downglacier ($\partial u/\partial x > 0$) is accompanied by a decrease in temperature ($\partial\theta/\partial x < 0$). In steady-state conditions, sensible heat flux divergence between the surface, and some height above the surface, z, is given by

$$Q_{H(z)} - Q_{H(o)} = \rho \, c_p \left[\int_0^z \theta \, \frac{\partial u}{\partial x} \, dz + \int_0^z u \, \frac{\partial\theta}{\partial x} \, dz \right] \quad (2.4)$$

where ρ is assumed to be constant with height. An analogous equation applies to the latent heat flux.

From Eq. (2.4) it is apparent that a reduction of horizontal gradients will reduce the flux divergence. At a sufficient distance from the glacier margin, these gradients may be negligible close to the surface, thus allowing the use of flux estimation procedures developed for boundary layer conditions.

Despite its importance, the problem of boundary layer development on glaciers has received little attention. It is known generally that boundary layers with temperature inversions are shallower than others (Orlanski, Ross and Polinsky, 1974), but there is a need to determine, by experiment, the existence and depth of the boundary layer
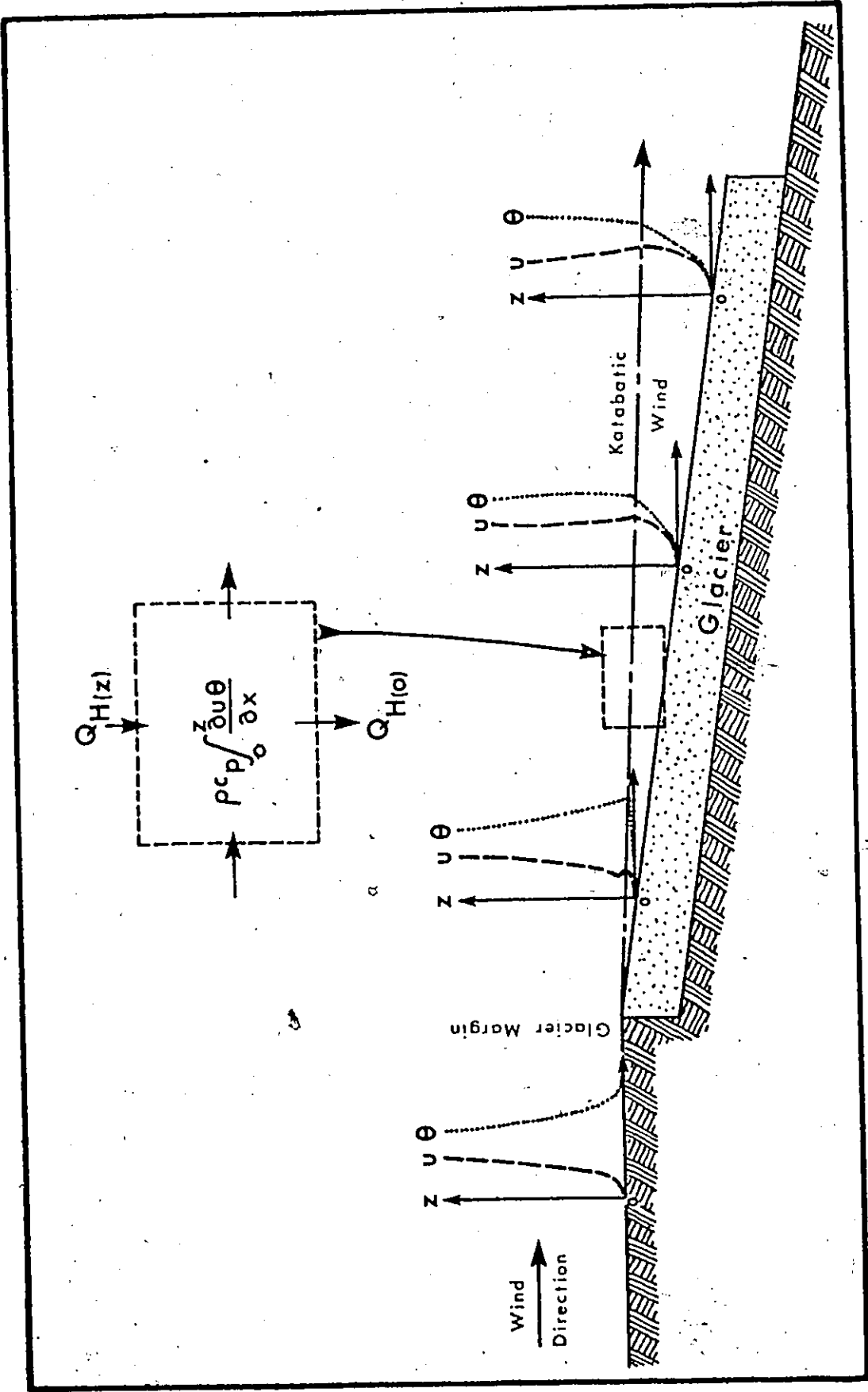
Figure 2.1.   Evolution of wind speed and temperature profiles over a melting glacier.

in katabatic flow. The depth is a crucial factor in applying boundary layer theory.

B. Transfer in Neutral Equilibrium

In neutral equilibrium the vertical temperature distribution is governed by dynamic effects alone. Turbulence is generated solely by mechanical energy resulting from the surface interaction with the wind. This state is well understood, and it forms the starting point for the investigation of more complex cases. Moreover, transfer models developed for the neutral case have been used in glaciological investigations (Havens, Müller and Wilmot, 1965; Müller and Keeler, 1969).

Neutral transfer models may be used to compute the height-integrated values of the eddy transfer coefficients in Eq. (2.1). This is done by expressing the fluxes in terms of the friction velocity, u_*, the friction temperature, θ_*, and the friction vapour pressure, e_*:

$$\tau = \rho \, u_*^2 \qquad (2.5a)$$

$$Q_H = \rho \, c_p \, u_* \, \theta_* \qquad (2.5b)$$

$$\text{and} \quad Q_E = \rho \, \frac{\lambda_{v\varepsilon}}{p} \, u_* \, e_* \qquad (2.5c)$$

From Prandtl's mixing length hypothesis, any friction parameter, y_*, may be expressed as

$$y_* = k \, z \, \frac{\partial y}{\partial z} \qquad (2.6)$$

in which k is von Kármán's constant. Within the boundary layer, Eq. (2.6) can be integrated over height, and the friction quantities written in terms of finite differences:

$$y_* = k \frac{\Delta y}{\Delta \ln z} \qquad\qquad (2.7)$$

The validity of the logarithmic expression is established for adiabatic flow.

The eddy transfer coefficients are assumed to be equal in adiabatic conditions. The validity of this assumption is supported by various studies (Rider and Robinson, 1951; Rider, 1954; Dyer, 1967; Harbeck, 1967; Oke, 1970; Dyer and Hicks, 1970; Webb, 1970), although discenting investigations have recently been reported (Businger et al., 1971; Pruitt, Morgan and Lourence, 1973; Högström, 1974). The question of similarity in neutral conditions can not be examined in this study, so the majority view, that the equality assumption holds, is accepted. This view also agrees with the theoretical position taken by Obukhov (1946) and Ellison (1957).

Consequently Eqs. (2.1a), (2.5a), (2.6) and (2.7) may be combined (using $y_* = u_*$) to define the general eddy transfer coefficient, $K = K_M = K_H = K_E$:

$$K = k^2 \frac{(\Delta u)^2}{(\Delta \ln z)^2} \left(\frac{\partial u}{\partial z}\right)^{-1} \qquad\qquad (2.8)$$

Substituting Eq. (2.8) directly into Eq. (2.1), and using finite difference approximations to the gradients,

$$\tau = \rho \, k^2 \, \frac{\Delta u^2}{(\Delta \ln z)^2} \qquad (2.9a)$$

$$Q_H = \rho \, c_p \, k^2 \, \frac{\Delta u \, \Delta \theta}{(\Delta \ln z)^2} \qquad (2.9b)$$

$$\text{and} \quad Q_E = \rho \, \frac{\lambda_v \varepsilon}{p} \, k^2 \, \frac{\Delta u \, \Delta e}{(\Delta \ln z)^2} \qquad (2.9c)$$

The logarithmic model must be modified to include buoyancy effects. Nevertheless, it has been assumed that errors introduced by thermal effects are small close to the ground. This assumption under-lies the use of the logarithmic framework over melting ice by some investigators (Havens, Müller and Wilmot, 1965; Grainger and Lister, 1966). However, Derikx (1971) found that a neutral framework, modified to include buoyancy effects, gave better flux estimates than the neu-tral form.

Melting ice differs from other natural surfaces in that the surface values of temperature and vapour pressure can be reasonably well specified. This offers an ideal situation for the application of bulk transfer procedures (Deacon and Webb, 1962). They involve the use of a dimensionless drag coefficient, C_D, which is obtained by integrating Eq. (2.6) between z and z_0, the surface roughness length, so that

$$\frac{y_*}{y - y_0} = \frac{k}{\ln (z/z_0)} = r \qquad (2.10)$$

where $C_D = r^2$. From Eqs. (2.5) and (2.10):

$$\tau = \rho \, C_D \, u^2 \tag{2.11a}$$

$$Q_H = \rho \, c_p \, C_D \, u \, (\theta - \theta_o) \tag{2.11b}$$

$$\text{and} \quad Q_E = \rho \, \frac{\lambda_v \epsilon}{p} \, C_D \, u \, (e - e_o) \tag{2.11c}$$

where $\theta_o = 0 \, C$ and $e_o = 611 \, Pa$.

The bulk transfer approach is useful in synoptic scale studies (Sheppard, 1958), and it can be applied to data taken from meteorological shelters or automatic weather stations. However, there is uncertainty about the use of a single C_D value for all fluxes. Several glaciological investigators have suggested that the wind profile z_o is larger than the temperature profile roughness length, z_H (Sverdrup, 1936; Liljequist, 1955; Hölmgren, 1971; Wendler and Ishikawa, 1973). It is also possible that the vapour pressure profile has a unique roughness length (Sheppard, 1958). Thus Γ may depend upon the specific friction quantity represented by y_*. Then a separate bulk coefficient would be required for each transfer.

C. Stability Parameters

Stability is characterized by thermal stratification in the air layer next to the ground. Thermally stratified conditions differ from the neutral case in that buoyancy becomes an additional turbulent energy term. Buoyant forces are caused by the vertical density differences arising from temperature gradients. Vapour pressure gradients also have an effect, but this is extremely small (Webb, 1965).

Two types of thermal stratification are recognized:

(1) Due to a decrease in temperature away from the surface (lapse), warm air near the ground rises, while cool air aloft sinks. Conditions are unstable since buoyancy augments turbulence, and vertical mixing is amplified.

(2) Due to an increase in temperature with height (inversion), air tends to remain in place. Conditions are stable since the buoyant force depletes turbulent energy, and vertical mixing is dampened.

This thesis deals exclusively with the second type.

Stability measures begin with a consideration of the forces contributing to the turbulent energy exchange, E_t. Richardson's (1920) analysis of the forces suggests that only mechanical and buoyant forces are important. Their contribution is summarized in the relationship

$$\frac{\partial E_t}{\partial t} = \tau \frac{\partial u}{\partial z} - \frac{g}{\theta_a} \frac{Q_H}{c_p} \qquad (2.12)$$

in which θ_a is the absolute air temperature. The ratio of these forces defines the flux Richardson number, Rf:

$$Rf = \frac{g \, Q_H}{\theta_a \, c_p \, \tau \, (\partial u/\partial z)} \qquad (2.13)$$

By this number:

(1) neutral equilibrium is defined at Rf = 0, since only the mechanical contribution remains in Eq. (2.12),

(2) unstable conditions are defined when Rf < 0, and

(3) stable conditions are defined when Rf > 0.

Furthermore, Richardson suggested that Rf = 1 was a critical value since Eq. (2.12) then equals zero, and turbulent energy vanishes. Hence, Rf has important theoretical implications as a criterion for determining the onset of turbulence, and is analogous to the Reynolds number in this respect. However, it is not a practical parameter since it requires a priori knowledge of the fluxes. This is contrary to the objective of the profile approach, which is to obtain the transfers as the end product.

The gradient form of the Richardson number, Ri, is practical. It is obtained by assuming $K_M = K_H$, and substituting Eqs. (2.1a) and (2.1b) into Eq. (2.13):

$$Ri = \frac{g}{\theta_a} \frac{(\partial\theta/\partial z)}{(\partial u/\partial z)^2}$$

(2.14)

However, Ellison (1957) suggested that the assumption, $K_M = K_H$, was invalid for any but neutral conditions. Despite this uncertainty, Ri has been used frequently because it is easy to evaluate from profile data. For this reason, it is sometimes used even when a better alternative is available (Swinbank, 1968).

Much attention has been devoted to determining a critical Ri value, Ri_c. This denotes the point at which turbulence ceases. Early work by Durst (1933) pointed to a value of 1.0, which would suggest that Ri is a valid substitute for Rf if Richardson's prediction was correct. More recent values are considerably smaller (Businger, 1955; Yamamoto, 1959; Kaimal and Izumi, 1965; Högström, 1967; Okamoto and

Webb, 1970). Individual estimates differ, but it seems that departures from the adiabatic framework are difficult to describe analytically beyond Ri greater than 0.1 or 0.2 (Dalrymple, Lettau and Wollaston, 1963; Oke, 1970; Webb, 1970). This is due to the sporadic occurrence of turbulence in strong stability (Portman, Elder, Ryznar and Noble, 1962; Okamoto and Webb, 1970).

An alternative to Ri employs the stability length scale, L (Obukhov, 1946; Lettau, 1949):

$$L = \frac{u_*^3}{k\,g\,Q_H/c_p\,\rho\,\theta_a} \tag{2.15}$$

which follows the same sign convention as Rf and Ri. Used in the form z/L, it becomes the basis of stability-corrected transfer models (Dyer, 1967; Dyer and Hicks, 1970; Businger et al., 1971). The difficulty posed by the need for a measurement of Q_H is overcome by combining Eqs. (2.5b) and (2.15) (Calder, 1966; Webb, 1970):

$$L = \frac{u_*^2\,\theta_a}{k\,g\,\theta_*} \tag{2.16}$$

Thus L can be evaluated from sufficiently detailed and precise profile measurements.

The z/L stability parameter has the advantages that it does not contain stability-dependent quantities, and it makes no assumptions about the equality of transfer coefficients. Moreover, the influence of height above ground is readily seen. Webb (1965) has outlined a

scheme in which turbulence becomes sporadic, and potential temperature gradients virtually disappear, at z/L = -1.

D. Transfer in the Stable Case

Investigators over the last 50 years have endeavored to model thermal stratification, and incorporate it into the adiabatic framework. Important theoretical work was done by Obukhov (1946), Lettau (1949) and Ellison (1957), but the main line of investigation has been experimental (Priestly, 1959; Lumley and Panofsky, 1964; Webb, 1965).

The effect of a temperature gradient is to introduce a basic inequality between the vertical and the horizontal deviations from the mean flow (Taylor, 1927). Equilibrium between friction parameters and gradients is altered so the equality in Eq. (2.6) no longer holds. This problem is approached by employing a dimensionless function of stability, ϕ. Following Webb (1965), ϕ is incorporated into Eq. (2.6):

$$y_* = \frac{k\,z}{\phi}\,\frac{\partial y}{\partial z} \qquad (2.17)$$

A number of ϕ functions have been derived experimentally from profile data (Holzman, 1943; Yamamoto, 1959; Elliott, 1960; Panofsky, 1961; Sellers, 1962). More recent work by Dyer (1967), and subsequent investigators (Dyer and Hicks, 1970; Businger et al., 1971; Pruitt, Morgan and Lourence, 1973) have included direct flux measurements in addition to profiles. Some of these incorporate data from stable conditions, but exact functional relationships for ϕ are not generally agreed upon.

The stable case is examined by considering the stability correction form proposed by Monin and Obukhov (1954), which expresses ϕ as an infinite series in z/L:

$$\phi = 1 + \alpha_1 \frac{z}{L} + \alpha_2\left(\frac{z}{L}\right)^2 + \alpha_3\left(\frac{z}{L}\right)^3 + \ldots \qquad (2.18a)$$

where α_1, α_2, α_3, ... are empirically determined constants. Monin and Obukhov, along with a number of subsequent investigators (Taylor, 1960; McVehil, 1964; Webb, 1970), have agreed that no term above first order need be considered for stable conditions.
Thus

$$\phi = 1 + \alpha \frac{z}{L} \qquad (2.18b)$$

in which α is referred to as the Monin-Obukhov constant. However there has been strong disagreement over the value of α. Past estimates vary from 0.6 (Monin and Obukhov, 1954; Swinbank, 1964) to 9.5 (Hogstrom, 1967). More recently, a value close to 5 has been suggested (Webb, 1970; Businger et al., 1971; Carl, Tarbell and Panofsky, 1973; Dyer, 1974).

Rearranging Eq. (2.18b) to express α as a derivative, and integrating with height,

$$\phi = \int_{z_0}^{z} \frac{\partial(\phi - 1)}{\partial z/L} \, dz/L = \alpha \frac{(z-z_0)}{L} \qquad (2.19)$$

in which ϕ is a height-integrated stability correction.

The ϕ correction is an essential component of the Monin-Obukhov model

$$y_* = k \ (y - y_0) \left[\ln\left(\frac{z}{z_0}\right) + \alpha \ \frac{(z - z_0)}{L} \right]^{-1} \qquad (2.20)$$

which is obtained by substituting Eq. (2.18b) into Eq. (2.17), re-arranging terms, and integrating over height. This expression, often referred to as the log-linear model, was independently derived by Liljequist (1955) in his analysis of heat transfer in Antarctic inversions.

The central problem in constructing profile based models of heat transfer in stable conditions is to determine if a single α value is suitable for all profiles. This is the same as determining if the eddy transfer coefficients are equal in stable conditions, since

$$\frac{K_H}{K_M} = \frac{\phi_M}{\phi_H} \qquad (2.21)$$

Similarity of transfer mechanisms in thermally stratified conditions has never been accepted with conviction in atmospheric studies. Moreover, Swinbank and Dyer (1967) provided convincing experimental evidence that K_M differs markedly in its behaviour from K_H and K_E in unstable conditions. Experimental evidence in unstable conditions suggests that ϕ_H and ϕ_E are equal, but different from ϕ_M (Dyer, 1967; Dyer and Hicks, 1970; Businger et al., 1971; Carl, Tarbell and Panofsky, 1973). The nature of the inequality is such that K_H and K_E are greater than K_M. This is in basic agreement with Ellison's (1957) theoretical predictions.

The stable situation is not as well documented. Stewart (1959) stated that there is no obvious justification for equality, and Ellison (1957) suggested $K_M > K_H$. However, experimental results of Webb (1970) and Oke (1970) point to an equality of K_H and K_M. Other experimenters find K_M greater than the other coefficients only in strong stability (Businger et al., 1971; Carl, Tarbell and Panofsky, 1973; Pruitt, Morgan and Lourence, 1973).

Allowing a different value for each atmospheric parameter used in Eq. (2.20) and taking $\Delta\phi$ between two heights, stability corrected friction parameters can be calculated, and substituted into Eq. (2.5):

$$\tau = \frac{\rho\, k^2\, \Delta u^2}{(\Delta \ln z + \Delta\phi_M)^2} \tag{2.22a}$$

$$Q_H = \frac{\rho\, c_p\, k^2\, \Delta u\, \Delta\theta}{(\Delta \ln z + \Delta\phi_M)(\Delta \ln z + \Delta\phi_H)} \tag{2.22b}$$

$$\text{and}\quad Q_E = \frac{\rho\, \lambda_v\, \epsilon\, k^2\, \Delta u\, \Delta e}{p(\Delta \ln z + \Delta\phi_M)(\Delta \ln z + \Delta\phi_E)} \tag{2.22c}$$

where the subscripts, E, H and M apply respectively to latent heat, sensible heat and momentum.

Theoretically, thermal stratification also affects the drag coefficients in Eq. (2.11). However, it is usually argued that stability effects are small enough to be ignored in practice. Some investigators have applied drag coefficients, determined in neutral conditions,

to the non-neutral case (Deacon and Swinbank, 1958). According to
Bradley (1972) this procedure is reasonable for unstable conditions, but
it results in flux overestimation in the stable case. Thus, it may be
necessary to modify Eq. (2.10) for stable conditions.

In order to make ϕ correction schemes operational, stability
must be measured from gradients alone. Although a correction based upon
z/L is theoretically sound, Ri is the only stability parameter which
meets this requirement. Therefore it is useful to examine the relation-
ship between Ri and z/L (Dyer and Hicks, 1970):

$$\frac{z}{L} = \frac{\phi_M^2}{\phi_H} \; Ri \tag{2.23}$$

An experimental evaluation of ϕ_H and ϕ_M can establish the relationship
between these two stability parameters. Dyer and Hicks (1970) found
$\phi_M^2/\phi_H = 1$ in unstable conditions, and thus Ri and z/L values which
are equivalent numerically. Webb's (1970) data for unstable conditions
seem to support this conclusion, but they indicate a different result
for the stable case.

CHAPTER THREE

EXPERIMENTAL PROCEDURE

A. Site and Observation Period

Peyto Glacier (51° 40' N, 116° 33' W) is located in the Canadian Rocky Mountains, about 100 km north of Banff, Alberta. The glacier occupies approximately 14 km^2, mostly in a large upper basin which is continuous with the Wapta Icefield (Fig. 3.1). It ranges in altitude from 2100 m to 3000 m, and faces the north-east. Most investigators consider the glaciers of this area to be temperate, that is their temperature is at the pressure melting point of ice throughout.

.The site offered particular advantages for this research. Since it was selected as a study basin for the International Hydrological Decade, it had a well established field camp set up by the Glaciology Division of the Department of Environment (Canada). Also, the basin was readily accessible.

Measurements were scheduled to begin in late June, 1971, but bad weather resulted in a one-month delay. Hence, observations were confined to August, and the first week of September, prior to the end of the ablation season.

KEY MAP

● PEYTO GLACIER

PEYTO GLACIER AREA

Peyto Lake

93

N

⊢1km⊣

BASE CAMP ▲

◆ EXPERIMENTAL SITE (elevation 2300m)

Peyto Creek Trail

Icefall

Peyto Glacier

WAPTA

ALBERTA
BRITISH COLUMBIA

ICEFIELD
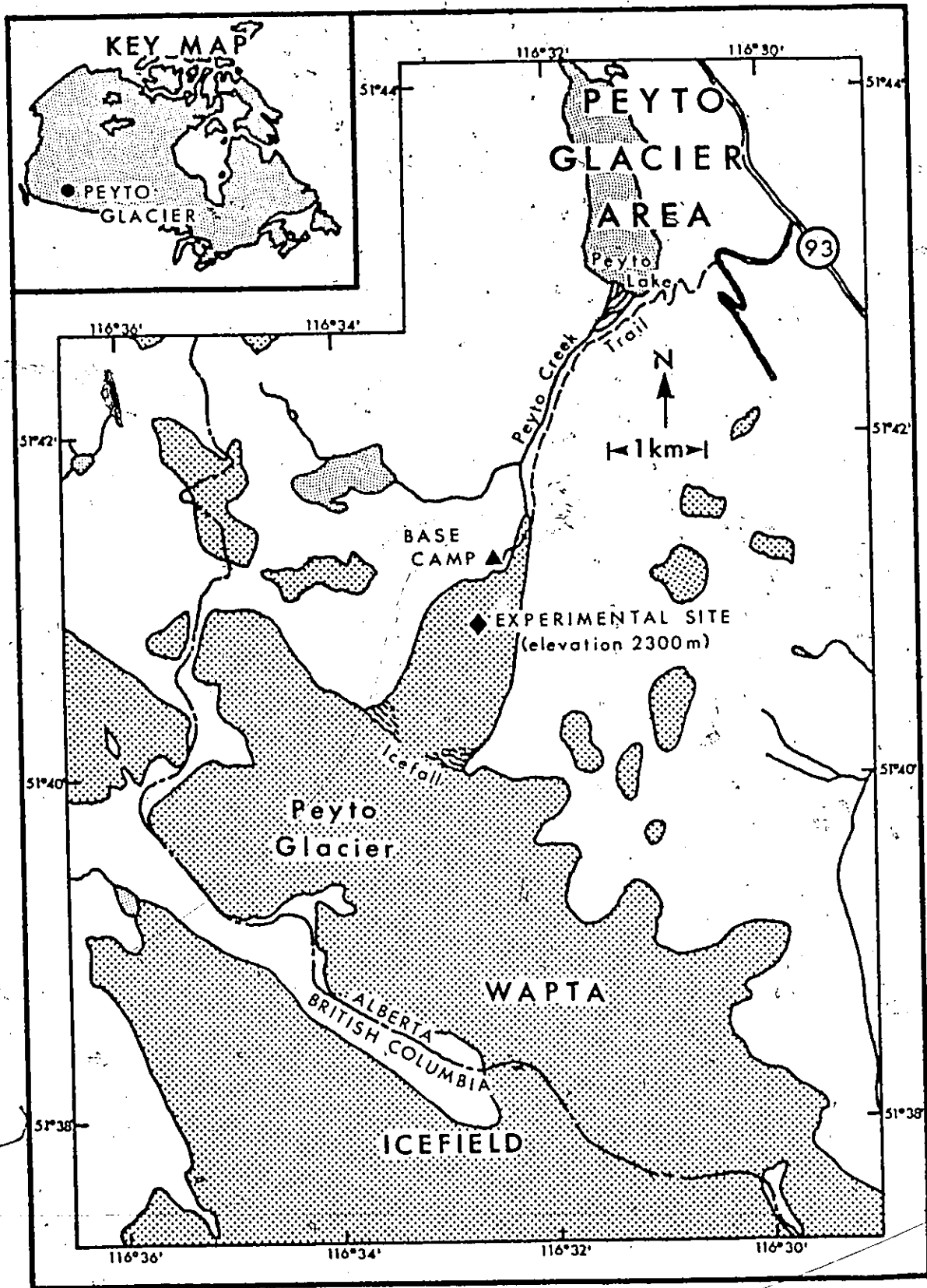
Figure 3.1. Location of experimental site.

B. Instrumentation

Instrument selection and placement were directed toward:

(1) accurate measurement of vertical profiles of wind speed, temperature and vapour pressure near the surface. These were needed to examine the depth of the boundary layer, stability relationships and surface roughness.

(2) accurate measurements of other energy terms to evaluate the energy balance:

$$Q_* + Q_H + Q_E + Q_I + Q_M = 0 \qquad (3.1)$$

in which Q_I is the heat conducted beneath the surface, Q_M the melt energy, and Q_* the net radiative transfer. This evaluation is needed to assess the performance of computation procedures developed for Q_H and Q_E.

1. Location of Sensors

A measurement site was established on the glacier tongue, about 1 km from the icefall (Fig. 3.1). The surface roughness elements appeared uniform over this distance, providing a fetch of 1000 m. According to an often-quoted rule-of-thumb, the overlying air is representative of the surface up to a maximum height of 1/100 the fetch, or 10 m in 1,000 m (Bradley, 1968a). Most measurements were made within 5 m of the surface.

In establishing the instrumental layout, a persistent down-

glacier wind was assumed (Fig. 3.2). Other wind directions occurred

only during stormy weather, when measurements were not made. An anemo-

meter mast, and a temperature mast were located side-by-side, upwind of

all other instrumentation. A net radiometer was mounted slightly down-

wind, and to one side of the masts. Melt measurements were made down-

wind from all the others. Signals were recorded in a hut to the side

of the melt plot. Power was supplied by one of two 1 kW generators,

located as far downglacier as possible, to avoid electrical interference

with the signals.

2. Profile Measurements

Wind and temperature sensors were mounted at heights of 0.25,

0.5, 0.75, 1, 1.5, 2 and 4 m above the surface (Fig. 3.3). On some

occasions dry bulb measurements were also taken at 6 m. Additional wind

speeds were measured at 2.5, 3, 3.5, 5 and 6 m. The base of each mast

was mounted on a flat rock. This arrangement maintained the sensors at

a constant height above the surface throughout the melt season.

The surface consisted of elongated ice hummocks (Fig. 3.3),

with a local relief of about 0.5 m. The irregularity raises the possi-

bility that the measurement heights were determined incorrectly. The

heights of the 0.25 m sensors were checked by performing a microrelief

survey of a 20 x 20 m grid (Fig. 3.2), with survey points at 0.5 m

intervals across the glacier, and at 1 m intervals upglacier. The mean

ice level was determined by fitting a first-order trend surface to the

data (Krumbein and Graybill, 1965). The height of the lowest sensor on
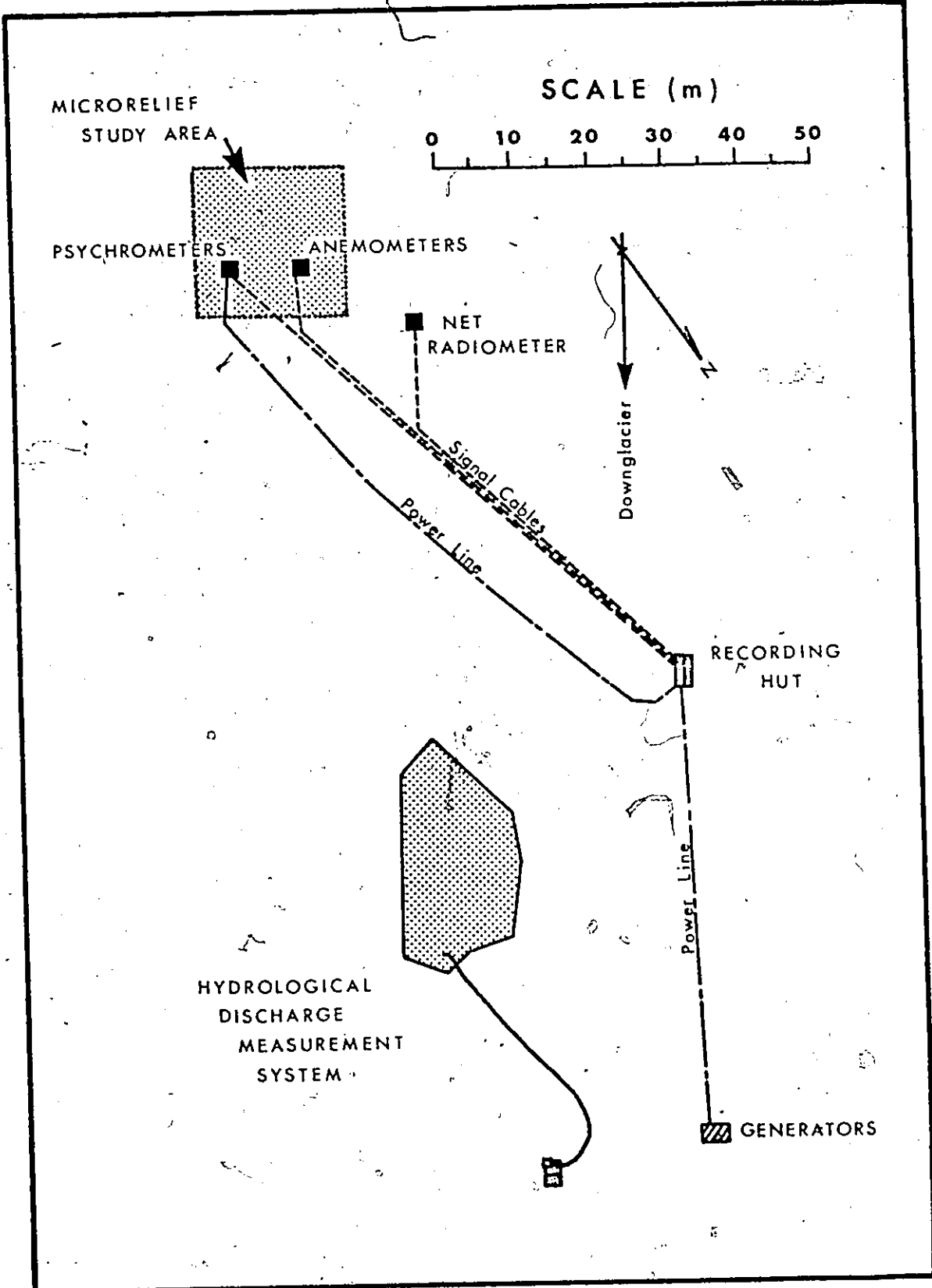
Figure 3.2. Experimental site plan.

28
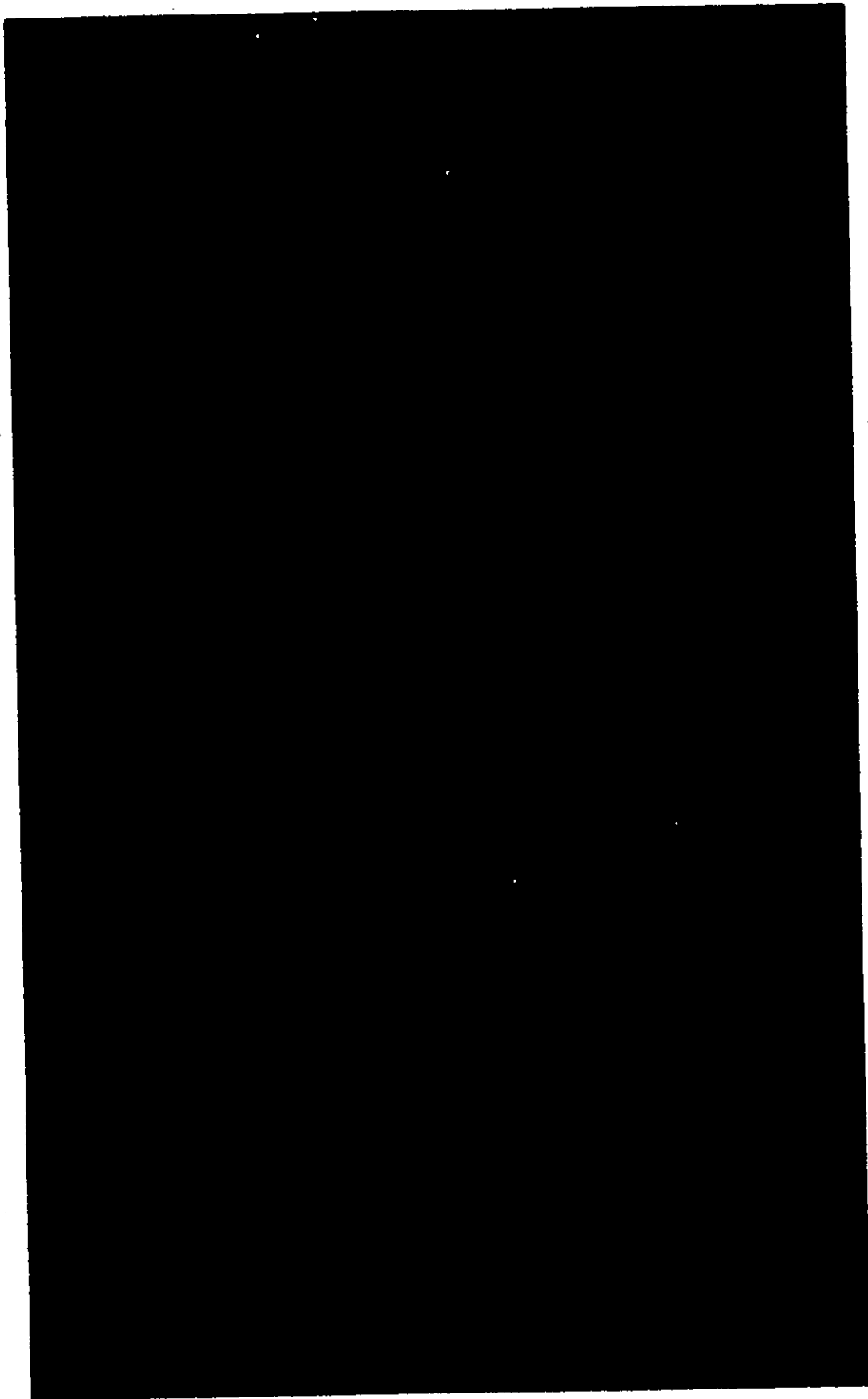
Figure 3.3. Downglacier view of experimental site.

each mast was measured relative to the trend. This differed from the originally chosen value (0.25 m) by -0.011 m for the temperature mast, and 0.003 m for the wind mast. Both discrepancies are within the standard error of the trend surface. Therefore the measurement heights were accepted as correct.

a. Wind Profile

Light-weight cup anemometers were used in this study (C.W. Thornthwaite Associates). The cup assembly (weight < 7 g) is supported on a low friction bearing, thus ensuring a low stall speed (about 0.1 m s^{-1}), and a fast response to wind speed variations. The anemometer distance constant* is roughly 0.6 m (Thornthwaite, Superior, Mather and Hare, 1961).

The anemometer operates on the principle of a shutter-interrupted light beam which generates an electric current by activating a photocell. Each cup revolution causes the current to vary through one cycle, and this increments a counter. The wind speed is related to the number of counts per unit time by a third-order polynomial equation

$$u = a_0 + a_1 \, f \, c - a_2 \, f^2 \, c^2 + a_3 \, f^3 \, c^3 \qquad (3.2)$$

in which a_0, a_1, a_2, a_3 are polynomial coefficients, c is the number of cup revolutions per minute, and f is a cup calibration factor (Appendix 2.C).

The inclusion of a cup calibration factor is necessary because individual cup assemblies differ slightly in performance. Calibration

---

* The distance which the wind must travel in order for the anemometer to respond to 62.3% of a step change in wind speed.

factors for each cup were determined:

(1) by a field intercomparison, with anemometers mounted at one level above the ground,

(2) by a factory recalibration of some of the sensors, and

(3) by visual inspection of profile plots (u vs. ln z). The last step, which followed the preceding two, was necessary because cup assembly characteristics can change during transport* (see Appendix 2.C).

Care was taken in mounting the anemometers since systematic errors can result:

(1) from interference between the anemometer and the mast,

(2) from interference due to insufficient vertical spacing be- tween anemometers, and

(3) from insufficient height above the surface.

Tanner (1963) reports that the first source of error can be eliminated by ensuring that the cup rotation, at the closest point to the mast, is in the same direction as the wind. This procedure was followed here. The lowest sensor height, and the minimum vertical separation (both equal to 0.25 m) were considered sufficient to prevent errors arising from (2) and (3) (Fig. 3.4).

b. Temperature Profiles

Ventilated dry and wet bulb psychrometry was used (Wexler, 1970). Successful application of the method depends on accurate tempera- ture probes, adequate radiation shielding and proper ventilation. Ther- mopile thermometers, based on a design by Lourence and Pruitt (1969),

* W.J. Superior, Thornthwaite Laboratories, personal communication.
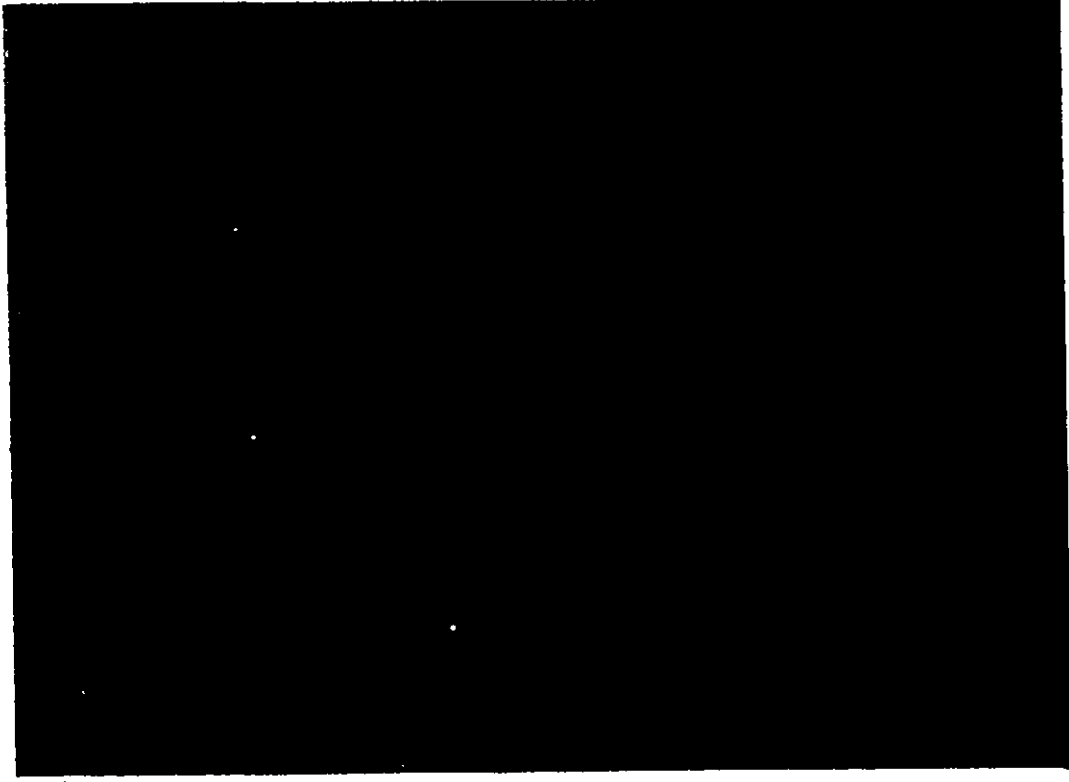
Figure 3.5.   Psychrometers near the surface.
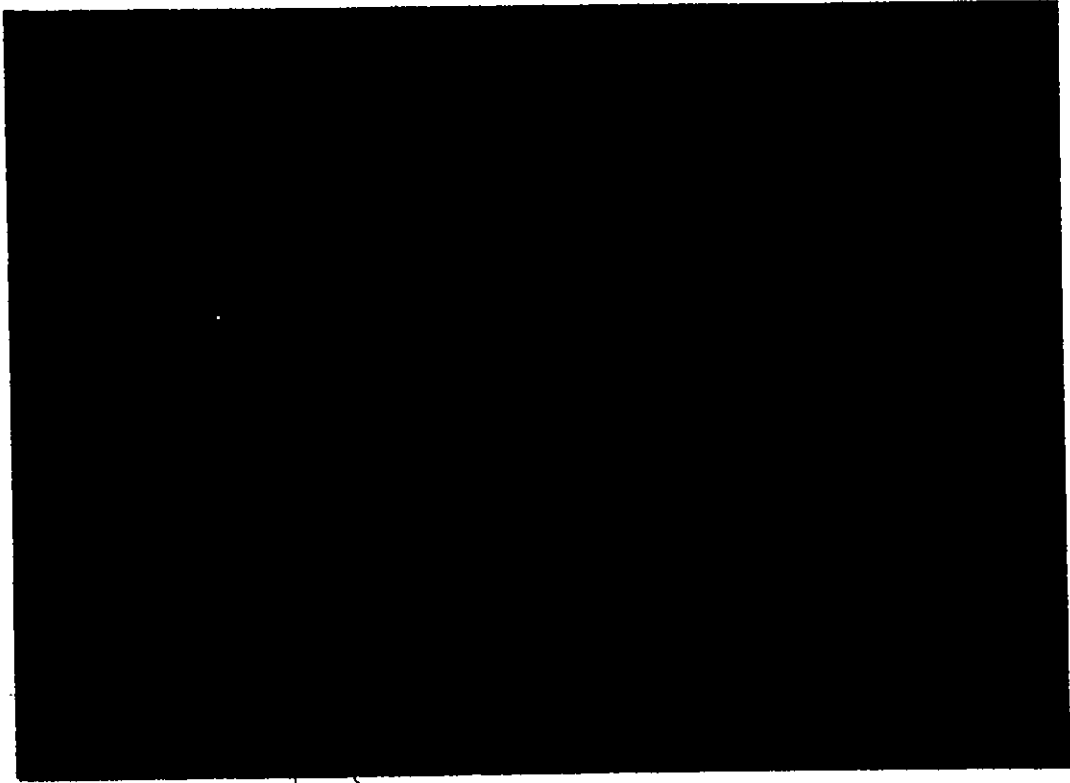
Figure 3.4.   Anemometers near the surface.

with modification by the author (Appendix 2.A), were used to measure temperature. Their time constants* were determined to be approximately one minute.

They were referenced to ice and water in a vacuum flask at the base of the mast. Their outputs were calibrated against a precision platinum resistance thermometer (Rosemount Engineering Company, Model 104MB16CCXA, Bridge Model 414L, precision $\pm$ 0.01 C) prior to and following the field study, over a temperature range of 20 C. From the the calibration data the following polynomial regression relationship was obtained:

$$T = a_0 + a_1 m - a_2 m^2 \qquad (3.3)$$

in which T is the temperature, and m the electromotive output in mV. Values obtained from Eq. (3.3) were converted to potential temperature by removing the influence of the adiabatic lapse rates.[@]

Pooled data from all of the probes employed in the field were used to establish Eq. (3.3). However, an examination of the residuals from the regression revealed that individual probes deviated systematically from Eq. (3.3), and that the deviations were virtually constant over the calibration range. To avoid systematic errors, the mean deviation for a probe was applied to Eq. (3.3) as a correction constant (Appendix 2.C).

---

* The time taken to respond to 62.3% of a step change in temperature.
@ 0.01 C m^{-1} for dry bulbs and 0.007 C m^{-1} for wet bulbs.

The sensor housings used in this study (Fig. 3.5) closely follow a design by Lourence and Pruitt (1969) which was intended to:

(1) eliminate temperature errors arising from the absorption of radiation by the probes,

(2) supply water to the wet bulb at a rate which is in equilibrium with the evaporation (to avoid erroneous wet bulb temperatures), and

(3) maintain a ventilation rate which is in accordance with the requirements of aspirated wet bulb psychrometry (> 4 m s^{-1} and < 11 m s^{-1}; List, 1966).

The radiation error was minimized by covering the probes with two shields, each painted flat black on the inside and covered on the outside with aluminized mylar, which has a high reflectivity for radiation (Fuchs and Tanner, 1965). The wet bulb was covered with a wick which led to a reservoir of distilled water. The wet bulbs were checked periodically to guard against drying out or excessive water supply. Lourence and Pruitt (1969) indicated that this system could provide a ventilation rate of approximately 5 m s^{-1}. This was confirmed for the housings used here in subsequent tests by Allen (personal communication). Further details appear in Appendix 2.A.

3. Other Measurements

In addition to the profile measurements, sufficient information for the evaluation of Q_*, Q_I and Q_M was obtained. Descriptive information about the wind direction and cloud cover was also collected.

a. Net Radiation

A shielded net radiometer (Swisteco Pty. Ltd., Type S-1) was used to measure Q_* (Fig. 3.6). This instrument utilizes the thermopile principle. Its output is related to the net radiative flux by a calibration constant of 6.06 W mV^{-1}.

Features of net radiometer construction, and sources of error are given by Funk (1959, 1962) and Latimer (1972). Among the sources of error to be considered are:

(1) change in calibration constant with time,

(2) unequal convective heat exchanges from the top and bottom sensing surfaces, and

(3) inadequate spatial sampling.

Precise calibrations before and after the field season could not be made. However intercomparisons with a second net radiometer, carried out at Peyto and at Simcoe, Ontario, supported the validity of the calibration constant. Convective heat exchanges from the top and bottom sensing surfaces were equalized by continuously purging the domes with nitrogen. This also prevented internal condensation. The instrument was mounted at 2 m above the surface, which ensured that 96% of the outgoing radiation came from an area of radius 10 m (Reifsnyder, 1967). The spatial sampling problem over ice was also noted by Langleben (1968; 1969), who used a 15 m mounting height over melting sea ice. Since the scale of surface texture variations was comparatively small in this study, the area seen by the net radiometer was considered to be sufficiently large to encompass all of the variations which were observed

Figure 3.6.   Net radiometer.
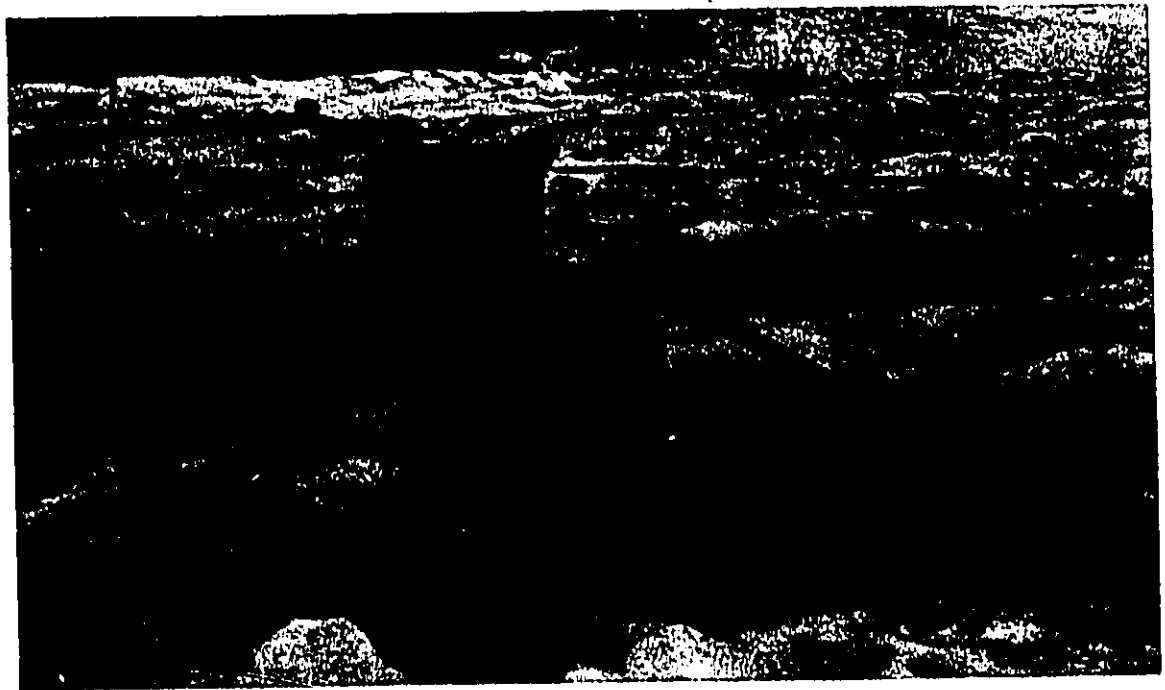
Figure 3.7.   Hydrological discharge measurement system.

(Figs. 3.3 and 3.6).

b. Ice Temperature

Ice temperature profile data taken by Paterson (1971) on Athabasca Glacier, 100 km to the North of Peyto, indicated temperatures slightly below the pressure melting point. These suggested that Peyto Glacier could also deviate from the temperate definition, in which case heat transfer into the surface would occur. Hence, the possibility that heat might be stored in the ice was investigated.

Thermopiles were embedded in the ice at 5, 10, 20 and 30 m below the surface. Temperatures at these depths showed no discernable deviations from 0 C. Therefore the glacier was accepted as temperate, and Q_I was assumed to be negligible.

c. Melt Energy

The amount of energy used in melting the ice was obtained from hydrological discharge measurements. A small area of the glacier surface was isolated with white plastic strips (Appendix 2.B). These protected the underlying surface from sunlight, thus causing the area to be isolated through differential ablation. A chain survey was used to measure the dimensions of the plot. The surface area was calculated to be 386 m^2.

Meltwater generated within the plot boundaries was collected in a pit at the downslope end, and siphoned into a tank (Fig. 3.7) fitted with a V-notch weir (22.5°)*. The water head at the notch was

* The system was designed by L. Derikx, Glaciology Division, Department of Environment (Canada) and assembled by R. Weaver.

recorded continuously on a water level recorder (Leopold and Stevens, drum type, Model F). Constant relevelling of the tank was required since the supports tended to melt into the ice. Significant levelling corrections resulted in a step change in the hydrograph, and this was distributed linearly over the affected portion of the record. A point-gauge, mounted near the V-notch, was used to calibrate the recorder (Appendix 2.B).

Head readings were taken in thousandths of a foot (precision $\pm$ 0.002 ft). These were converted (British Standards Institution, 1961) to discharge by

$$D = \frac{2}{15} \sqrt{2\,g}\ C\ h^{5/2} \tag{3.4a}$$

in which C is the discharge coefficient, D the discharge, and h the head. The discharge coefficient was functionally related to the head:

$$C = 0.65 - 0.396\ (h^{1/4} - 0.798) \tag{3.4b}$$

Since Eq. (3.4a) gives discharge in $ft^3\ s^{-1}$, the value for D was con-verted to $m^3\ s^{-1}$, and the melt energy was obtained from

$$Q_M = \frac{\rho_W\ \lambda_f\ D}{A_p} - \frac{\lambda_f}{\lambda_v}\ Q_E \tag{3.4c}$$

in which A_p is the plot area, λ_f the latent heat of fusion of ice, and

ρ_w the density of water. Q_E is incorporated into Eq. (3.4c) to correct for the transport of water between the atmosphere and the plot. In practice, the correction was found to be small. Direct measurements of discharge from the tank agreed well with results from the discharge equation (Appendix 2.B).

Care was required to guard against leaks developing in the walls of the plot, and malfunctioning of the siphon, but otherwise the system worked well. Good results were obtained with a 1000 m^2 plot on Peyto Glacier in an earlier study (Derikx, 1971), and with an 84 m^2 plot on the McCall Glacier, Alaska (Wendler and Ishikawa, 1973).

d. Descriptive Information

Wind direction was taken four times an hour. It was measured, to the nearest five degrees, in direction left or right of the long axis of the glacier tongue.

Cloud cover was recorded with the same frequency as the wind, noting high, medium and low cloud, in tenths of sky covered. Barometric pressure was recorded on an aneroid barograph (Lambreckt, No. 290).

4. Recording, Data Reduction and Averaging

Electrical interference can be a source of error (Tanner, 1963). This is particularly important in thermopile thermometry since signals seldom exceed 2 mV. Consequently, the practice of using shielded signal cable, and grounding all shields to a common point, was adopted. Care was also taken to ensure that power cables did not cross signal cables.

A ground could not be made because ice is a poor conductor. However, according to Goodman (personal communication), an effective substitute could be obtained by constructing a Faraday cage around the hut. This was done with aluminium screening to which the shields were grounded.

a. Wind Profile Record

Cup revolutions were automatically recorded on registers every half hour. Readings were precise to $\pm$ 0.047 rpm. Data were transferred from the register outputs to computer cards for subsequent analysis.

b. Temperature and Vapour Pressure Profile Records

Temperature signals were recorded on a two-pen recording potentiometer (Honeywell Electronik 194). One pen recorded dry bulb signals, while the second pen was used for the wet bulb. The recorder precision was $\pm$ 0.25% of full range with a dead band error of $\pm$ 0.15% of full range.

Each level was recorded sequentially, using a stepping switch with gold-plated contacts to minimize signal noise. The stepping rate was one cycle per minute. For a probe time constant of one minute, this sampling frequency lies between suggested rates of once every three minutes (Angus, 1963) and twice a minute (Suomi and Tanner, 1958). Data were transferred from the chart paper to computer cards by a digitizer, which resolved the recorder trace to $\pm$ 0.16% of full range.

The signal data were converted to temperature by Eq. (3.3), and subsequently meaned over 30 minutes. These were then converted to potential temperatures. Half-hourly means of dry and wet bulb temperature, θ and θ_w, were used to compute the vapour pressure profiles from

$$e = E \exp\left[\frac{A\,\theta_w}{\theta_w + B}\right] - \gamma\,(\theta - \theta_w)\,\frac{p}{p_0} \tag{3.5}$$

in which A and B are empirical constants, E is the vapour pressure at the ice point, p_0 is a reference pressure (10^5 Pa), and γ is the psychrometric constant. This equation is adapted from standard relationships, which deal with saturation vapour pressure and vapour pressure deficit (List, 1966; Dilley, 1968).

c. ## Net Radiation Record

A similar recording procedure to the above was used for $Q_\star$. The signal was recorded once every minute, and the calibration constant was used to obtain the net radiation value. Individual values were meaned over half an hour.

c. ## Melt Record

Water level recorder charts gave a continuous record of head. The charts were reduced by hand. Six values for each half hour were transferred to computer cards, and converted into energy fluxes by Eq. (3.4). These were then meaned for the half-hour period.

C. Data Quality

The quality of data is a function of the accuracy and precision of the measurements (Cook and Rabinowicz, 1963). The conclusions which are drawn from data should be weighed against the sources of error. Fuchs and Tanner (1970) have shown how error analysis can assess the quality of heat flux computations from profile data. It has also been used to determine errors in radiometrically derived surface temperatures (DeWalle and Parmelle, 1974).

Accuracy refers to the size of any systematic error in a measurement system. This type of error can lead to incorrect conclusions unless it is small. However, it is also difficult to assess. Concern for sensor design and exposure is directed toward minimizing this type of error.

Precision refers to the size of the random error in a set of measurements. It may be reduced by careful calibration of sensors, and the use of high resolution recording equipment. Any value, Y, can be expressed as a function of fundamental measurements, X_1, X_2, X_3 ..., which have errors, dX_1, dX_2, dX_3 ... associated with them:

$$Y = f (X_1 \pm dX_1, X_2 \pm dX_2, X_3 \pm dX_3 \ldots) \tag{3.6a}$$

The total error in Y, dY, is given by the total derivative

$$dY = \frac{\partial Y}{\partial X_1} dX_1 + \frac{\partial Y}{\partial X_2} dX_2 + \frac{\partial Y}{\partial X_3} dX_3 \ldots \tag{3.6b}$$

The probable error in Y is smaller. It is calculated by taking the root-mean-square of Eq. (3.6b):

$$\delta Y_{rms} = \left[\left(\frac{\partial Y}{\partial X_1}\delta X_1\right)^2 + \left(\frac{\partial Y}{\partial X_2}\delta X_2\right)^2 + \left(\frac{\partial Y}{\partial X_3}\delta X_3\right)^3 + \ldots\right]^{\frac{1}{2}} \quad (3.6c)$$

The errors, δX_1, δX_2, $\delta X_3 \ldots$, are evaluated either from _a priori_ knowledge or, where mean values are used, by taking the standard errors, σ_{X_1}, σ_{X_2}, $\sigma_{X_3} \ldots$ (Fogel, 1962). The quantity, $\delta Y/Y$, defines the relative error in Y. It is expressed as a percentage.

1. Profile Measurements

a. Wind Speed

The precision of a wind speed measurement is affected by the error in the cup calibration factor ($\pm$ 0.5%), and the read-out error ($\pm$ 0.047 rpm). They give rise to relative errors of 0.5% over the range of wind speeds encountered in this study, with slightly greater error for $u \leq 1$ m s^{-1} (Table 3.1a).

The errors in wind speed differences between any two levels are larger (Table 3.1b). Since they depend upon the overall wind speed, a range of 4 to 5 m s^{-1} was chosen as being representative of the data obtained in the first metre (see Chapter Four).

Overestimates of the wind speed may result from (MacCready, 1966; Bernstein, 1967; Acheson, 1970):

(1) deviations of the wind vector from the horizontal plane, which create an additional vertical component,

TABLE 3.1

Wind Profile Errors

(a) Wind speed.

$u \ (m \ s^{-1})$	$\delta u \ (m \ s^{-1})$	$\delta u/u \ (\%)$
0	0.001	-
1	0.005	0.5
2	0.010	"
3	0.015	"
4	0.020	"
5	0.025	"
6	0.030	"
7	0.035	"
8	0.040	"
9	0.045	"
10	0.050	"

TABLE 3.1 (cont'd.)

Wind Profile Errors

(b) Wind speed difference between two levels, a and b (u_a = 4 m s^{-1}, u_b = 4 to 5 m s^{-1}).

Δu (m s^{-1})	$\delta \Delta u$ (m s^{-1})	$\delta \Delta u / \Delta u$ (%)
0.0	0.028	—
0.1	0.029	29.0
0.2	0.029	14.5
0.3	0.030	10.0
0.4	0.030	7.5
0.5	0.030	6.0
0.6	0.030	5.0
0.7	0.031	4.4
0.8	0.031	3.9
0.9	0.032	3.6
1.0	0.032	3.2

(2)   differences between the vector wind, and the average wind in the mean direction, and

(3)   inertial effects within the anemometer, which make it insensitive to lulls in the wind speed (overrun error).

The first two are likely to be negligible, since deviations of most quantities are relatively small in stable conditions (Lumley and Panofsky, 1964).

Overrun error may be substantial in unstable conditions, but can probably be ignored in the stable case. This is supported by Hyson's (1972) analysis, in which the overrun error was found to be zero for $\sigma_u/u \leq 0.12$, where σ_u is the standard deviation of the wind speed. An estimate of σ_u was not available for this study, but using $\sigma_u = 2 u_*$ as representative of stable conditions (Lumley and Panofsky, 1964), gives $\sigma_u/u < 0.12$ for most of the measurement period. In addition, Hyson's anemometer had approximately twice the distance constant of the anemometers used in this study, so they should have been more susceptible to inertial effects (MacCready, 1970). Therefore, a larger value of σ_u/u could probably be tolerated here.

b.   Temperature

The probable error in T was assessed from the error in the calibration constant ($\pm$ 0.00937 C mV^{-1}), and the resolution error in extracting data from the recorder charts ($\pm$ 0.0067 mV). The results (Table 3.2a) represent the errors in the half-hour mean temperatures, θ and θ_w. They indicate relative errors of less than 1% over most of the calibration range.

TABLE 3.2

Temperature Profile Errors

(a) Temperature ($T = \theta$ or θ_w).

T (C)	δT (C)	$\delta T/T$ (%)
0	0.034	-
2	0.035	1.8
4	0.035	0.9
6	0.036	0.6
8	0.038	0.5
10	0.039	0.4
12	0.041	0.3
14	0.043	0.3
16	0.045	0.3
18	0.048	0.3
20	0.050	0.3

TABLE 3.2 (cont'd.)

Temperature Profile Errors

(b) Temperature difference ($\delta\theta = 0.04$ C).

$\Delta\theta$ (C)	$\delta\Delta\theta$ (C)	$\delta\Delta\theta/\Delta\theta$ (%)
0.0	0.057	-
0.2	"	28.5
0.4	"	14.3
0.6	"	9.5
0.8	"	7.1
1.0	"	5.7
1.2	"	4.8
1.4	"	4.1
1.6	"	3.6
1.8	"	3.2
2.0	"	2.9

These error estimates may be too small. In cases where mean values are obtained from discretely sampled data, MacCready (1970) has stated that it is more appropriate to assess how representative a measurement may be. This is done for independent samples by computing the standard error of the mean, but these data are autocorrelated.[*] Thus the computation of standard errors requires a detailed knowledge of the time series properties (Leith, 1973). Consequently, the error analysis was based solely upon calibration and recorder error.

The error in potential temperature differences between two levels is listed (Table 3.2b) over the range of temperature differences observed in the first metre (see Chapter Four). The analysis indicates that $\Delta\theta$ in excess of 1 C is required for the determination of temperature differences to better than $\pm$ 5%.

Measurement accuracy could have been affected by radiation error, and failure to keep the reference bath at 0 C. The design features intended to minimize these errors have already been described, but quantitative estimates of their magnitude could not be made. However, radiation errors could result in higher than expected temperatures, while reference bath errors would tend to reduce the temperature below the true value. Therefore, the net error was thought to be small.

c. Vapour Pressure

The precision of the vapour pressure calculations depends upon the precision of the dry and wet bulb temperature measurements. The

---

[*] This applies to time-ordered data, in which each value is correlated with the preceding value.

results of the error analysis are shown (Table 3.3a) for vapour pressures which encompass the range observed in this study.

An evaluation of the probable error in vapour pressure differences between two levels (Table 3.3) indicates that a vapour pressure difference of at least 50 Pa is required in order to keep the relative error within $\pm$ 10%. Observed differences were usually smaller than this (see Chapter Four).

The accuracy of e depends on the performance of the dry and wet bulb sensors. The probable causes of temperature errors have already been noted, but the wet bulb deserves special consideration because it is crucial (Lourence and Pruitt, 1969). Incorrect water feed rates and inadequate ventilation can lead to erroneously high wet bulb values, which raise the vapour pressure measurement above the true value. This problem was not satisfactorily solved.

2. Other Measurements

a. Net Radiation

The error in Q_* depends upon the resolution in the signal reading ($\pm$ 0.33 mV), and the calibration error. The latter was set at $\pm$ 5%, which is a liberal estimate for this type of radiometer (Latimer, 1972).

The error analysis (Table 3.4) indicates a relative error of $\pm$ 5%, with greater error for $Q_* < 300$ W m^{-2}. The errors for small Q_* are probably overestimates. The recorder was normally changed to a smaller range for these values, thus improving the scale resolution.

TABLE 3.3

Vapour Pressure Profile Errors

(a) Vapour pressure.

e (Pa)	δe (Pa)	$\delta e/e$ (%)
0	2.4	-
100	2.5	2.5
200	2.6	1.3[a]
300	2.7	0.9
400	2.8	0.7
500	2.9	0.6
600	3.0	0.5
700	3.1	0.5
800	3.2	0.4
900	3.2	0.4
1000	3.3	0.3

TABLE 3.3 (cont'd.)

Vapour Pressure Profile Errors

(b) Vapour pressure difference.

Δe (Pa)	δΔe (Pa)	δΔe/Δe (%)
0	4.2	-
10	"	42.0
20	"	21.0
30	"	14.0
40	"	10.5
50	"	8.4
60	"	7.0
70	"	6.0
80	"	5.3
90	"	4.7
100	"	4.2

TABLE 3.4

Net Radiation Errors

Q_* (W m^{-2})	δQ_* (W m^{-2})	$\delta Q_*/Q_*$ (%)
0	1.5	-
50	3.3	6.6
100	5.0	5.0
200	10.2	"
300	15.0	"
400	20.0	"
500	25.0	"
600	30.0	"
700	35.0	"
800	40.0	"
900	45.0	"
1000	50.0	"

Systematic errors could have resulted from the incorrect mounting and operation of the net radiometer, but these could not be evaluated. The precautions for minimizing these have already been described.

b. Melt Energy

The precision of the melt estimates depends upon the error in the discharge coefficient ($\pm$ 1%), and the tolerance in reading the hydrograph ($\pm$ 0.002 ft.). These lead to relative errors of less than $\pm$ 5% over most of the range between 0 and 1000 W m^{-2} (Table 3.5). They are about the same as the errors usually encountered in stream gauging with weirs (Gray and Wigham, 1970).

Systematic errors could have been caused by leaks in the melt plot, malfunctioning of the siphon and tilting of the weir. Precautions for minimizing these have been described.

TABLE 3.5

Melt Energy Errors

Q_M (W m^{-2})	δQ_M (W m^{-2})	$\delta Q_M/Q_M$ (%)
0	0.1	-
50	2.8	5.6
100	4.3	4.3
200	6.6	3.3
300	8.8	2.9
400	10.0	2.0
500	11.5	2.3
600	12.9	2.2
700	14.3	2.0
800	15.7	2.0
900	17.2	1.9
1000	18.7	1.9

CHAPTER FOUR

RESULTS AND DISCUSSION

A. Wind Speed, Temperature and Vapour Pressure Data

1. General Features of Data Obtained

Since the instrumentation required constant attention, continuous measurement over long periods was not attempted. Instead most of the data were collected over daylight periods, when the melt rate was high. However four longer periods, each of which exceeded 24 hours, included night-time data. The data are listed in Appendix Five. Local Apparent Time (LAT) is used throughout.

Wide ranges of wind speed, temperature and vapour pressure were encountered (Table 4.1). Air temperatures, large relative to the surface temperature, indicate a strong potential for heat transfer to the glacier. In contrast, atmospheric vapour pressure fluctuated around the ice point value of 611 Pa, so that the vapour flux was directed upward on some occasions and downward on others. Hence, over the melt period, the net exchange of latent heat was small. Horizontal wind speed usually exceeded 3 m s^{-1}, providing vigorous mixing in cases of fully developed turbulent flow.

Cloud conditions were typical of the melt season. Cloudless periods, which have the experimental advantage of minimizing fluctuations

TABLE 4.1

Peyto Glacier, 1971, Summary of Data Collected at z = 1 m

Time of Start (LAT)	Duration (hr)	Clear Periods (Total hr 1/10 or less cloud)	Wind Speed (m s^{-1}) Max.	Min.	Temperature (C) Max.	Min.	Vapour Pressure (Pa) Max.	Min.	Cloud Cover (Tenths) Amt.	Type
Aug. 1 – 1200	5	5	7.6	6.8	5.7	4.7	660	610	0-1	Cu
2 – 0730	9.5	4.5	6.3	3.3	15.6	9.9	950	640	0-8	Cu
3 – 0700	9	0	7.7	4.5	12.2	9.0	660	450	3-9	Cl,Cu
12 – 1000	7	0	5.1	3.3	13.0	9.0	620	570	0-1	Cu,Smoke
13 – 0700	34	3	8.7	1.0	13.6	6.0	830	340	0-8	As,Cl, Cu,Smoke
16 – 0700	4.5	2	5.4	3.4	9.0	6.1	530	440	0-10	Cu
18 – 1300	6	0	4.6	2.5	6.1	5.6	680	620	9-10	Sc
19 – 0700	12	1	4.8	3.2	11.1	6.0	740	670	1-9	Cl,Cu
20 – 0700	34	6	6.7	3.4	11.6	7.8	620	520	1-10	As,Cl,Cu
24 – 1100	12	7	7.8	3.3	9.7	5.1	630	600	1-8	Cu
25 – 0800	12	4.5	4.7	3.1	9.4	6.4	600	500	0-6	Cl,Cu

TABLE 4.1 (cont'd.)

Time of Start (LAT)	Duration (hr)	Clear Periods (Total hr 1/10 or less cloud)	Wind Speed (m s⁻¹) Max.	Min.	Temperature (C) Max.	Min.	Vapour Pressure (Pa) Max.	Min.	Cloud Cover (Tenths) Amt.	Type
Aug.28 - 1100	52	28.5	6.3	2.0	11.3	4.3	840	500	0-10	Ac,As,Cl, Cu,Cs
Sept.2 - 1200	6	0	4.0	2.2	3.7	2.3	580	520	6-10	Cu
3 - 0800	11	0.5	3.7	2.2	5.2	2.5	670	500	1-10	Sc
4 - 0900	30	7	9.4	2.5	7.4	4.4	690	430	0-10	Cu,Sc

in radiation, were encountered only sporadically. Wind direction was usually downglacier, within 45 degrees of the long axis of the glacier tongue. Barometric pressure varied slightly with the weather, but was always close to 7.8×10^4 Pa. This value was used in calculations.

2. Time Variation of Wind Speed, Temperature and Vapour Pressure

Data from the longest collection period (August 28-30) serve to illustrate time variations of wind speed, temperature and vapour pressure. Half-hourly means of these parameters, measured at a height of 1 m, are plotted in Fig. 4.1. The selection of this height will be justified later.

Only the wind shows a tendency to vary diurnally. Speeds were higher by day than at night. This is probably due to a local valley breeze circulation. Air in the valley below the glacier was warmed by day, while the air over the glacier was cooled. Cold air flowed into the valley in response to density and topographical differences, resulting in relatively strong winds. At night the air in the valley was also cooled, and both the density difference and the resulting valley wind were reduced. This agrees with Sedgewick's (1966) findings for Peyto. Diurnal variations of temperature and vapour pressure were not observed, presumably because they were controlled by air mass characteristics.

Wind speed varied considerably over periods of a few hours, particularly at night. According to Lettau (1966) this type of variation characterizes katabatic winds.
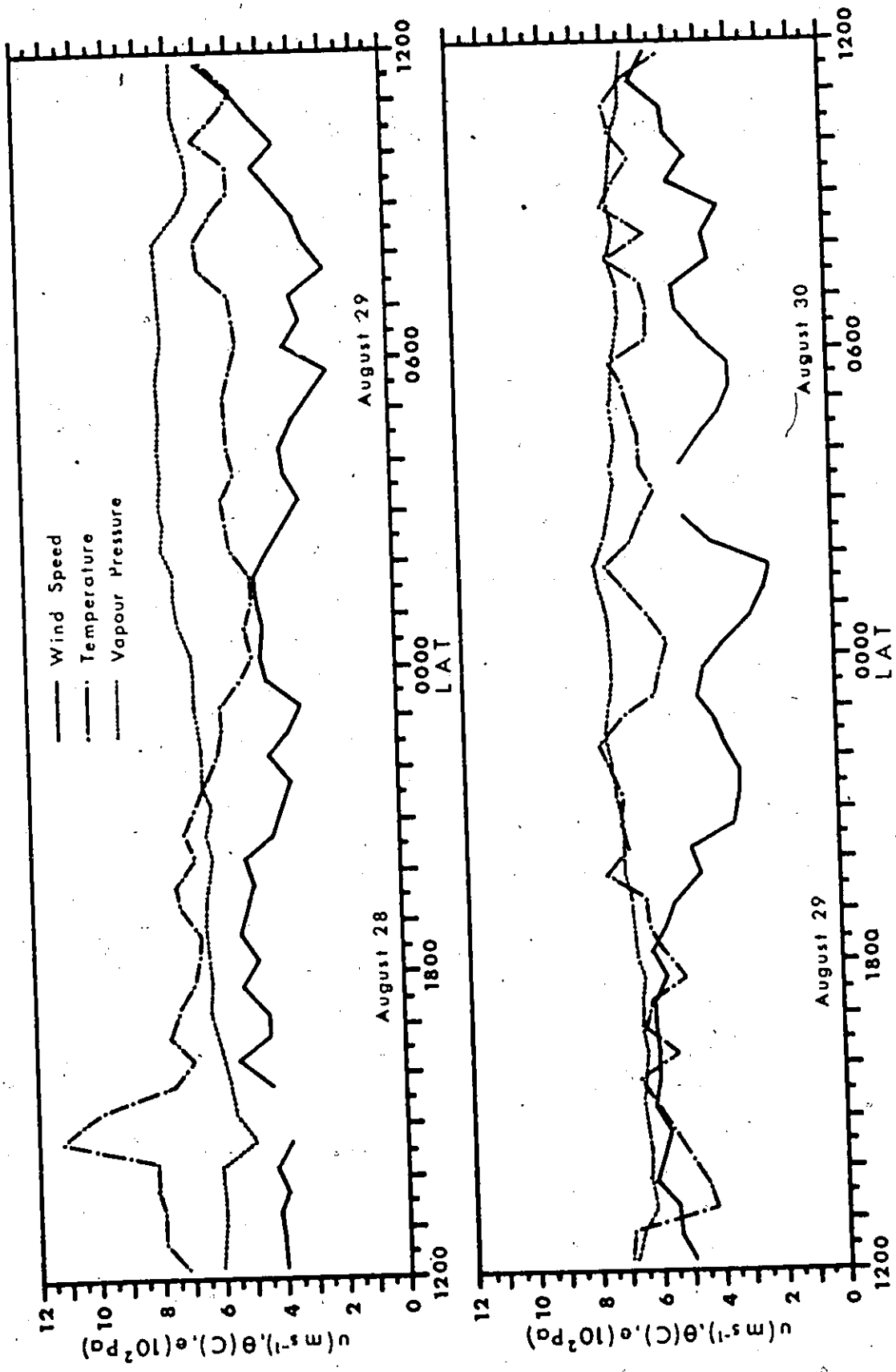
Figure 4.1. Wind speed, temperature and vapour pressure at z = 1 m, August 28 - 1200 to August 30 - 1200.

Short-term variations in temperature were related to wind speed. Relative temperature minima usually corresponded with relative wind speed maxima. This can be expected when air is cooled from below by turbulent mixing, since turbulence should increase with wind speed. As turbulence increases, so does the degree of cooling at a given height, resulting in a temperature decrease. Reduced wind speed produces relative warmth. This effect was also observed over periods of a few minutes. Lulls in the wind were quickly followed by noticeably warmer temperatures. Short-term variations in vapour pressure also responded to wind speed variations, but the response was weaker than that for temperature, since the vapour pressure was always close to the ice point.

These variations indicate that steady-state conditions did not strictly apply. Nevertheless, a steady state can be assumed, since the flux divergence is negligibly small. This is illustrated by evaluating the finite difference approximations to $\rho \partial u/\partial t$ and $\rho c_p \partial \theta/\partial t$ in Eq. (2.2). For the Peyto data $\Delta \tau/\Delta z < 10^{-3}$ Pa/m and $\Delta Q_H/\Delta z < 1$ W m^{-2}/m, over half-hourly periods. Larger flux divergence values could have occurred due to gusts and lulls within the half-hour averaging period. However, the resultant errors would off-set one another, since they would be similar in magnitude but of opposite sign.

The assumption of horizontal uniformity rests upon the argument advanced earlier (Chapter 2.A), that horizontal gradients of u, θ and e should be negligible close to the surface away from the glacier margin. It could not be tested with the data obtained here.

3. Profiles of Wind Speed, Temperature and Vapour Pressure

Profiles of wind speed, dry and wet bulb temperatures, and vapour pressure are plotted in Fig. 4.2. Wind speed measurements showed a smooth curvilinear variation with height. Relatively few anomalies were found, a reflection of good anemometer performance. The incidence of anomalous readings was greater for dry bulb temperatures, but the profiles approached the consistency of those obtained for the wind. The results of the wet bulb and derived vapour pressure profiles are poorer by comparison due to problems in providing a correct water supply to the wicks (see Chapter Three).

Wind speed gradients generally decrease with increasing height above the surface, but in some cases (e.g. August 29 - 0300) the gradient above 2 m became extremely shallow, and even reversed. The temperature gradient also showed a decrease with increasing height, within 2 m of the glacier surface. Above this level it was either very shallow or exceedingly steep on occasion (Fig. 4.2b), suggesting that the flow above 2 m behaved differently from that below. Vapour pressure gradients were small, and consequently patterns of variation with height were difficult to detect. A decrease of the gradient with height is indicated when the profile shows a consistent height variation (e.g. August 29 - 0500).

Not all of the data were equal to the standard exhibited in Fig. 4.2a,b. Instrumental malfunctions, and recording errors often caused anomalies to appear in the wind and temperature profiles. These were usually difficult to detect in the type of plot shown in Fig. 4.2,
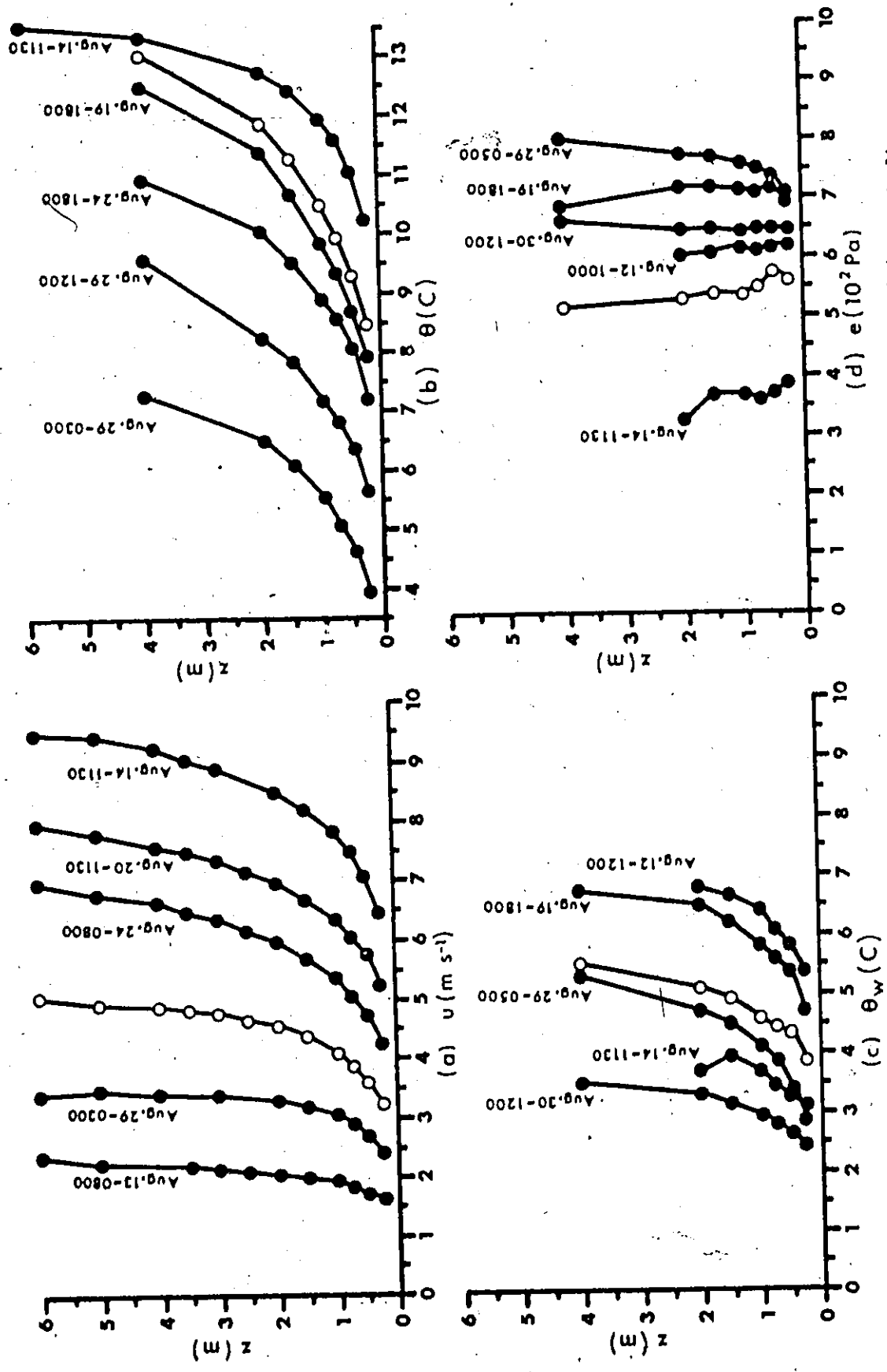
Figure 4.2. Selected profiles, (a) wind speed, (b) dry bulb temperature, (c) wet bulb temperature, and (d) vapour pressure. Open symbols: August 20 - 1400.

but became apparent in later stages of the analysis. Therefore it was
necessary to discard some data. This was preferred to the procedure
of smoothing data, employed by some authors (Businger et al., 1971;
Pruitt, Morgan and Lourence, 1973), since the possibility of causing
bias was avoided.

The need to be selective is further illustrated by the
results of the error analysis (Chapter 3.C.1). Values for Δu of 0.3 -
0.6 m s^{-1} are common. Error analysis showed that these have a preci-
sion of 5 - 10%. The range of $\Delta \theta$ is usually 0.4 - 1 C, with an error
of 6 - 14%. Vapour pressure differences are very small, with absolute
values of < 10 - 30 Pa. Thus the relative errors in Δe were rarely
less than 15%, more often close to 40%. Due to the obvious short-
comings in the vapour pressure data, vapour pressure profiles were
given a minor role in the analysis. Emphasis is placed upon the wind
speed and temperature profiles, from which most of the conclusions
about transfer over the ice are drawn.

B. Profile Structure of the Air Above the Ice

1. Katabatic Influence

The tendency of the air layer near the surface to behave
differently from that above is further illustrated by logarithmic pro-
files of u and θ (Fig. 4.3). These profiles follow the established
stable form within the first meter. However, eye-drawn extrapolations
for greater heights diverge substantially from measured values. Above
1 - 2 m, measured values are smaller than the extrapolated. This is
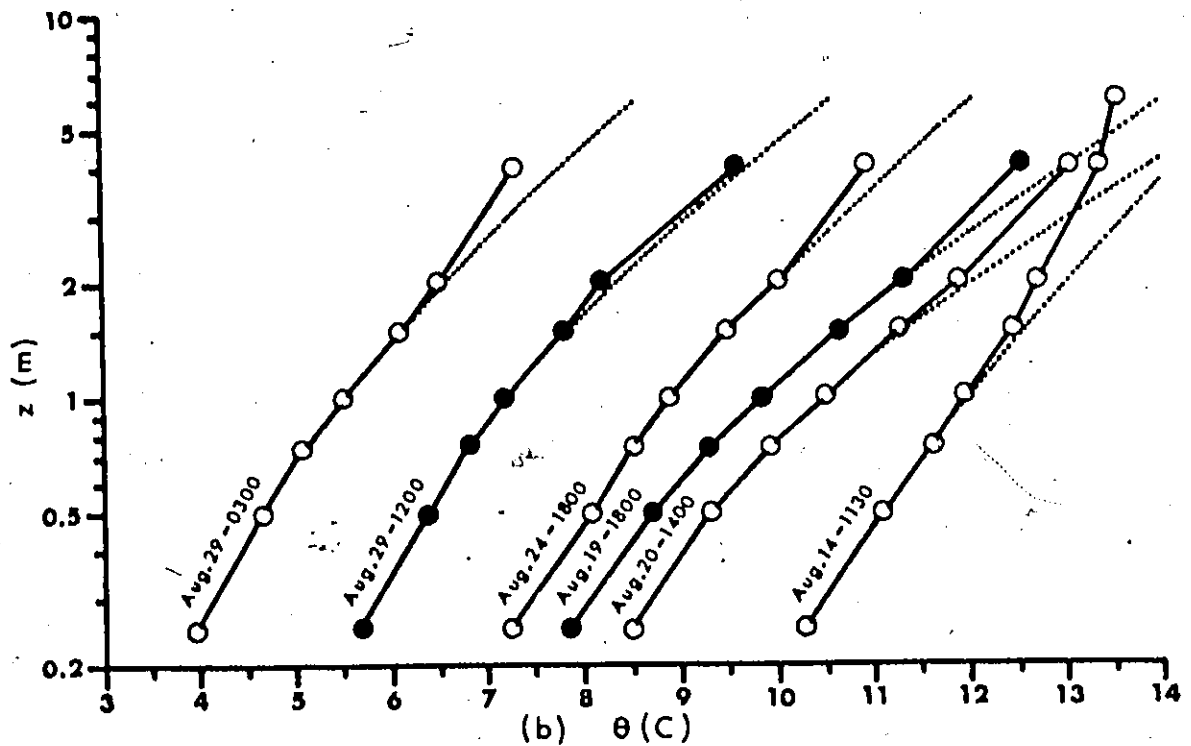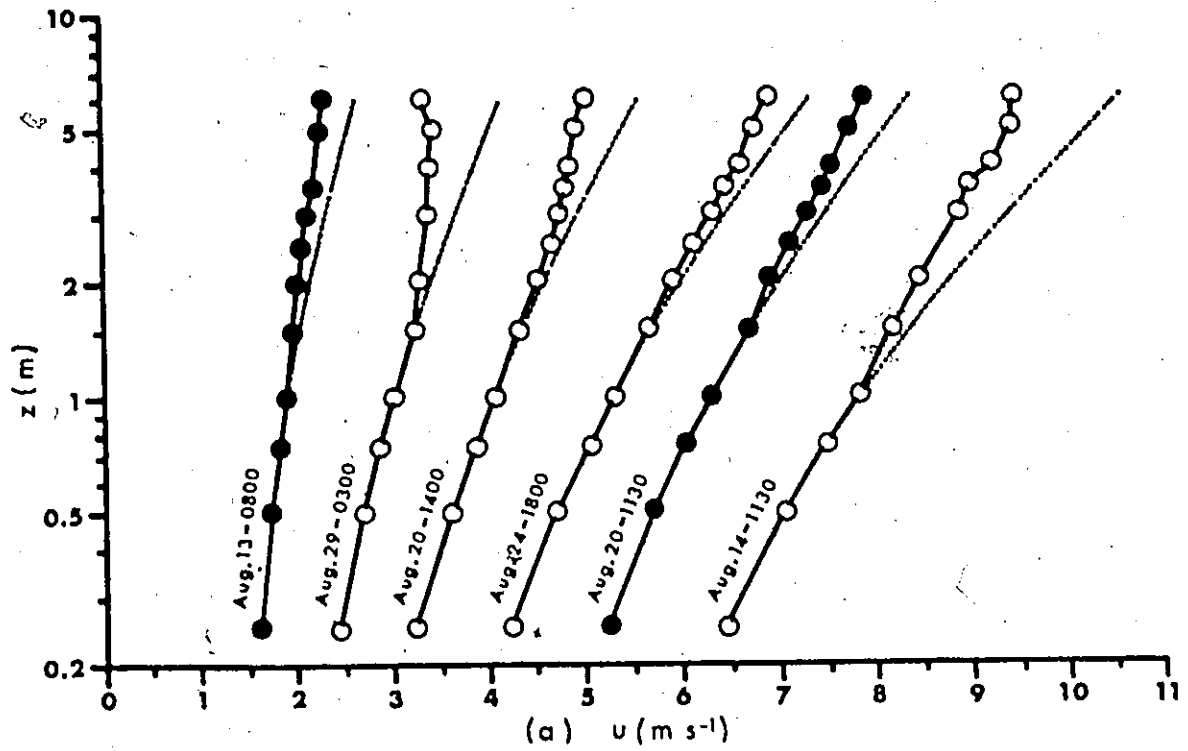
Figure 4.3. Selected profiles plotted on a logarithmic height scale,
(a) wind speed, and (b) temperature. Open symbols:
simultaneous wind speed and temperature profiles. Dotted
lines are eye-drawn extrapolations of the lower profile
form.

interpreted to be a consequence of katabatic flow.

Katabatic flow was detected in the wind profiles where $\partial u/\partial z = 0$. An example, accompanied by a thermocline, is shown in Fig. 4.4. The association is inevitable. From Eqs. (2.1b), (2.5b) and (2.17)

$$K_H = \frac{k^2 z^2}{\phi_M \phi_H} \frac{\partial u}{\partial z} \tag{4.1}$$

Hence, when $\partial u/\partial z = 0$, $K_H = 0$, and heat transport is accomplished only through molecular motion. This means that when warm air is advected over the glacier, turbulent cooling is confined to a shallow layer near the surface. As the air continues downglacier this surface layer becomes increasingly colder than the original invading air, and a distinct boundary develops between the two. This is marked by a thermocline, a feature which has been observed elsewhere over glaciers (Hubley, 1957; Hölmgren, 1971).

Reversals of the wind speed gradient were detected infrequently in the observed profiles, but all profiles were influenced by katabatic flow. Vertical flux divergence of heat and momentum probably occurred, since τ and Q_H should approach zero at the level where the katabatic force is strongest (where K_M and K_H approach 0). However, values equal to zero are unlikely. Hölmgren (1971) has noted that a certain amount of momentum transfer across the core of the katabatic wind is possible through wave motion. In addition, molecular heat transfer can take place across the thermocline.
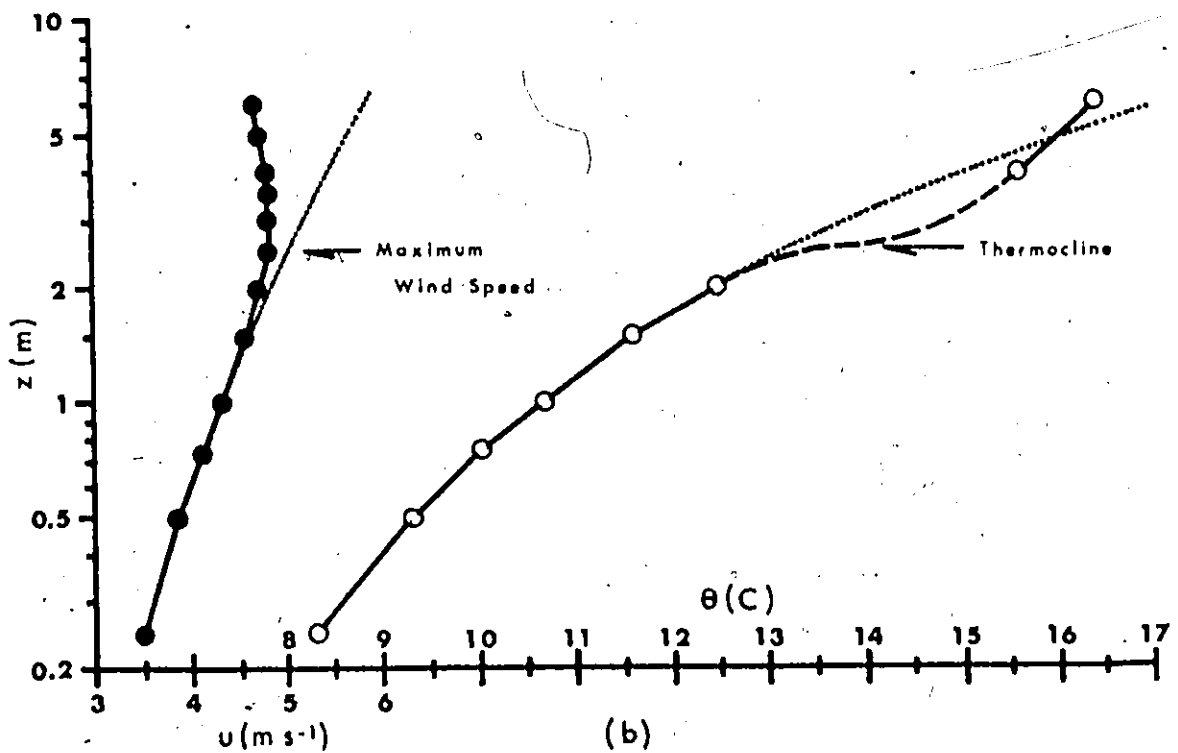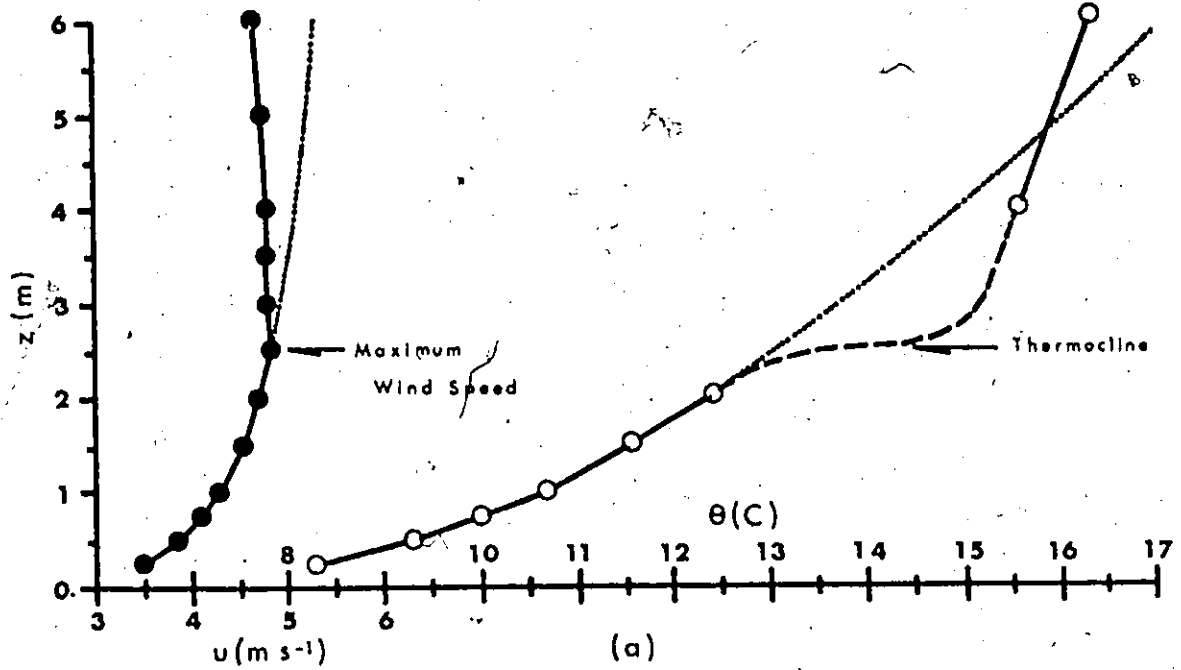
Figure 4.4. Example of katabatic wind profile (closed symbols) and associated temperature profile (open symbols), August 12 - 1430, (a)arithmetic height scale, and (b) logarithmic height scale. Dotted lines are eye-drawn extrapolations of the lower profile form.

The flux divergences of heat and momentum associated with the katabatic flow appeared to be small close to the surface. An approximate evaluation of the momentum flux divergence is obtained from (θ'/θ_0) $\rho g \sin \psi$ in Eq. (2.3). Hölmgren (1971) suggested that $\rho c_p u\theta'/\Delta x$ could be used in assessing sensible heat flux divergence, where θ' is set equal to the temperature difference between the highest and lowest measurement levels. This procedure was followed here, and $\theta' \simeq 3.5$ C represents the usual temperature change encountered. Taking $u \simeq 4$ m s^{-1} and $\Delta x \simeq 5$ km, values of $\Delta\tau/\Delta z \simeq 0.005$ Pa/m and $\Delta Q_H/\Delta z \simeq 3$ W m^{-2}/m are obtained. Computed values of the surface fluxes are substantially greater (see Fig. 4.15). Hence vertical flux divergence does not seem to be a critical factor within the first metre above the ice.

Although the profiles follow the usual stable form within the first 1 - 2 m, it is not certain if the log-linear form is appropriate or not. This was determined by analyzing friction parameters computed from the wind and temperature data.

2. Procedure for the Analysis of Friction Parameters

The height variations of the profile-derived quantities u'_*/k and θ'_*/k are examined. The primes signify that these values must be corrected in order to obtain accurate friction parameters. The procedure follows that devised by Webb (1970) for analyzing profiles in stable equilibrium. It was not applied to vapour pressure profiles because the data were not sufficiently precise.

Rearranging Eq. (2.20), and dividing by $\Delta \ln z$ for any atmospheric property, y,

$$Y = \frac{y*}{k} \left[1 + \frac{\alpha}{L} X \right] \qquad (4.2)$$

where $Y = \Delta y/\Delta \ln z$, and $X = \Delta z/\Delta \ln z$. The quantity, Y, is equal to u'_*/k or θ'_*/k. As z approaches zero, it converges to the correct value $(u_*/k$ or $\theta_*/k)$, since z/L becomes negligibly small close to the surface. The value of X may be taken as the height difference through the air layer between the two measurement levels used in computing Y. It is close to the geometric mean of the two heights, which is used commonly in assigning a height to quantities derived from finite differences.

Values of Y and X were obtained from all possible combinations of height pairs in a profile. Subsequently, Y was plotted against X, as a scatter diagram. In a log-linear regime, Y should increase linearly with X from a positive value at $X = 0$.

3. Profiles of Friction Quantities and Delimitation of Boundary Layer

The characteristic plot for the stable case occurs within the first meter (Fig. 4.5). Above, the distribution is markedly different from the expected result. Webb (1970) also showed deviations (above 8 m) in strong stability.

For u'_*/k (Fig. 4.5a) values reach a maximum near 1.5 m, then decrease with height, becoming negative above 3.5 m (i.e., where
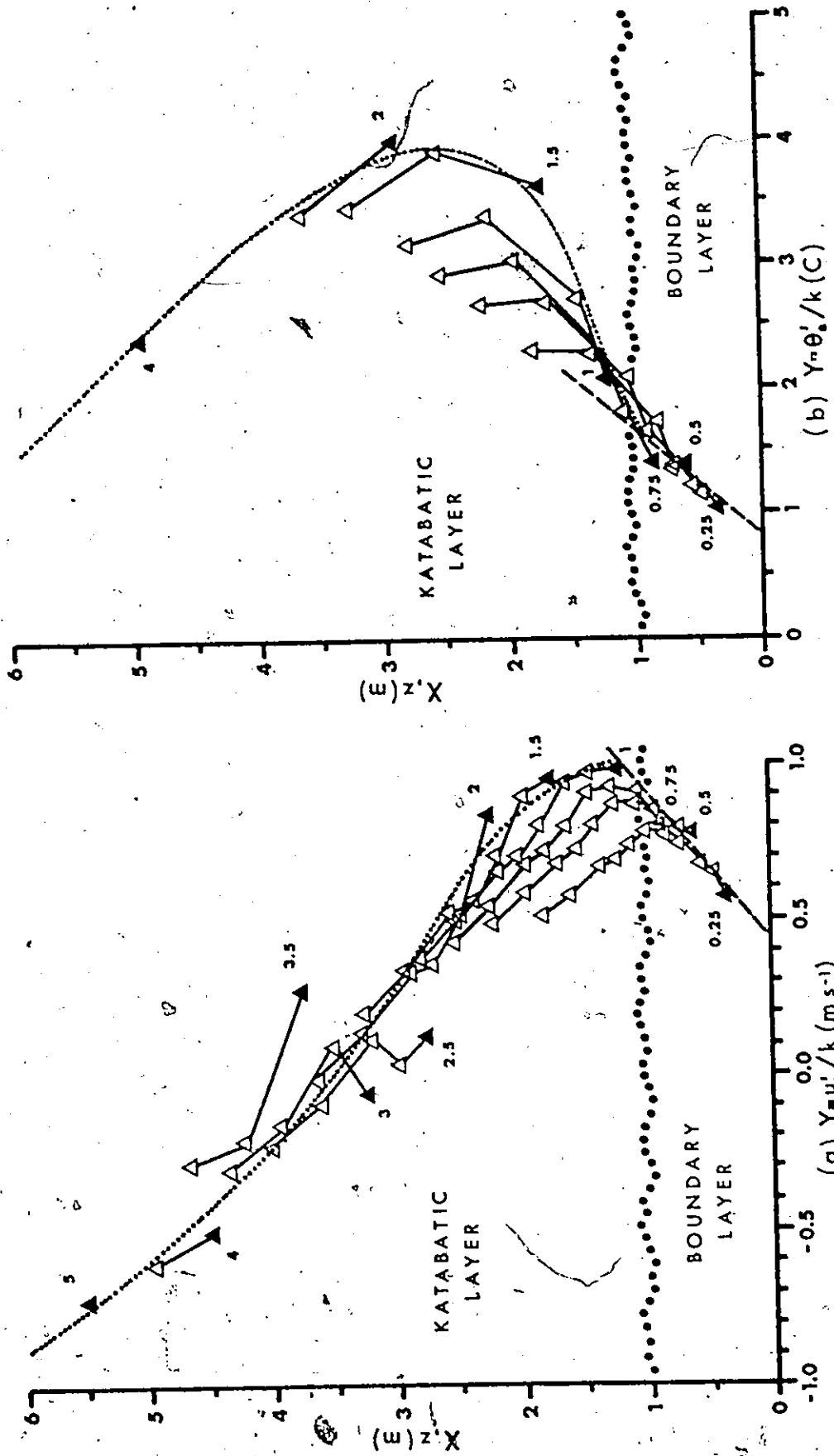
Figure 4.5. Example of air layer analysis, August 13 – 2100, (a) from wind profile data, and (b) from temperature profile data. The approximate height of the boundary layer (bold dotted line), best-fit line to boundary layer points (dashed line) and general trend of points above the boundary layer (thin dotted line) are indicated. Closed symbols: adjacent height pairs, with height of lower level marked; open symbols: other height pairs.

$\Delta u/\Delta \ln z = 0$). Between 1 and 2.5 m, scatter in the data is large. The data were ordered by joining all points with the same lower level for $\Delta \ln z$. Fig. 4.5a shows that points joined in this way follow the expected stable distribution below 1 m, and parallel one another above this level. Webb (1970) showed similar results, except that he joined points with the same upper level.

The θ'_*/k distribution (Fig. 4.5b) is similar to that for u'_*/k below 1 m. Above this height values of the parameter increase rapidly, due to the strong temperature gradient of the thermocline, reaching a maximum near 3 m. Values then decrease with height as the temperature gradient decreases.

Both distributions indicate that a boundary layer, where the fluxes are constant with height, exists close to the ice surface. This conclusion is inferred from the apparent log-linear variation of Y for $z \le 1$ m. Above, the fluxes probably decrease with height, and become small within the katabatic layer.

4. Thickness of the Boundary Layer and the Frequency of Its Occurrence

The thin boundary layer implies that the placement of instruments according to boundary layer adjustment criteria for horizontal surfaces can be misleading. The height of the maximum katabatic wind speed is important, since the thickness of the boundary layer should be related to it. A model which predicts the katabatic wind spatially is required, but is beyond the scope of this study.

Therefore, a descriptive assessment for this site is offered here.

Boundary layer thickness was determined by examining individual plots of u_*'/k and θ_*'/k. Examples are shown in Fig. 4.6. In most cases the thickness was about 1 m. Departures from this value were rare. It was more common for the boundary layer to disappear altogether.

Obvious cases of katabatic winds ($u_*'/k < 0$) were also rare. The height decrease of u_*'/k from the maximum value near 1 m was usually small, which may indicate that the wind gradient reversal occurs above 6 m. However, it is also possible that the geostrophic wind exerts substantial control over the surface flow, and that the katabatic force is not sufficiently strong in such cases to obliterate it.

The disappearance of the boundary layer was investigated further to see if it would seriously influence the use of turbulent transfer relationships. Fig. 4.7 shows that the boundary layer was observed relatively frequently. Hence the turbulent transfer approach is justified for most flow conditions. Since the katabatic layer thickens downglacier (Hölmgren, 1971), the boundary layer in the upper basin of the glacier may be even thinner than that observed on the tongue. This hypothesis is supported by wind profiles measured in the upper basin of the Vallée Blanche, French Alps, by de La Casinière (1974), where the wind speed gradient vanishes within 1 m of the surface. In this study it disappeared at about 3 m, or not at all.

In conclusion, turbulent transfer theory may be used over melting ice if the thickness of the boundary layer is determined, and measurements are made within it. Assuming that the lower portions of
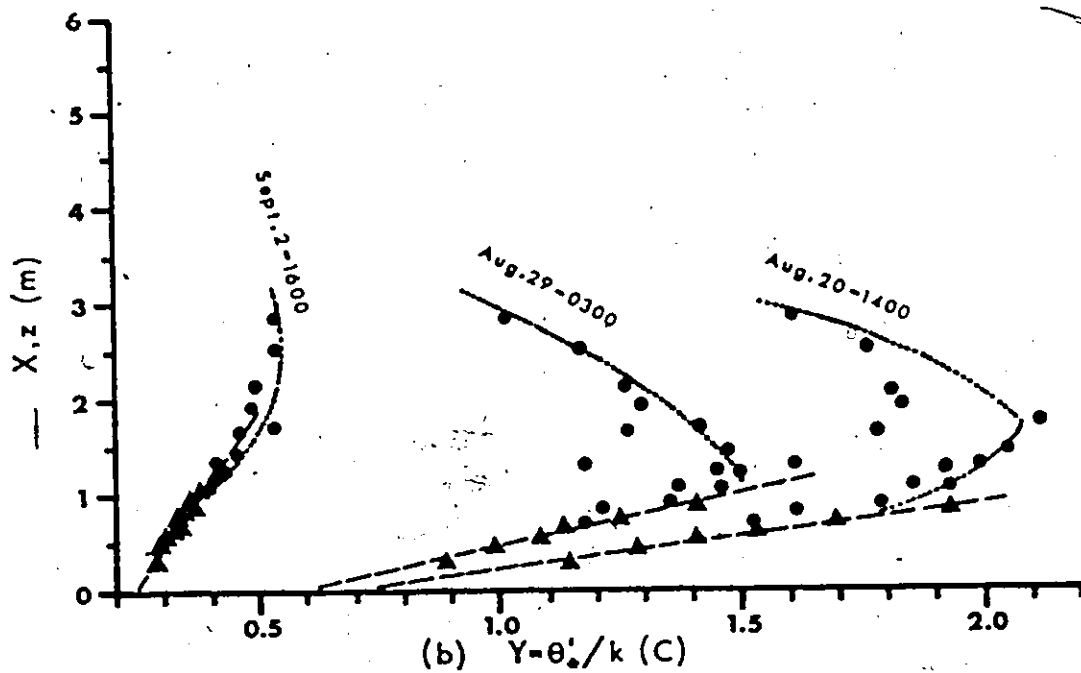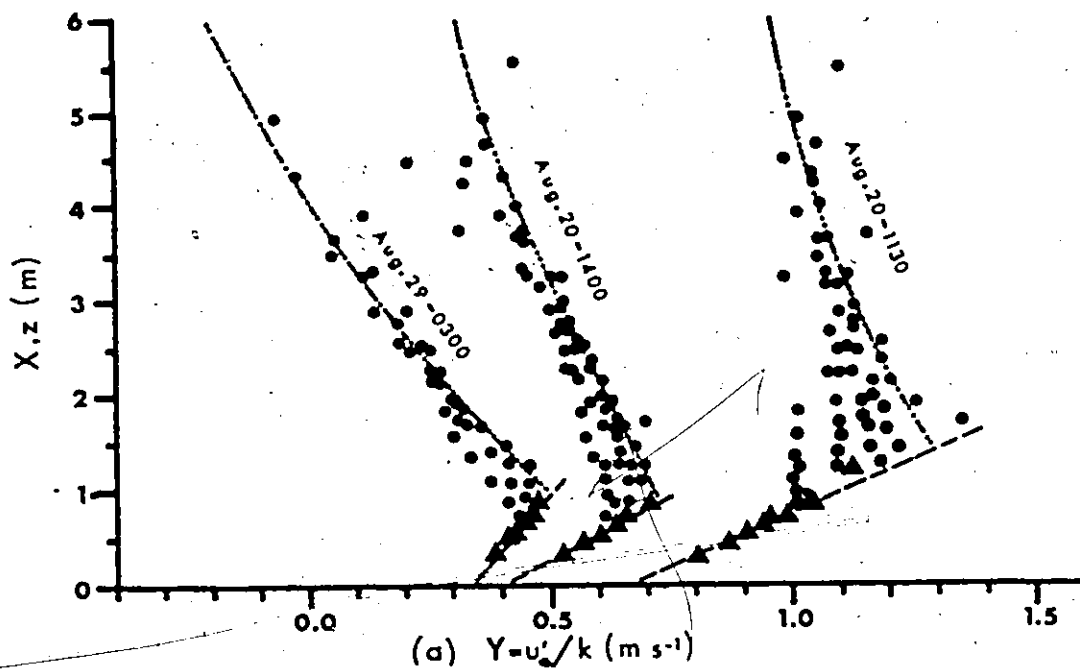
Figure 4.6. Selected friction parameter profiles, (a) from wind profile data, and (b) from temperature profile data. Profile form within the boundary layer (dashed line and triangles) and above (dotted line and circles) is shown.
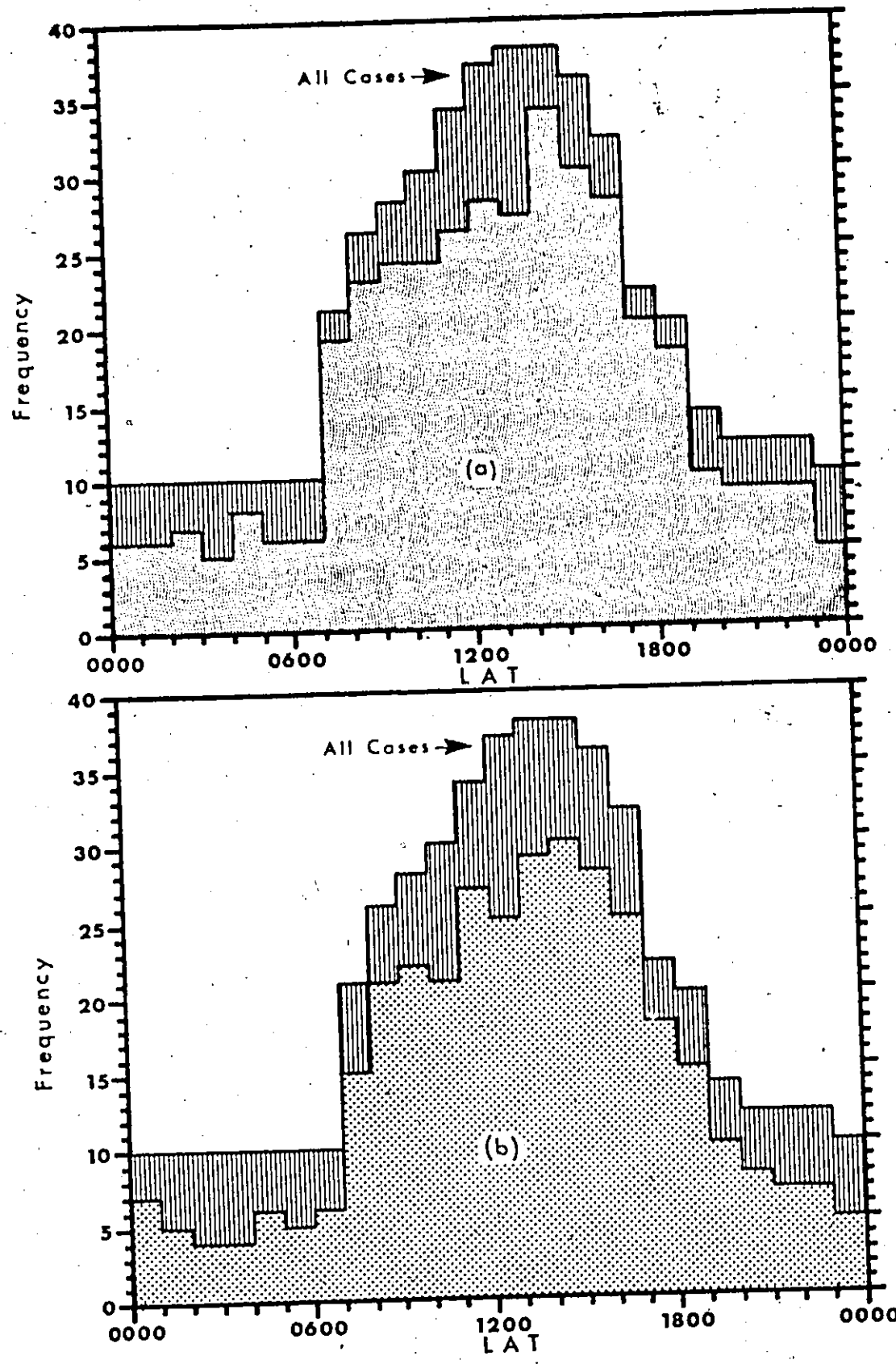
Figure 4.7. Frequency of observed boundary layer cases, (a) from wind profiles, and (b) from temperature profiles. Vertical hatching shows the difference between all cases observed and boundary layer cases.

the profiles in Fig. 4.6 represent the boundary layer, stability corrections for them can be established.

C. Stability Analysis of the Boundary Layer

1. Selection of Boundary Layer Cases

Only measurements within the first meter of the surface were used for the stability analysis. These yielded six sets of Y and X values for each profile. Examples (Fig. 4.8a, b) show the expected linear relationship.

Fluxes can be obtained from these distributions by fitting regression lines, with Y dependent on X. From Eq. (4.2), $\phi = 0$ at X = 0 (i.e., $z = z_0$), and the intercept value is equal to y_*/k (u_*/k or θ_*/k). τ and Q_H are then obtained from Eqs. (2.5a) and (2.5b), while L is evaluated from Eq. (2.16).

The use of only six points meant that only the best data could be used. Substantial error at any one point would influence the regression. The only observations considered here were those in which an aerodynamic, and a thermal boundary layer were observed together. Moreover, a complete data set was required. This eliminated data for the first three days of August, since the anemometer at 0.75 m did not function. The standard error of the intercept was used to assess the data quality. Cases where the standard error of either u_*/k or θ_*/k exceeded 20% were eliminated, since these were associated with an unacceptably wide scatter of points about the regression line.

This is effectively a two-stage selection procedure.
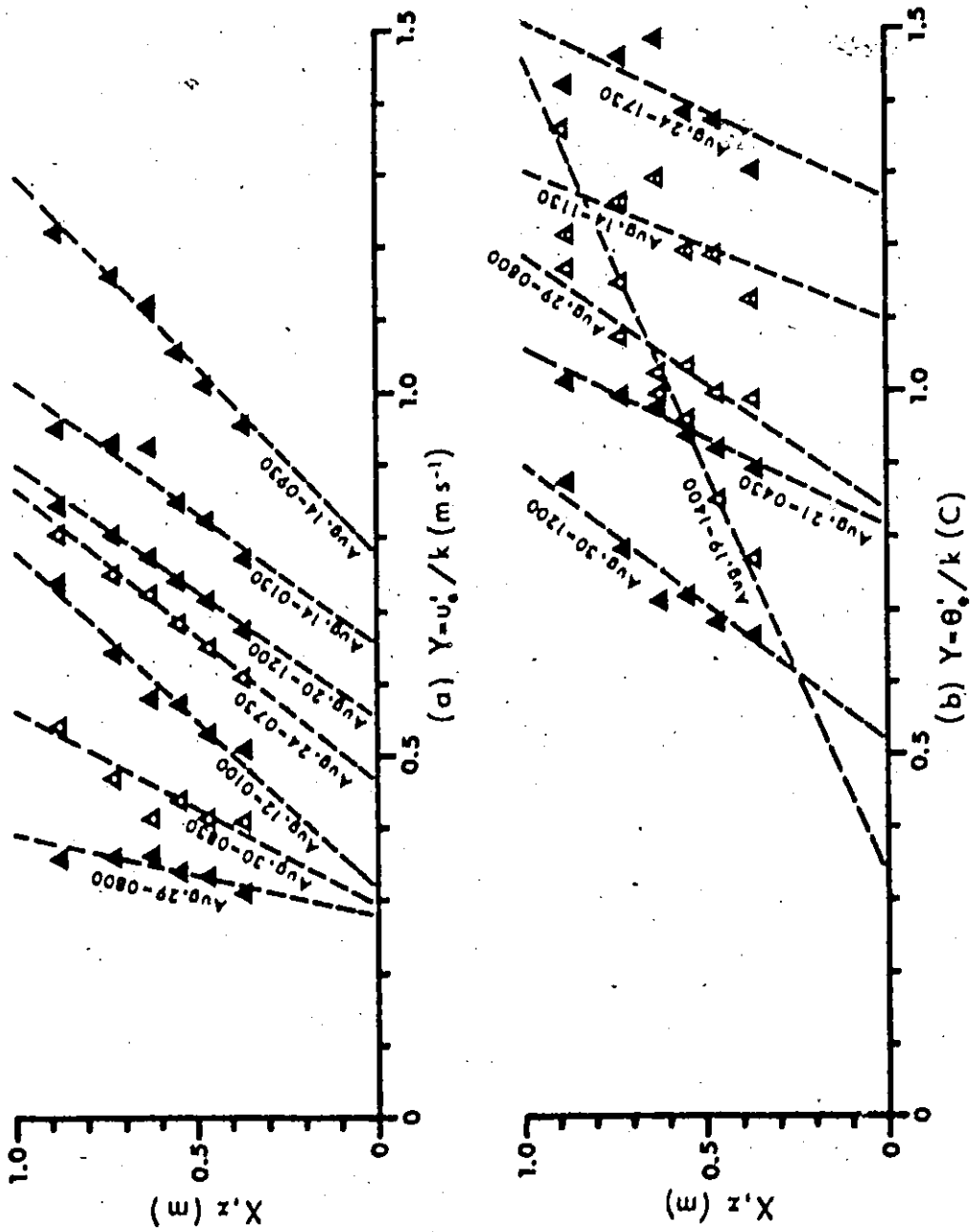
Figure 4.8. Selected boundary layer profiles, not corrected for stability, (a) friction velocity, and (b) friction temperature.

Firstly, it requires that boundary layer conditions prevail for both profiles, and secondly, it demands the best data. A total of 124 cases were selected (Appendix Four).

2. Similarity Analysis

The shape function method of Swinbank and Dyer (1967) was used to test for similarity between wind speed and temperature profiles. It is derived from the finite difference form of Eq. (2.1) for any flux Q_x. Assuming a constant flux layer, and evaluating Q_x from two different pairs of measurements,

$$S_x = \frac{\Delta y}{(\Delta y)_o} \tag{4.4}$$

where S_x is the shape function. The null subscript designates a reference difference, which is measured here between 0.25 and 0.5 m. The other difference is calculated from any possible height pair for $z \leq 1$ m, while an adjacent height pair is specified for $z > 1$ m.

The shape function responds to stability variations, and change of position in the flow field. If wind speed and temperature profiles have similar responses, their shape functions will be identical. Thus equality of transfer coefficients can be accepted, if the neutral values are equal.

Shape functions for wind speed, S_M, and temperature, S_H, were calculated for each data set, and meaned over 124 runs. These

are plotted against the mean Richardson number in Fig. 4.9. Since the Ri values are taken at different heights above the ground, the analysis illustrates shape function variation with height as well as stability.

A small systematic difference between S_M and S_H is indicated for $z \leq 1$ m. Large standard deviations are associated with each point, and it is not clear if the difference is significant. The comparison was clarified by counting the number of data sets (S_M and S_H) below 1 m which indicated $S_H < S_M$. These amounted to 72% of the total. According to a standard test of proportions (Appendix 3.A) this differs significantly from 50%, the value which would be expected if the shape functions were similar. Hence, it is likely that temperature and wind profile responses to stability are different. This implies that $K_H > K_M$ in stable conditions, a conclusion which is at variance with most previous work. A few investigative results agree with the Peyto finding (Businger et al., 1971; Carl, Tarbell and Panofsky, 1973), but this other work also finds $K_H > K_M$ in neutral stability. Here, however, the equality of transfer coefficients in neutral conditions is assumed.

The analysis above 1 m parallels McVehil's (1964) findings for South Pole wind and temperature distributions, where an apparent decrease of K_H/K_M (increase of S_H/S_M) with height was found, for Ri > 0.08. He associated this with a decay of turbulent flow at some height above the surface. In his study the decay occurred near 4 m, while the log-linear model described the flow between 0 and 4 m. The analysis for Peyto indicates decay near 1 m, and log-linear profiles between 0 and 1 m.
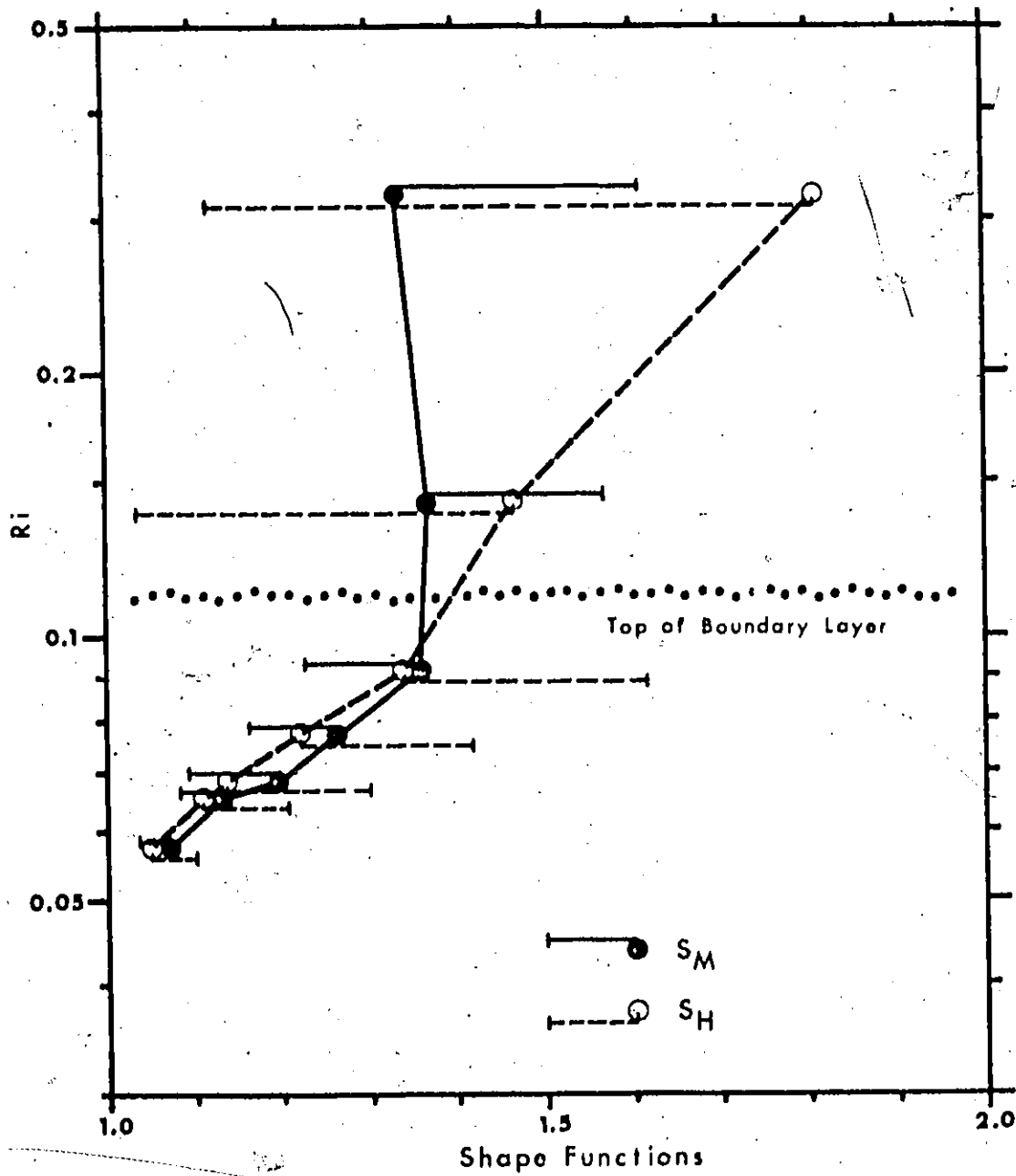
Figure 4.9. Results of shape function analysis. Bars denote standard deviation about the mean.

The analysis contains an apparent inconsistency in that $S_H >$ S_M above 1 m, but the inequality is reversed below 1 m. If the decay of turbulent flow due to increasing stability alone accounted for the changes in shape functions, the inequality should be the same at all levels. However the air above 1 m lies outside the boundary layer, in a zone where the effects of vertical flux divergence are also important. Here the tendency toward thermocline formation results in large S_H values, since temperature gradients are large, while the weakening of wind speed gradients in katabatic flow causes S_M to be small.

3. Investigation of Monin-Obukhov Constants

A computerized version of the procedure used by Webb (1970) for estimating α was developed. The linear regressions of Fig. 4.8 were extended to intercept the X axis at $Y = 0$ (Fig. 4.10).

Let the value of X at $Y = 0$ be ς. Substituting into Eq. (4,2)

$$\alpha = - \frac{L}{\varsigma} \tag{4.5}$$

Individual α values can be evaluated from Eq. (4.5) for each profile, using the appropriate value of ς. This differs from Webb's procedure in that his α values were derived by using Ri instead of L. Assuming similarity between transfer coefficients, he obtained

$$L = \frac{z}{Ri} \left[1 + \alpha \frac{z}{L} \right]^{-1} \tag{4.6}$$
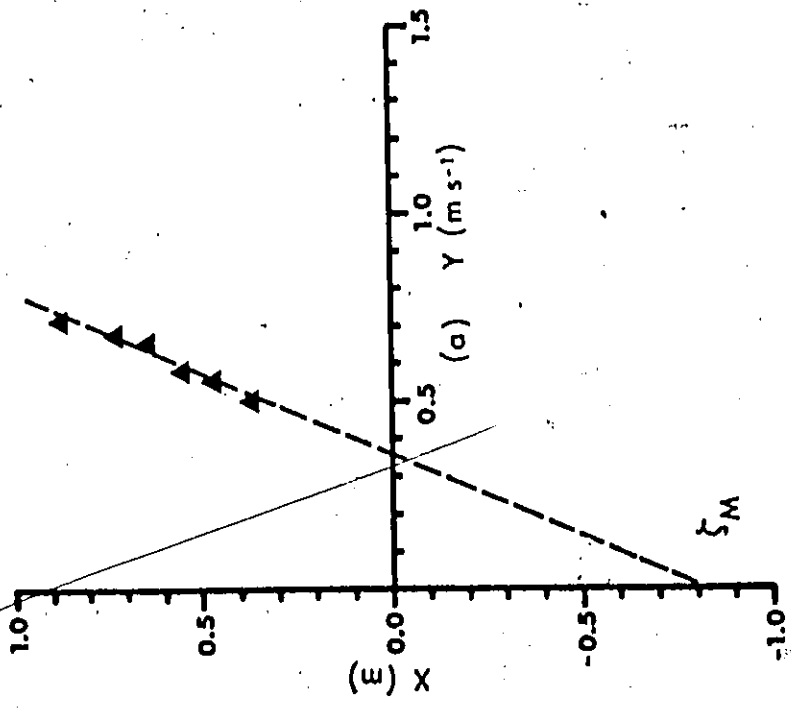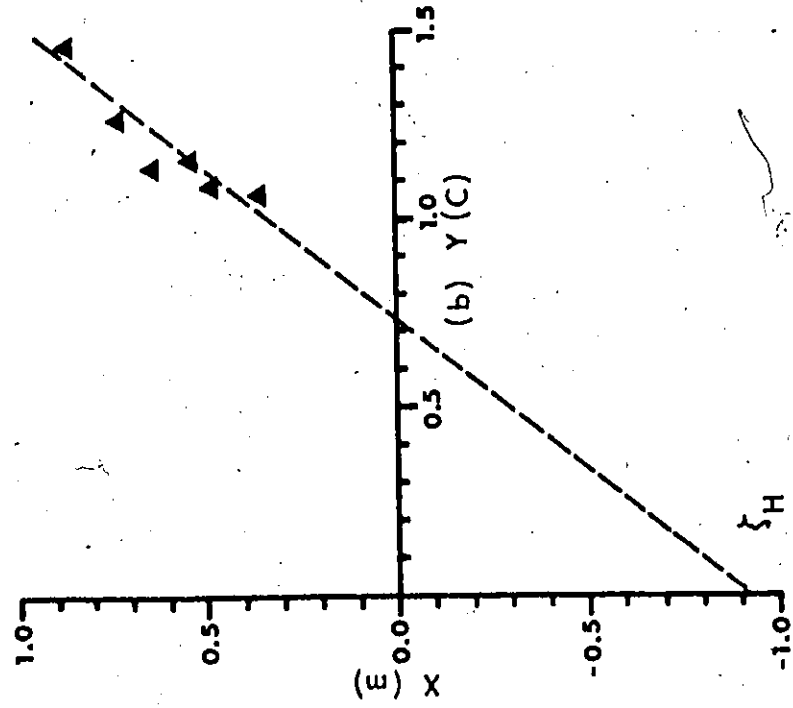
Figure 4.10. Example of ζ value computations, August 25 - 1300, (a) friction velocity case, and (b) friction temperature case.

Then, using Eq. (4.5),

$$\alpha = \frac{z}{Ri_z (z - \zeta)} \tag{4.7}$$

where z refers to the geometric mean of the two measurement levels used in determining Ri.

The use of Ri is advantageous in that it is evaluated directly from Δu and $\Delta \theta$ data. On the other hand L must be evaluated from Eq. (2.16), which uses estimates of u_*/k and θ_*/k. These are the intercept values (at $z = 0$) in the regression analysis of u_*'/k and θ_*'/k (Fig. 4.8). They are very sensitive to measurement error, since only six points are used in fitting each line, and consequently a low resolution in determining L can be expected. This was shown by performing the analysis with both types of stability parameter. The α determinations from Eq. (4.7) showed a smaller range than those from Eq. (4.5). However the use of Ri requires that $K_H = K_M$ in stable conditions. The shape function analysis suggests that this requirement can not be met. Hence the results from Eq. (4.5) are used (Appendix Four).

A value of α was computed for each wind speed and temperature profile, and two values, respectively α_M and α_H, were obtained from individual runs. Most of the values computed from the temperature profile were smaller than those from the wind profile. Also the range of α_H was greater than that of α_M, and included a few extremely large values. The reason for these relatively large values can be seen in

the plot of data for August 19 - 1400 in Fig. 4.8b, where θ_*/k increases rapidly with height. An anomalously low value for ζ, and a correspondingly high estimate for α_H result. In the wind profile analysis slopes showed less variation and fewer extreme values.

Smaller α values were obtained from the temperature profile than from the wind profile in 60% of the samples. This proportion was found to be statistically significant (Appendix 3.A). It suggests that $\phi_H < \phi_M$, and that $K_H > K_M$ in stable conditions. This agrees with the results from the shape function analysis.

Individual α values were meaned to arrive at the Monin-Obukhov constant for each profile (Table 4.2a). Arithmetic means yield 7.14 for the wind profile, and 34.09 for the temperature profile. Geometric means, which are preferred by some authors (Crawford, 1965; Webb, 1970), give values of 5.41 for wind, and 3.58 for temperature. These discrepancies might reflect non-normality in the data distributions. Therefore they were tested for skewness (Appendix 3.B). Arithmetically distributed data were found to be positively skewed, while geometrically distributed data were normal. The skewness of the arithmetically distributed data is attributed to overestimates of α which result from unusually large L calculations. It is possible that the anomalous L values reflect imprecise data. Consequently new means were obtained for α_M and α_H from a subset of the data, which contained all cases wherein the standard errors of u_*/k and θ_*/k did not exceed 10% (Table 4.2b). The results are essentially the same as those of the full sample, except that the standard errors of the Monin-Obukhov constants are

TABLE 4.2

Determinations of Monin-Obukhov Constants

(a) Mean of 124 values (standard error of friction parameters $\leq$ 20%).

	α_M	α_H
Arithmetic mean	7.14	34.09
Geometric mean	5.41	3.58
Standard error of geometric mean	3.9%	12.8%

(b) Mean of 73 values (standard error of friction parameters $\leq$ 10%).

	α_M	α_H
Arithmetic mean	6.79	24.47
Geometric mean	5.44	2.64
Standard error of geometric mean	4.6%	21.2%

larger. Hence the geometric means of the full sample, $\alpha_M = 5.4$ and $\alpha_H = 3.6$, are accepted. The former is close to the experimental results of other investigators (Webb, 1970; Sheppard, Tribble and Garratt, 1972; Dyer, 1974).

The smaller constant for temperature does not agree with the conclusions of others, which support a single value of the Monin-Obukhov constant for all profiles. An explanation for the Peyto result is offered here in the form of a tentative hypothesis. Rewriting Eq. (2.1a, b) to include the effect of molecular transfer,

$$\tau = \rho (K_M + \nu) \frac{\partial u}{\partial z} \tag{4.8a}$$

$$\text{and } Q_H = \rho c_p (K_H + \nu_H) \frac{\partial \theta}{\partial z} \tag{4.8b}$$

in which ν is the kinematic viscosity, and ν_H the thermal diffusivity. In fully turbulent flow, the molecular transfer coefficients can be safely ignored since they are negligible by comparison with their eddy counterparts. However they may be important in strongly stable conditions, where the decay of turbulent flow is well advanced. From Eq. (4.8)

$$\frac{\partial u}{\partial z} = \frac{\tau}{\rho (K_M + \nu)} \tag{4.9a}$$

$$\text{and } \frac{\partial \theta}{\partial z} = \frac{Q_H}{\rho c_p (K_H + \nu_H)} \tag{4.9b}$$

Hence, gradients (or finite difference approximations) are governed by the combined mechanisms of eddy and molecular transport. As K_M and K_H approach 0, the denominator of Eq. (4.9) approaches the value of the molecular coefficient. At Peyto the convergence occurs within a few metres of the surface, since Ri increases rapidly with height. As $\nu_H > \nu$, the relative change in $\partial u/\partial z$ with increasing stability is eventually greater than that for $\partial\theta/\partial z$. This results in a greater change of u'_*/k with height than is the case for θ'_*/k. Thus $\alpha_M > \alpha_H$ since a greater change with height also implies a greater change with stability.

It follows that any form of analysis which employs profiles to examine the stable case must be influenced by molecular transfer. Therefore the ratio of the two ϕ functions reflects the ratio of the combined eddy and molecular transfer coefficients for heat and momentum. Thus Eq. (2.21) is written

$$\frac{K_H + \nu_H}{K_M + \nu} = \frac{\phi_M}{\phi_H} \qquad (4.10)$$

As z/L becomes very large the eddy transfer coefficients should approach negligible values, and $\phi_M/\phi_H \simeq \nu_H/\nu$. The functions, ϕ_M and ϕ_H, were evaluated from Eq. (2.18b) for different stabilities by using α_M and α_H, respectively, in place of α (Table 4.3). The limiting value of ϕ_M/ϕ_H, as turbulence ceases, is approximately 1.5. This is close to the ratio of $\nu_H/\nu = 1.43$ (at 10 C).

Since the ratio of the Monin-Obukhov constants is determined by the molecular transfer coefficients in this case, α_E can be evaluated from

TABLE 4.3

Evaluation of ϕ Functions at Different Stabilities

z/L	ϕ_M	ϕ_H	ϕ_E	ϕ_M/ϕ_H	Ri
0	1	1	1	1	0
0.01	1.05	1.04	1.04	1.02	0.009
0.02	1.11	1.07	1.07	1.04	0.017
0.05	1.27	1.18	1.17	1.08	0.037
0.1	1.54	1.36	1.34	1.13	0.057
0.2	2.08	1.72	1.68	1.21	0.08
0.5	3.7	2.8	2.7	1.32	0.102
1	6.4	4.6	4.4	1.39	0.112
10	55	37	35	1.49	0.122
100	540	360	340	1.5	0.123

$$\alpha_E = \frac{\nu}{\nu_E} \alpha_M \tag{4.11}$$

in which ν_E is the diffusion coefficient of water vapour. Using standard values of the molecular coefficients at 10 C (List, 1966), $\alpha_E = 3.4$. Applying appropriate Monin-Obukhov constants to Eq. (2.18b),

$$\phi_M = (1 + 5.4 \, z/L) \tag{4.12a}$$

$$\phi_H = (1 + 3.6 \, z/L) \tag{4.12b}$$

$$\text{and} \quad \phi_E = (1 + 3.4 \, z/L) \tag{4.12c}$$

The difference between ϕ_H and ϕ_E is not crucial in flux determinations, since it is small for $z/L < 1$ (Table 4.3).

Stability parameters can be related using Eqs. (4.12a, b) and (2.23):

$$Ri = \frac{(1 + 3.6 \, z/L)}{(1 + 5.4 \, z/L)^2} (z/L) \tag{4.13}$$

Values of Ri in Table 4.3 were computed from this relationship. The function was plotted along with experimentally determined Ri and z/L values at $z = 0.5$ m (Fig. 4.11). In the case of the Richardson number, 0.5 m refers to the geometric mean of the two measurement levels used (0.25 and 1 m). Individual L values (Appendix Four) were used to
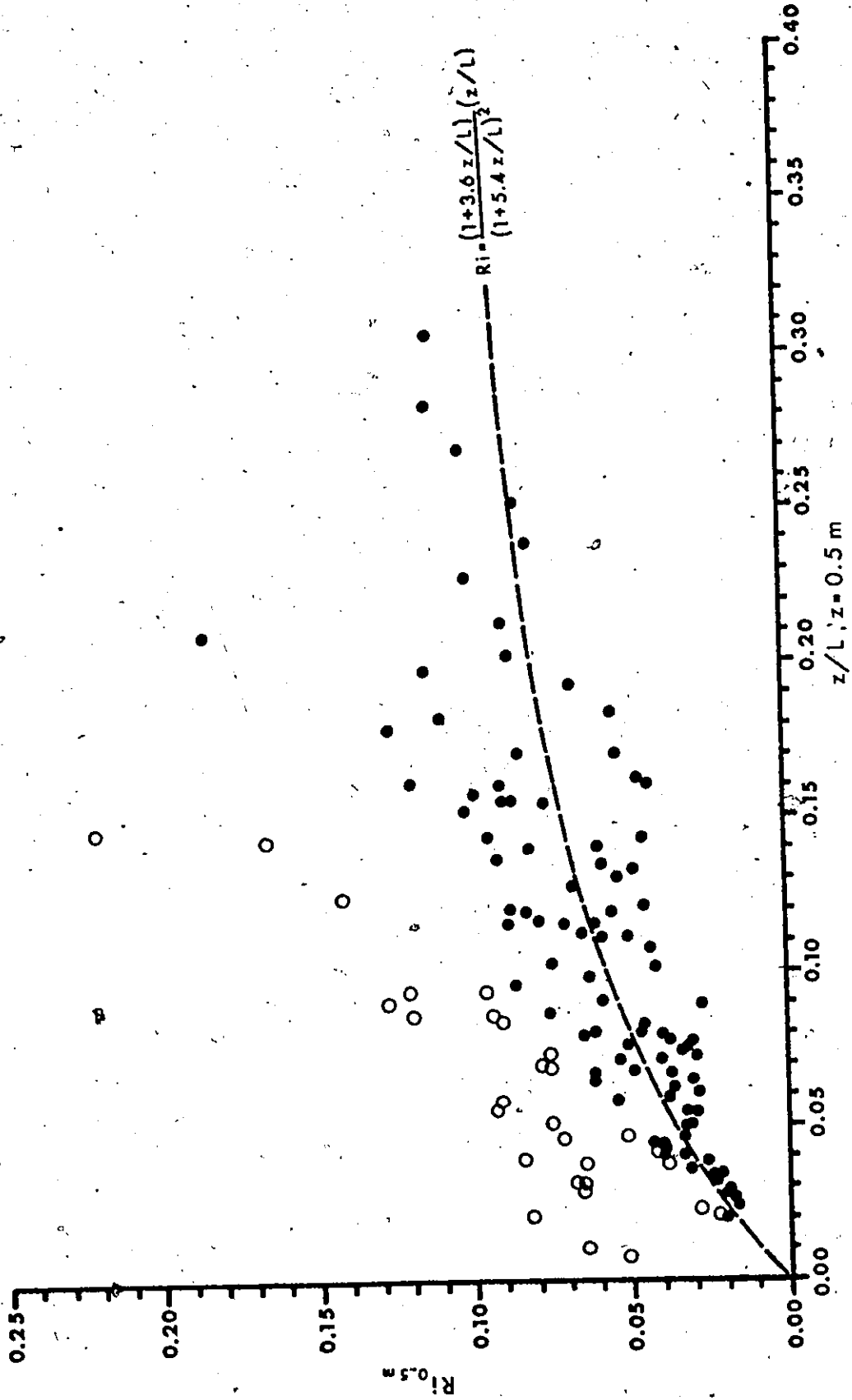
Figure 4.11. Relationship between Ri and z/L. Closed symbols: z/L > Ri; open symbols: z/L < Ri.

obtain z/L. Eq. (4.13) provides a description of the observations in cases where z/L > Ri. Data points for z/L < Ri are affected by the unusually large θ_*'/k increases with height noted earlier. The limiting value of Ri, as z/L becomes indefinitely large, is close to 0.125 (Table 4.3). This can be taken as a critical value at which turbulent decay is complete. A value of $Ri_c = 0.125$ lies within the range of values (0.1 - 0.2) defined by most other work.

D. Surface Roughness Parameters

1. Estimation Procedure

Usually z_0 is obtained from wind profiles in neutral stability. In such conditions a plot of u vs ln z is linear, and ln z_0 is obtained by extrapolation to u = 0. In the absence of neutral conditions at Peyto, a different method for estimating z_0 in stable conditions had to be devised. The method, which involves two steps, is based on the knowledge that the stability correction function is linear in the stable case (Fig. 4.12). Firstly, apparent ln z_0 values are obtained from each possible pair of wind speed measurements by joining the points with a straight line, and extending the line to intercept the ln z axis at u = 0 (Fig. 4.12a). These are denoted by $(ln z_0')_i$ for the ith measurement pair, and the prime indicates that it is influenced by stability. Then

$$\frac{(\Delta u)_i}{(\Delta \ln z)_i} = \frac{u_z}{\ln z - (\ln z_0')_i} \qquad (4.14a)$$
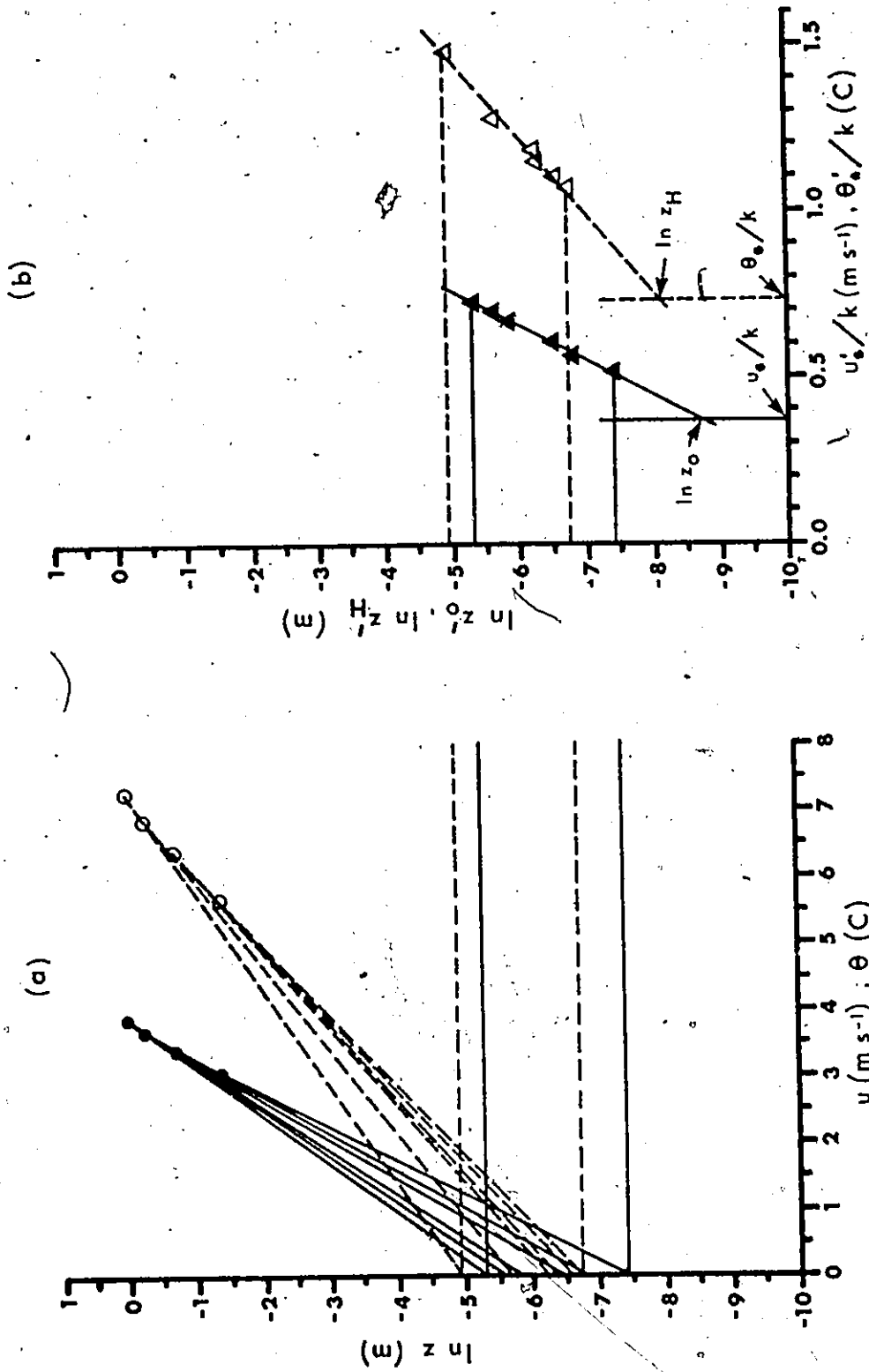
Figure 4.12. Example of z_0 and z_H evaluation, August 25 - 1300, (a) determination of ln z_0 and ln z_H values, and (b) determination of ln z_0 and ln z_H. Closed symbols: wind profile data; open symbols: temperature profile data.

$$\text{and} \quad (\ln z_0')_i \approx \ln z - \frac{u_z (\Delta \ln z)_i}{(\Delta u)_i} \qquad\qquad (4.14b)$$

in which z refers to the higher level of the measurement pair. Secondly, the influence of stability was removed by regressing $\ln z_0'$ against u_*^1/k (Fig. 4.12b). The value of $\ln z_0$ is defined at u_*/k, which represents neutral conditions. Since the surface temperature is known, the same procedure may be applied to the temperature profile (Fig. 4.12).

2. Estimates of Roughness Parameters

Mean z_0 and z_H values were calculated. Langleben (1972) obtained different values, depending upon whether individual z_0 or $\ln z_0$ were meaned. He chose the mean of $\ln z_0$ on the grounds that the logarithmic value is used in the neutral wind profile. A skewness test (Appendix 3.B) was applied to the distributions of $\ln z_0$ and $\ln z_H$, and they were found to be normal. Consequently means of $\ln z_0$ and $\ln z_H$ are used here.

The geometric mean value of z_0 is 0.073 mm (standard error 4.1%) which agrees well with 0.07 mm, obtained over snow covered lake ice by Hicks and Martin (1972). It is slightly smaller than most other determinations. Hölmgren (1971) lists values ranging from 0.1 mm to 1.3 mm, depending on surface conditions, while Langleben (1972) reports 0.5 - 3 mm over sea ice. Liljequist (1955) obtained a value of 0.12 mm over snow in Anarctica. Relatively large values would result if a neutral wind profile was assumed in stable conditions.

The geometric mean z_H value is 0.156 mm (standard error 9.3%), about twice that for z_0. The relative magnitudes of z_0 and z_H contradict previous glaciological opinion, which suggests that z_H is several orders of magnitude smaller than z_0 (Sverdrup, 1936; Hölmgren, 1971). This seemingly contradictory finding is examined against results from measurements made over other surfaces, which suggest that $\ln(z_0/z_H)$ depends upon the degree of turbulence in the flow (Owen and Thompson, 1963; Chamberlain, 1968; Thom, 1972; Garratt and Hicks, 1973). It is indicated by the roughness Reynolds number, $Re_\star$, (Sutton, 1953):

$$Re_\star = \frac{u_\star z_0}{\nu} \qquad (4.15)$$

Calculated values of $Re_\star$ were meaned geometrically and plotted against the mean of $\ln (z_0/\bar{z}_H)$, together with data compiled by Garratt and Hicks (1973). The sample point for Peyto lies among their values (Fig. 4.13), indicating that $z_H > z_0$ for small $Re_\star$ values. It is also close to the result obtained by Hicks and Martin (1972) over lake ice.

The agreement shown in Fig. 4.13 probably does not form the basis of a predictive relationship for $\ln (z_0/z_H)$. As Thom (1972) has pointed out, such an approach is weakened by the appearance of z_0 in both axes of Fig. 4.13. Characteristically, experimentally derived z_0 values vary through several orders of magnitude (Untersteiner and Badgely, 1965; Hicks and Martin, 1972), due to measurement and sampling errors. In addition, the range of $u_\star$ is relatively small. Therefore it is possible that the mean of $\ln (z_0/z_H)$ would be suitable over the range of conditions
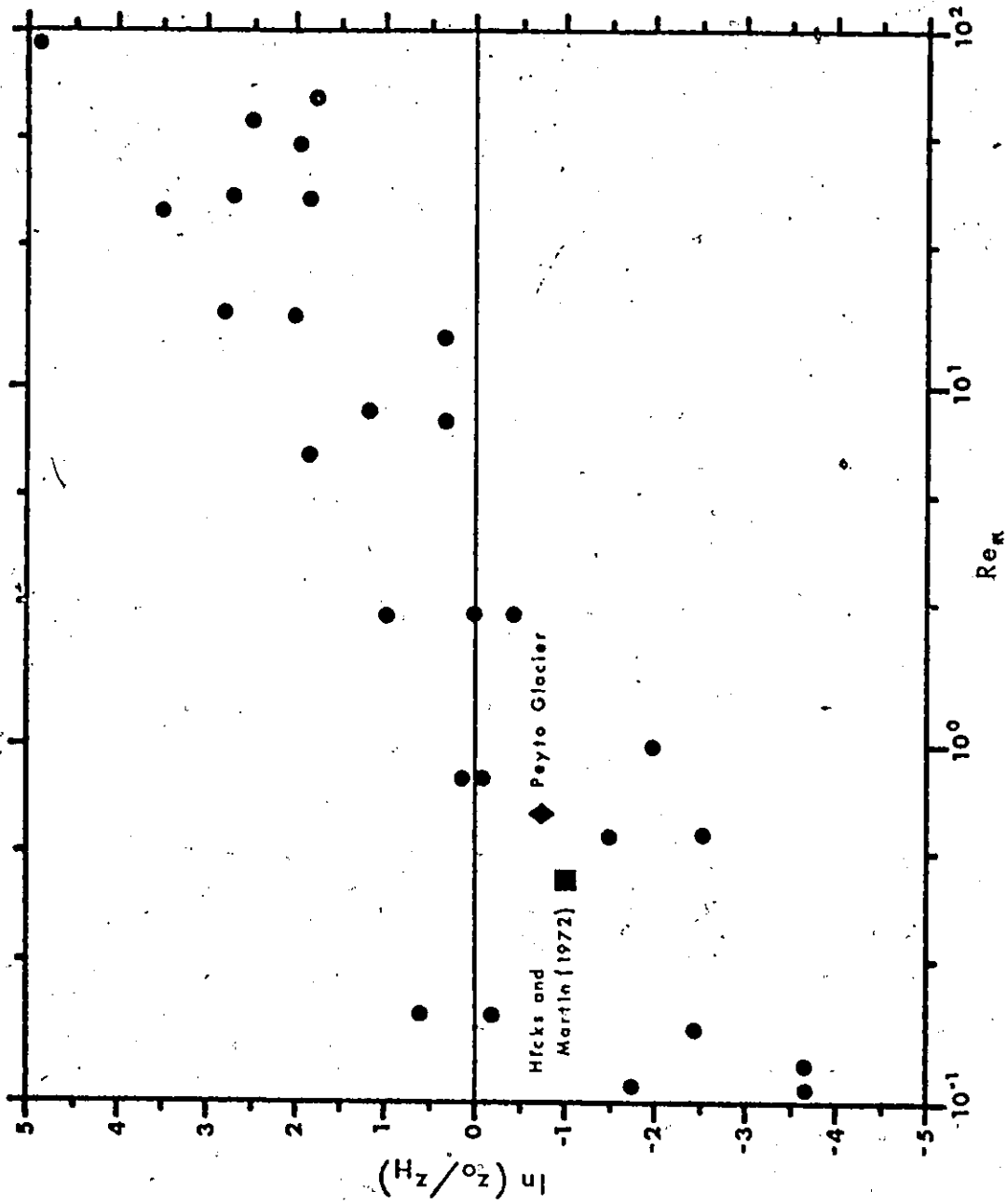
Figure 4.13. Relationship between ln (z_0/z_H) and Re_* as shown by Garratt and Hicks (1973).

experienced on the glacier. It also seems appropriate to use z_H for the vapour pressure profile, since existing experimental evidence does not indicate that a different value should be used (Monteith, 1973).

The finding that $z_H > z_0$ has important implications for glacier energy exchange studies, since it contradicts a long-standing belief. The importance of this is seen in Föhn's (1973) study on Peyto. He initially computed Q_H with $z_0 \gg z_H$, and obtained poor results. Better results were obtained by assuming $z_0 = z_H$, which is close to the result in this study.

3. Investigation of Roughness Parameter Variations

Fig. 4.13 suggests that z_0 and z_H vary with the degree of turbulence. Previously, roughness length changes over water have been related to u_* (Sverdrup, 1951; Sheppard, Tribble and Garratt, 1972). However, the computation of u_* requires detailed profile measurements, or an a priori knowledge of z_0. Therefore it is more common to look for a possible relationship with the wind speed at some reference level.

A tendency for z_0 to decrease with increasing wind speed over frozen surfaces has been suggested by Liljequist (1955), Unter-steiner and Badgely (1965), and Hölmgren (1971). However, in this study z_0 and z_H were plotted against wind speed at 1 m, and a relationship was not indicated. The possibility of time-variant roughness lengths was suggested by the observation that the ice surface was rough and easy to walk over by day, but slippery at night. This is due to differential ablation, resulting from the penetration of shortwave radiation into

the ice. The roughness parameters were plotted against time of day, and no detectable temporal change was found in either. Hence, mean values were used in the computation of drag coefficients.

4. Drag Coefficients

Given fixed roughness length values, the computation of drag coefficients from Eq. (2.10) is straightforward. The use of z_0 gives r_0 for the wind speed. r_H is calculated from z_H for temperature and vapour pressure. The drag coefficient, $C_D = r_0{}^2$, is retained in Eq. (2.11a), but is replaced by $C_H = r_0 r_H$ in Eq. (2.11b, c). These are shown in Table 4.4 for $z = 1$ m and $z = 10$ m. The values at 10 m were computed for comparison with those of Hicks and Martin (1972), which were obtained using eddy correlation measurements of τ, Q_H and Q_E. Excellent agreement is obtained for C_D, but C_H is smaller. It is not clear whether the difference relates to measurement error or other causes. Comparisons with other studies of this type are needed.

E. Flux Computations

1. Estimation Procedure

The foregoing results may be used in estimating τ, Q_H and Q_E. Two procedures for doing this from the available data are possible, each yielding the same answers. One is to compute the fluxes from Eq. (2.22), using the appropriate stability correction. The 0.25 and 1 m measurement levels would be used to obtain the largest possible gradients of u, θ and e within the boundary layer. A second approach is to use the bulk transfer coefficients for 1 m from Table 4.4, and measurements of u, θ

TABLE 4.4

Bulk Transfer Coefficients

	Momentum	Heat and Water Vapour
z_0, z_H (m)	0.73×10^{-4}	1.56×10^{-4}
r_0, r_H at 1 m	4.36×10^{-2}	4.74×10^{-2}
r_0, r_H at 10 m	3.51×10^{-2}	3.75×10^{-2}
C_D, C_H at 1 m	1.90×10^{-3}	2.25×10^{-3}
C_D, C_H at 10 m	1.23×10^{-3}	1.32×10^{-3}
C_D, C_H at 10 m (Hicks and Martin, 1972)	1.20×10^{-3}	$*1.72 \times 10^{-3}$

* mean of separate determinations by Hicks and Martin for heat and water vapour.

and e at z = 1 m in Eq. (2.11). However, a modification for stability is required. The latter is the more precise of the two, since the errors in gradients have been shown to be relatively larger than those for single measurements in Chapter Three.

The modification of the bulk transfer procedure involves a stability correction in Eq. (2.10). Rearranging Eq. (2.20):

$$\frac{y_*}{y_z - y_0} = \frac{k}{\ln{(z/z_0)} + \alpha(z - z_0)/L} \qquad (4.17)$$

Since roughness lengths are negligible compared to z,

$$\Gamma_0 = \frac{k}{\ln{(z/z_0)} + \alpha_M z/L} \qquad (4.18a)$$

$$\Gamma_H = \frac{k}{\ln{(z/z_H)} + \alpha_H z/L} \qquad (4.18b)$$

$$\text{and} \quad \Gamma_E = \frac{k}{\ln{(z/z_H)} + \alpha_E z/L} \qquad (4.18c)$$

where z = 1 m (i.e. $(z - z_0)$ and $(z - z_H) = 1$ m). In addition, the stability correction for Eq. (2.22) is obtained from Eq. (2.19), evaluating ϕ at 0.25 and 1 m. Hence, stability corrections for both the bulk and gradient approaches are easily obtained within the framework of the Monin-Obukhov scaling length.

z/L can not be obtained directly from gradient measurements. The Richardson number is easily computed from gradients, but it is not

readily incorporated into Eq. (4.12). Moreover, stability correction functions which are based upon Ri must be integrated numerically over the height difference between the measurement levels (Lettau, 1962). A method whereby z/L is computed from Ri, and subsequently used in Eq. (4.12) is required. Eq. (4.13) is unsuitable for this purpose since it can not be rearranged to express z/L in terms of Ri.

Approximate z/L estimates were obtained from Ri, at z = 0.5 m, by rearranging Eq. (4.6):

$$z/L = \frac{Ri}{(1 - \alpha' Ri)} \tag{4.19}$$

The value of α' was chosen so that it minimized the error in ϕ over the range of most frequently encountered Ri values (0 < Ri < 0.09; Fig. 4.11). A similar procedure has been applied to the results of Businger et al. (1971) by Binkowski (1975).

The error was examined in relation to the stability correction for momentum because, having the largest α, it was the most sensitive to error. The relative error in ϕ_M was assessed by comparing the true ϕ_M correction with its approximate value. The true ϕ_M correction was obtained from Eq. (4.12a), with an assumed z/L. The corresponding value of Ri was computed from Eq. (4.13), and inserted into Eq. (4.19) to calculate an approximate z/L value. Eq. (4.12a) was subsequently re-evaluated, using the new z/L, to obtain an approximate ϕ_M correction. This was done for various α' values (Fig. 4.14). Relative errors in ϕ_M showed little sensitivity to α' for small Ri, but the sensitivity increased as Ri
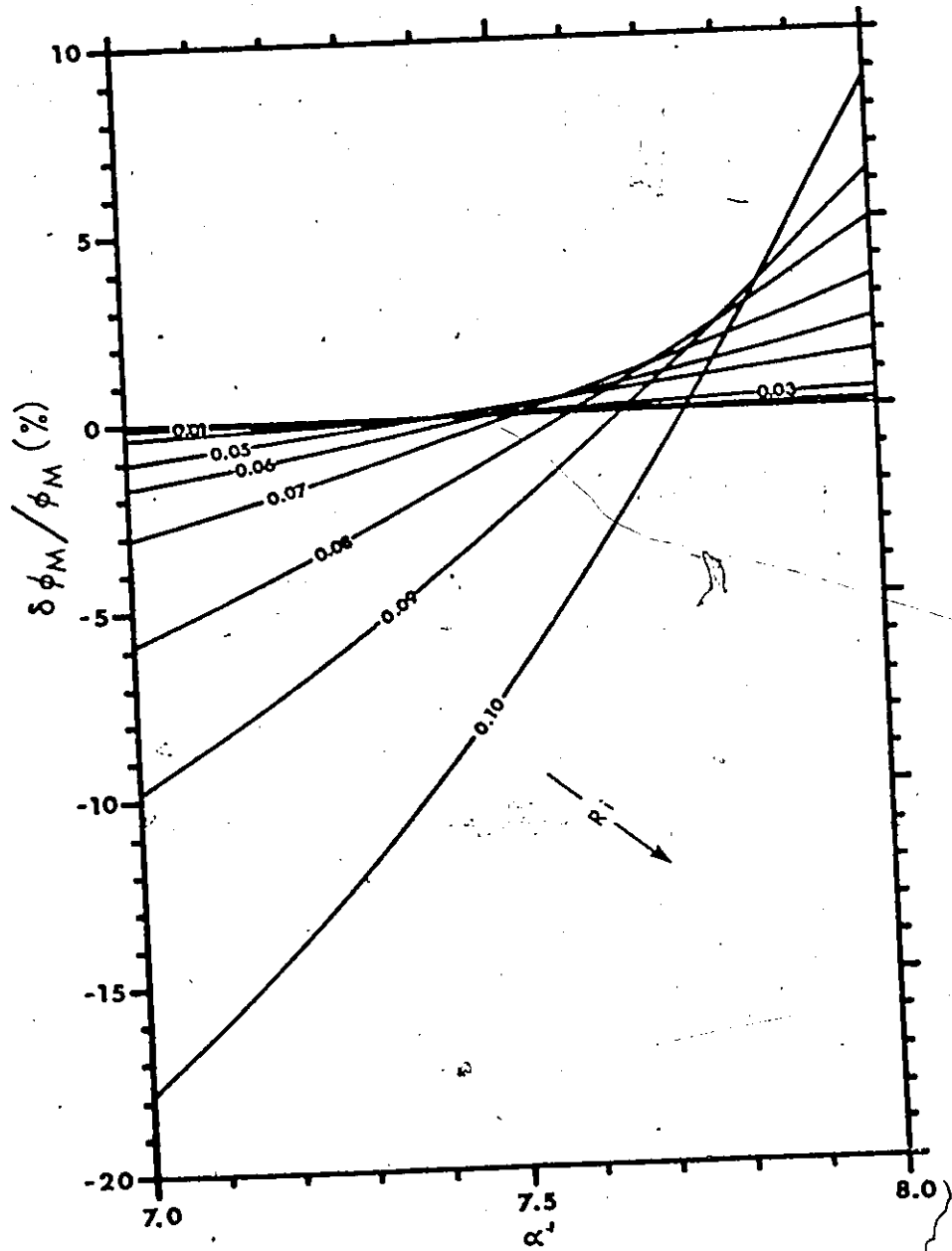
Figure 4.14. Relative error in ϕ_M as a function of α' and Ri.

increased. The value, $\alpha' = 7.5$, was adopted for use in flux calculations, since $\delta\phi_M/\phi_M$ was within 5% for Ri < 0.9, and negligible for Ri < 0.7.

The bulk transfer approach demands less instrumental precision, and lends itself to simpler measurement procedures, which require a minimum of attention in the field. In addition, stability influences have a much greater impact upon gradient estimates than is the case for the bulk method (Table 4.5). It follows that an error in determining ϕ will have a less serious effect upon the bulk transfer method. For these reasons, it was adopted for flux calculations.

Bulk estimates of the momentum and sensible heat fluxes agree with the friction estimates from Eq. (2.5) (Fig. 4.15). The wide scatter in the comparison of Q_H estimates (Fig. 4.15b) is due to errors in θ_*. These are caused by large variations in the slope of the θ_*/k regression analysis referred to earlier. Error analysis indicated that most of the uncertainty in the bulk estimates could be attributed to the evaluation of Γ from Eq. (4.18). Measurement errors in u, θ and e were negligible by comparison. Hence, the bulk transfer procedure appears to be the best method of calculating Q_E, given the difficulties encountered in obtaining vapour pressure gradients. Accounting for errors in the roughness lengths, Monin-Obukhov constants and z/L, the relative error in bulk estimates of fluxes is generally 15%.

2. Diurnal Distribution of Fluxes

Short-term energy balance estimates are a useful aid to understanding glacier melt hydrology. Values of Q_H and Q_E are plotted against time in Fig. 4.16, along with the measurements of Q_* and Q_M. The time

TABLE 4.5

Flux Estimates Meaned over 124 Individual Computations with and without
Stability Corrections

(a) Gradient method.

	Uncorrected	Corrected
Momentum (Pa)	0.0703	0.0340
Sensible heat (W m^{-2})	125	55.9
Latent heat (W m^{-2})	-14.8	-5.99

(b) Bulk method.

	Uncorrected	Corrected
Momentum (Pa)	0.0429	0.0357
Sensible heat (W m^{-2})	84.2	65.4
Latent heat (W m^{-2})	-2.47	-2.68
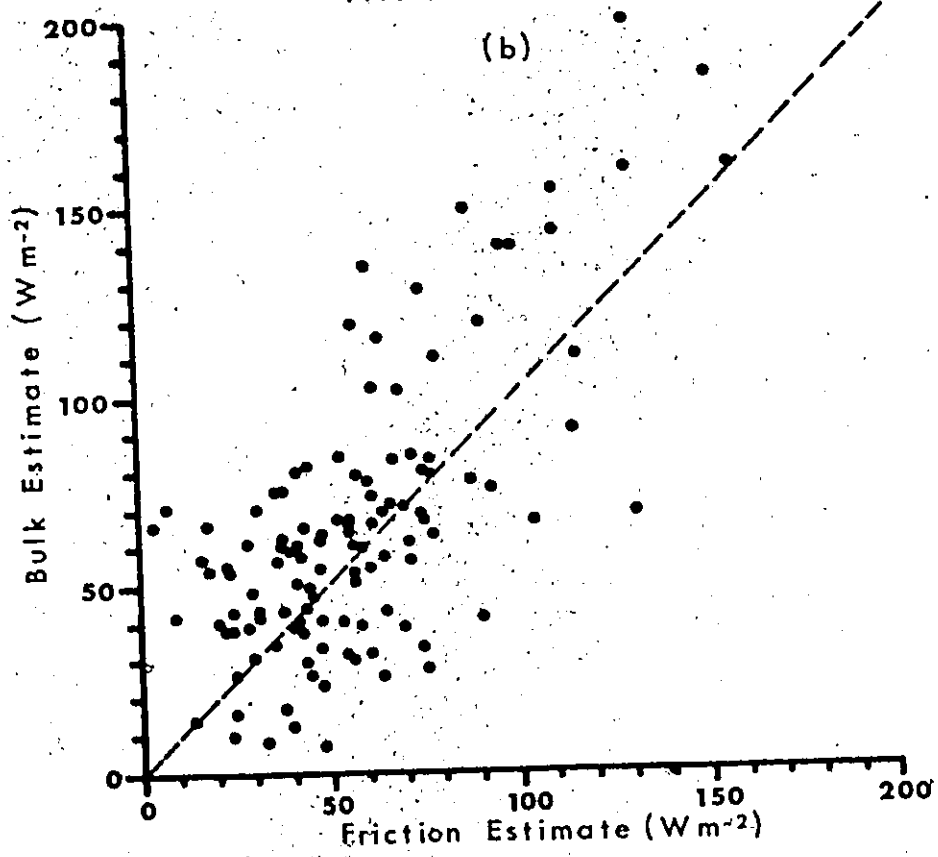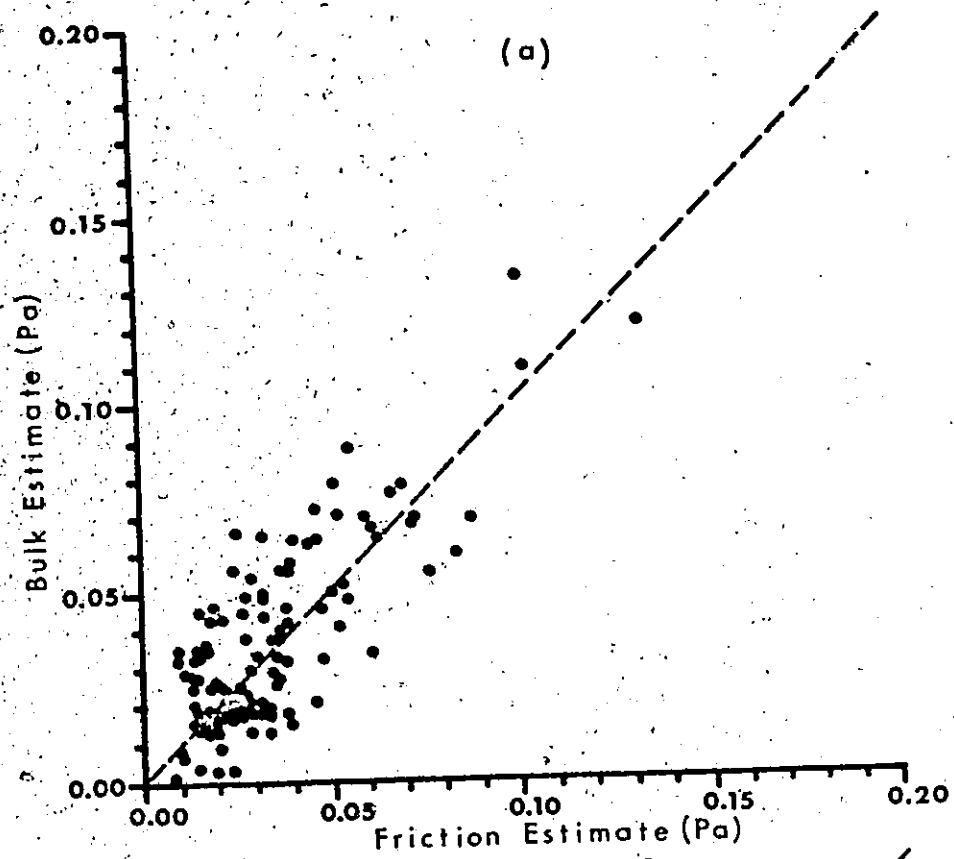
Figure 4.15. Comparison of bulk estimates and friction estimates of fluxes, (a) momentum, and (b) sensible heat.
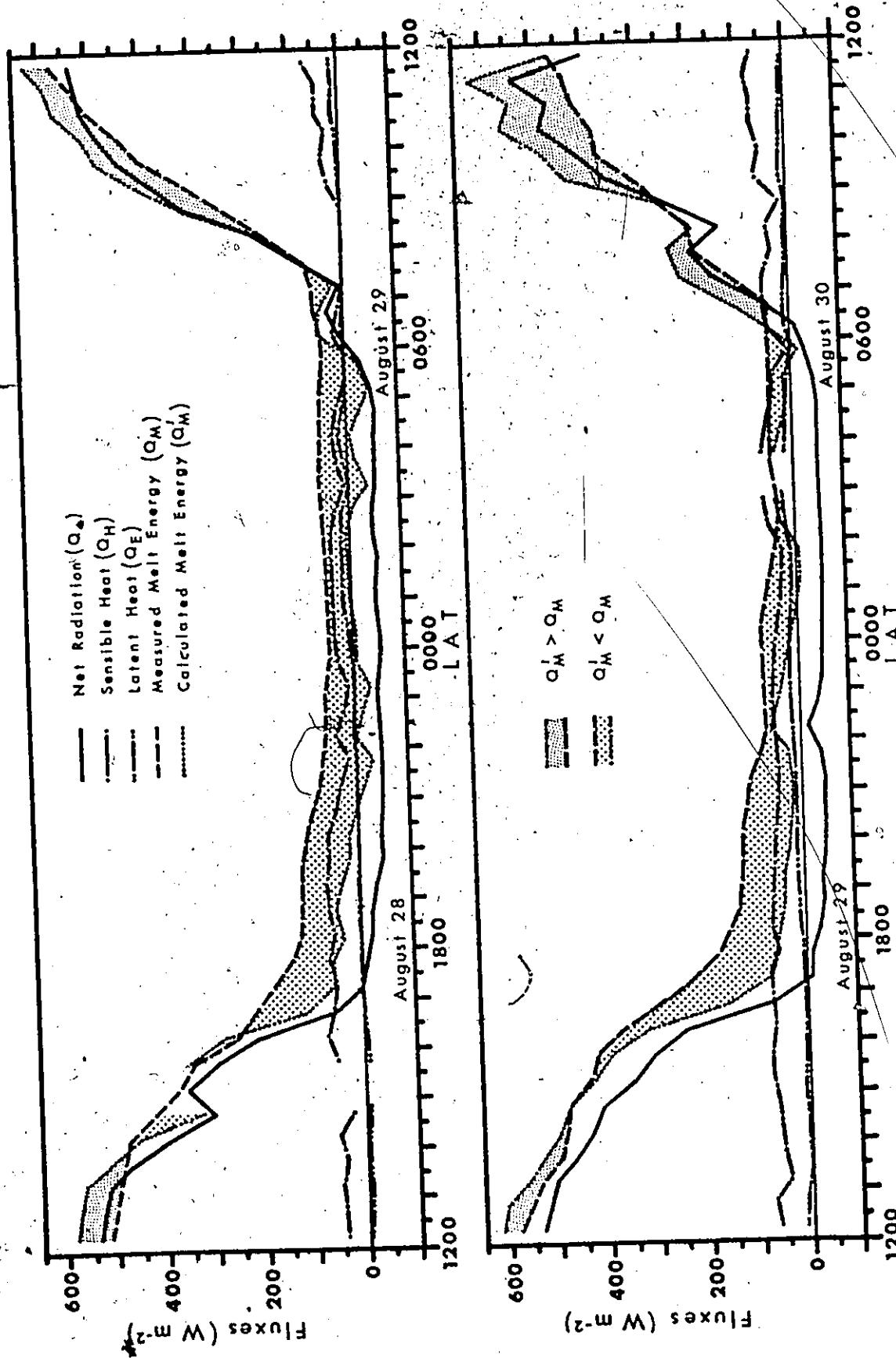
Figure 4.16. Short-term variation of energy balance components, August 28 - 1200 to August 30 - 1200.

period is the same as that of Fig. 4.1.

It can be seen that Q_M responds mainly to change in Q_*. The turbulent fluxes show a small variation over the course of a day, depending mainly upon wind speed (compare Fig. 4.1). The contribution of Q_H to the melt is positive. The magnitude of Q_E is small, oscillating around $0\ W\ m^{-2}$, in response to variations of e about the ice point.

Fig. 4.16 is probably unique in the glaciological literature, both with respect to the precision of the estimates, and the small time segments used. The earlier study of Derikx (1971) used one-hour estimates, but less precise profile measurements. Other studies have been concerned solely with daily totals.

Energy balance estimates of the melt energy, Q_M', were obtained by summing Q_*, Q_H and Q_E. They represent the energy input to the melt process. A comparison of the computed and measured short-term variations of melt energy indicates that Q_M lags behind Q_M'. This indicates that the surface hydrologic system is complex, since it requires time to respond to changes in energy input. Hence, the surface is a hydrologic zone within which storage effects are important.

3. Daily Totals

Daily totals of the measured melt energy were compared with those which were computed from the energy balance. Comparison was not made for shorter time periods because of lags in the hydrograph created by storage effects (Fig. 4.16), ensuring differences between the

predicted and measured values. This is readily observed in the late afternoon periods, where the value of Q_M obviously exceeds the sum of the other components.

Five independent periods of 24 hours duration were found among the data. Daily totals of Q_*, Q_H, Q_E and Q_M, as well as the predicted melt energy, Q_M', are listed in Table 4.6. The relative importance of Q_*, Q_H and Q_E corresponds with most other studies, where Q_* was found to be the greatest energy source and Q_E was the smallest (Paterson, 1969). However, the energy balance persistently underestimates the melt.

The underestimation of Q_M may be due to two features of the glacier surface hydrologic system. The first is that base flow occurs. This has been observed in snow packs (Davar, 1970), and it is seen in Fig. 4.16, where Q_M never goes to zero, even though the sum of the other energy balance terms is at times negative. Therefore, Q_M can be influenced by the melt events of preceding time periods. The second is that some water is trapped among the ice grains at the surface. As the grains melt, trapped water is released along with meltwater, thus leading to discharges which are greater than those predicted from the energy balance. Relatively high Q_* values should correspond to periods when differential ablation creates cracks in the ice which store water, thus reducing the effect of trapped water release. This could result in Q_M' exceeding Q_M, though this was not observed among the small number of cases obtained here. Müller and Keeler (1969) have shown that Q_M'/Q_M tends to be greater than unity when Q_* is relatively large, and less than

TABLE 4.6

Daily Totals of Energy Balance Components, Beginning at 1200 (MJ m^{-2})

Date	Net Radiation	Sensible Heat	Latent Heat	Measured Melt	Calculated Melt
Aug. 13 - 14	21.1	17.0	-3.5	51.4	34.6
Aug. 20 - 21	18.8	14.0	-1.1	41.9	31.7
Aug. 28 - 29	22.0	6.8	0.8	34.2	29.6
Aug. 29 - 30	22.6	9.4	2.1	36.3	34.1
Sept. 4 - 5	13.7	9.5	0.7	30.0	23.9

1.0 on days when Q_* is small. Also, Stenborg (1970) indicated that late
in the ablation season glacier basin run-off exceeds values computed
from climatic parameters. It is not known whether his result necessarily
applies to the small-scale system studied here. A satisfactory answer
to this question must be based upon the analysis of continuous measure-
ments throughout the ablation season.

The effectiveness of the energy balance method in estimating
ablation is assessed by changing Q_M and Q_M' into measures of surface
lowering (mm of water equivalent to melt energy, or mm w.e.). Daily
totals of Q_M and Q_M' are plotted along with the results of other investi-
gators (Fig. 4.17). Although differences between measured and calculated
ablation are all of the same sign, they are relatively small.
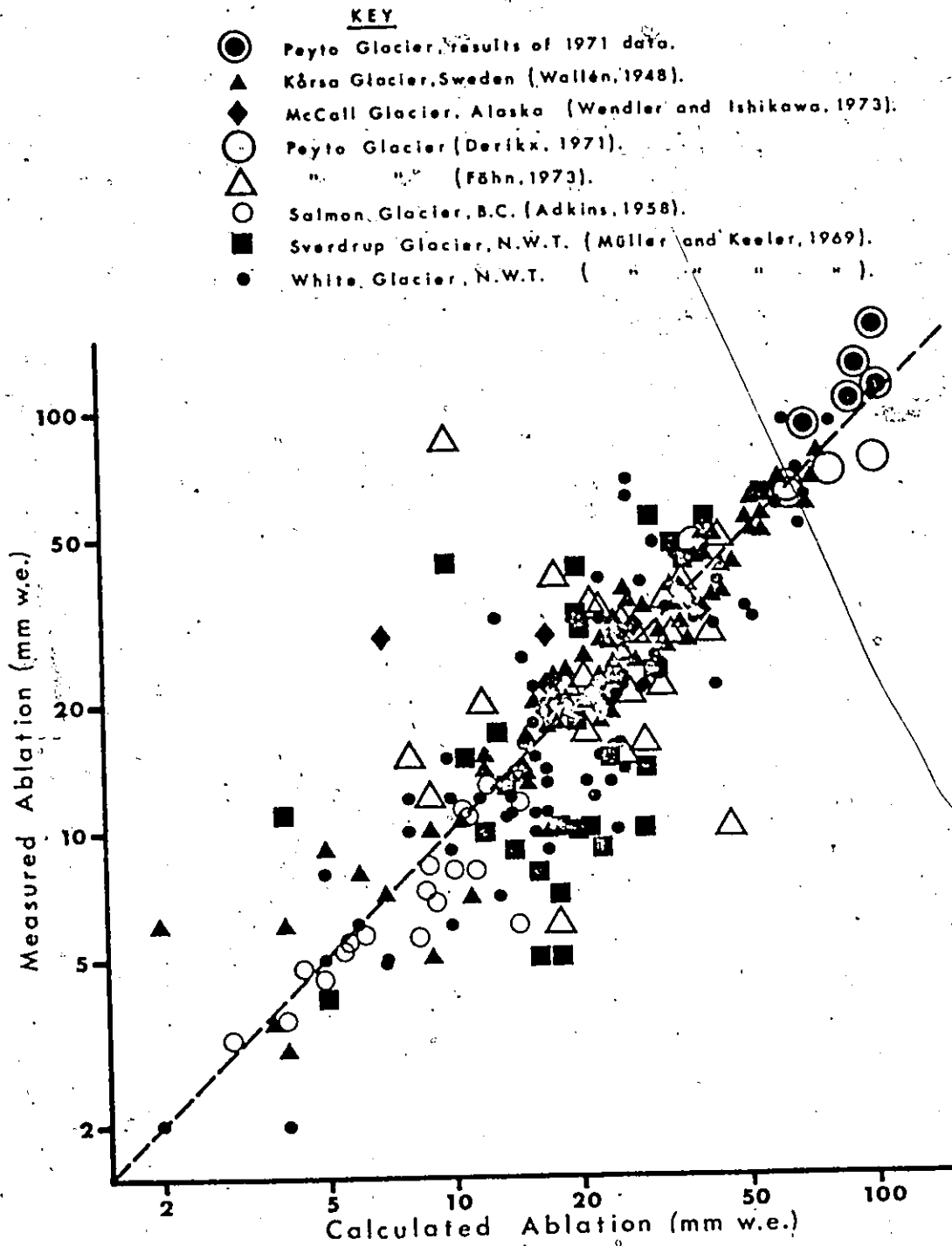
Figure 4.17. Comparison of computed and measured ablation from Peyto and other glaciers.

CHAPTER FIVE

CONCLUSION

This study sought to obtain short-term estimates of the turbulent heat fluxes, Q_H and Q_E, over melting ice. It was stated at the beginning that this requires a detailed experimental examination of flux-profile relationships near the surface. The theory, and experimental procedure for doing this were described.

This experiment succeeded in its purpose, and provided new information about the glacier boundary layer. Three important findings are included among the results:

(1) The boundary layer, in this case, is about 1 m in depth. Most previous energy balance studies have used profile measurements taken at greater heights above the surface. In some of these the boundary layer depth may have been adequate for the application of turbulent transfer theory. However the results of such investigations should be viewed with caution, particularly where there has been little examination of profile variation with height.

(2) The log-linear framework satisfactorily describes stability influences within the boundary layer. It is necessary to apply this framework to both the gradient, and the bulk transfer methods in order to obtain accurate flux estimates. The correspondence of the correction

109

scheme for the wind profile with that of other studies suggests that stability affects katabatically influenced flow in the same way that it affects flow over horizontal surfaces. The smaller value of the Monin-Obukhov constant for the temperature profile is an unusual result, but it could explain some of Wallén's (1948) findings for the Kårsa Glacier, Sweden. His results also point toward a weaker dependence of temperature on stability than is the case for wind.

(3) Sinks for the momentum and heat fluxes are different, as the different z_0 and z_H values indicate. Although this was expected, the direction of the inequality, $z_0 < z_H$, is opposite to what is usually assumed in glaciology. This is important in using the bulk transfer method.

The possible thickness of the boundary layer should be con- sidered in future studies before measurements are made. This is an important consideration for all methods stemming from turbulent transfer theory. In this connection, experimental studies of katabatic flow over glaciers, with a view to determining boundary layer development spatially, would be useful. The crucial questions are boundary layer thickness in relation to fetch, and possible temporal variations in thickness.

The stability correction procedure used here served the pur- pose of obtaining fluxes from wind speed, temperature and vapour pressure measurements. However, two measurement levels were required to determine the magnitude of the correction. A true bulk transfer model should use measurements from one level alone to determine stability corrections. The

use of a bulk Richardson number has been suggested for this purpose (Deacon and Webb, 1962), but its relationship to z/L is uncertain. Investigation in this area is needed. In addition, the finding of different Monin-Obukhov constants for wind speed and temperature requires further clarification.

The value of z_0, and the determination of z_H from profiles are important inputs to larger scale heat balance studies over glaciers. They should be useful to investigators who rely upon measurements taken from meteorological shelters for heat flux estimates, since the bulk transfer procedure must be used for this type of data. They could also be important parameters in synoptic-scale determinations of melt from glacier basins. This would be an improvement over semi-statistical models of the type used by Stenborg (1970). However, it would have to be done with an understanding of the spatial behaviour of katabatic flow, including its profile structure close to the surface.

The future direction of glacier climate research will probably be toward basin (meso-scale) studies, since this is the scale at which the hydrological role of glaciers can be assessed. By way of contributing to this, additional work in glacial microclimatology could be directed toward studies of katabatic flow, the incorporation of katabatic influences into flux estimation procedures, and the improvement of bulk transfer methods. This would be useful in obtaining continuous short-term estimates of energy balance components, extending over the melt season. In this way a better understanding of the influence of changing weather conditions upon the energy balance of the glacier surface, and its consequent hydrologic response, might be gained.

APPENDIX ONE

NOTATION

Upper Case Roman

A	constant in Eq. (3.6), equal to 17.269	dimensionless
A_p	area of meltwater discharge plot	m^2
B	constant in Eq. (3.6), equal to 237.3	C
C	discharge coefficient	dimensionless
C_D	drag coefficient for momentum	"
C_H	" " " heat and water vapour	"
D	discharge	$m^3\ s^{-1}\ (ft^3\ s^{-1})$
E	vapour pressure at the freezing-point of ice	Pa
E_t	turbulent energy exchange	$Pa\ s^{-1}$
K	general eddy transfer coefficient, subscripts E, H and M applying to water vapour, heat and momentum respectively	$m^2\ s^{-1}$
L	stability length scale	m
Q_E	latent heat flux due to water vapour transport	$W\ m^{-2}$
Q_H	sensible heat flux, subscripts o and z applying to values at the surface and at some height above the surface respectively	"
Q_I	heat flux below the ice surface	"
Q_M	melt energy	"

112

Q'_M	energy balance estimate of melt energy	$W\ m^{-2}$
Q_x	general flux notation	$Pa;\ W\ m^{-2}$
Q_*	net radiative flux	$W\ m^{-2}$
Re_*	roughness Reynolds number	dimensionless
Rf	flux Richardson number	"
Ri	gradient Richardson number, subscript c denoting the critical value	"
S	shape function, subscripts H and M applying to heat and momentum respectively	"
T	temperature, not corrected for adiabatic lapse rate	C
X	any independent variable, specified in text	
Y	any dependent " " " "	

Lower Case Roman

a	polynomial regression coefficient, order denoted by numerical subscript	
c	number of anemometer cup revolutions	rpm
c_p	specific heat of air at constant pressure	$J\ kg\ C^{-1}$
e	vapour pressure, surface value denoted by o subscript	Pa
e_*	friction vapour pressure, prime denoting value not corrected for stability	"
f	anemometer cup calibration factor	dimensionless
g	gravitational acceleration	$m\ s^{-2}\ (ft\ s^{-2})$

h	hydrologic head	ft
k	von Kármán's constant, equal to 0.415	dimensionless
m	electromotive output	mV
p	air pressure, reference value denoted by o subscript and set equal to 10^5	Pa
t	time	s
u	wind speed, z subscript referring to a partic- ular height above the surface	$m\ s^{-1}$
u_*	friction velocity, prime denoting value not corrected for stability	$m\ s^{-1}$
x	distance along the wind direction	m
y	any profile parameter, surface value denoted by o subscript, value at specific height above the surface by z subscript	
y_*	any friction parameter	
z	height above the surface	m
z_H	temperature profile roughness length, prime denoting value not corrected for stability	"
z_o	wind profile roughness length, prime denoting value not corrected for stability	"
z/L	stability parameter	dimensionless

Upper Case Greek

Γ	partial drag coefficient, subscripts E, H and o applying to water vapour, heat and momentum respectively	dimensionless

ϕ height-integrated stability correction, subscripts

E, H and M applying to water vapour, heat and

momentum respectively   dimensionless

Lower Case Greek

α Monin-Obukhov constant, subscripts E, H and M

applying to water vapour, heat and momentum

respectively   dimensionless

γ psychrometric constant equal to 66   Pa C^{-1}

ϵ ratio of molecular weight of water to air

constant equal to 0.622   dimensionless

ζ X-intercept value used in determination of

Monin-Obukhov constants   m

θ air temperature (potential value), surface

value denoted by o subscript   C (K)

θ_a absolute air temperature used in computation

of stability indices   K

θ_w wet bulb temperature (potential value)   C

θ_* friction temperature, prime denoting value

not corrected for stability   "

θ' temperature disturbance $(\theta - \theta_o)$ K

λ latent heat, subscripts f and v referring to

fusion and vapourization respectively   J kg^{-1}

ν kinematic viscosity, subscripts E and H

applying to diffusion coefficients of water

vapour and heat respectively $m^2 s^{-1}$

ρ	air density, subscript w denoting water density	$kg\ m^{-3}$
σ_u	standard deviation of the wind speed	$m\ s^{-1}$
τ	momentum flux (shearing stress)	Pa
ϕ	stability correction, subscripts E, H and M applying to water vapour, heat and momentum respectively	dimensionless
χ	any of the entities, momentum, heat and water vapour.	
ψ	slope angle	degrees

APPENDIX TWO

INSTRUMENTATION DETAILS

The ventilated psychrometer system, patterned after the system of Lourence and Pruitt (1969), and the hydrological discharge measurement system are described in this appendix. The accompanying diagrams illustrate the basic proportions, the arrangement of parts, and the overall dimensions. British units are used, in accordance with present North American industrial practice.

A. Ventilated Psychrometer System

1. Sensor Housing

The sensor housing is comprised of a set of shields, a T-junction, a water reservoir, and a ventilation unit (Figure A2.1a). An inner, and an outer shield are used. Both are covered with aluminized mylar on the outside, and flat black paint on the inside. The outer shield is constructed of acrylic tubing (2" I D), to which a hood of tinned steel is added. The mouth is inclined at 60 degrees to the horizontal, thus shielding the interior from direct sunlight. PVC tubing (1" I D) is used for the inner shield, which has small holes drilled near the downstream end, to allow purging of the air between the inner and outer shields. A support keeps the dry bulb centred in the air stream.

The T-junction is a standard PVC plumbing fitting, (1-1/2"
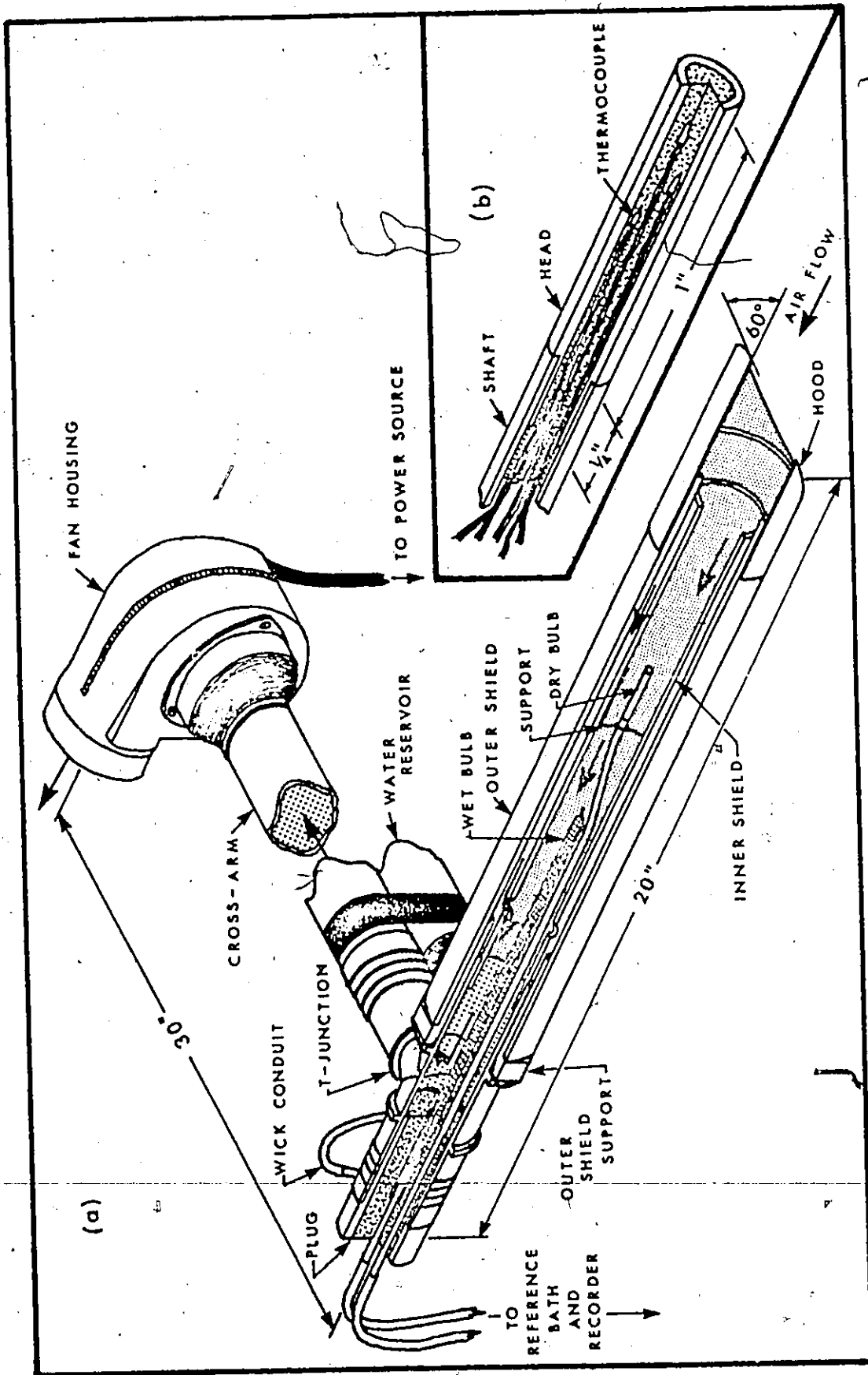
Figure A2.1. Ventilated psychrometer system (scale 1:3), (a) complete system, and (b) thermopile detail.

O D), which supports the inner shield. The outer shield support is a plastic sleeve, fitted over one end of the T-junction. A plug, which holds the dry and wet bulb probes in place, is inserted into the opposite end. Holes of appropriate diameter are drilled in the plug to allow the passage of a wick.

A one foot length of plastic tubing (1-1/2" O D) is used for a water reservoir. This is plugged at both ends, and access for re-supply of water is provided by drilling a small hole in the top. Water leaves along a wick which passes through a hole in the end closest to the T-junction. A wick conduit is constructed from an appropriate length of plastic tubing, which has short pieces of stainless steel tubing (3/16" O D) fitted to each end. These fit the holes in the plug and reservoir. The reservoir is suspended from the cross-arm by electrical tape.

The ventilation unit is a 115 V ac fan (Rotron Mfg. Co., NTO 120), contained within a housing, which is attached to the cross-arm. The cross-arm is made from a length of PVC tubing (1" I D). This arrangement ensures that the ac and dc parts of the system are separated, thus minimizing chances of interference with the temperature signals. During operation, air is sucked in through the shield opening, passes through the system, and exits from the fan housing (Figure A2.1a).

All exterior surfaces are painted white to minimize heating by solar radiation. Exceptions to this are the shield exteriors, since aluminized mylar is a superior coating in this respect, and the fan housing, which is far removed from the sensors.

2. Thermopile Construction

Five-junction thermopiles were used (Figure A2.1b). These are constructed from #30 awg copper-constantan thermocouple wire. The junctions are welded, and covered with heat-shrink tubing to insulate them from electrical contact. They are potted inside a small length (1-1/4") of aluminium tubing (3/16" O D), filled with polyester resin. The aluminium tubing is turned down along part of its length, and fitted into a relatively thin-walled piece of stainless steel tubing (3/16" O D). Individual wires are led back through white plastic tubing to a reference sensor of the same construction. One of the copper wires is cut near the reference sensor, and the two leads thus formed (positive and negative) are soldered to copper signal cable, which is attached to the recorder.

The reference probes are approximately 8" in length. Wet bulb probes are 11" long, and covered with a wick. Dry bulb probes are 14" long. This extra length is needed to ensure that the dry bulb is the first to encounter the air flow, and is thus unaffected by the environment of the wet bulb (Figure A2.1a).

B. Hydrological Discharge Measurement System

1. Description of System

The system is drawn schematically in Figure A2.2. The main component is a holding tank, approximately 4' long, 3' wide and 2' deep. Water enters the tank through a siphon, and leaves by falling over a 22.5° V-notch weir. The siphon drains water from a sump, which collects all of the water melted from a known area. This area is cut
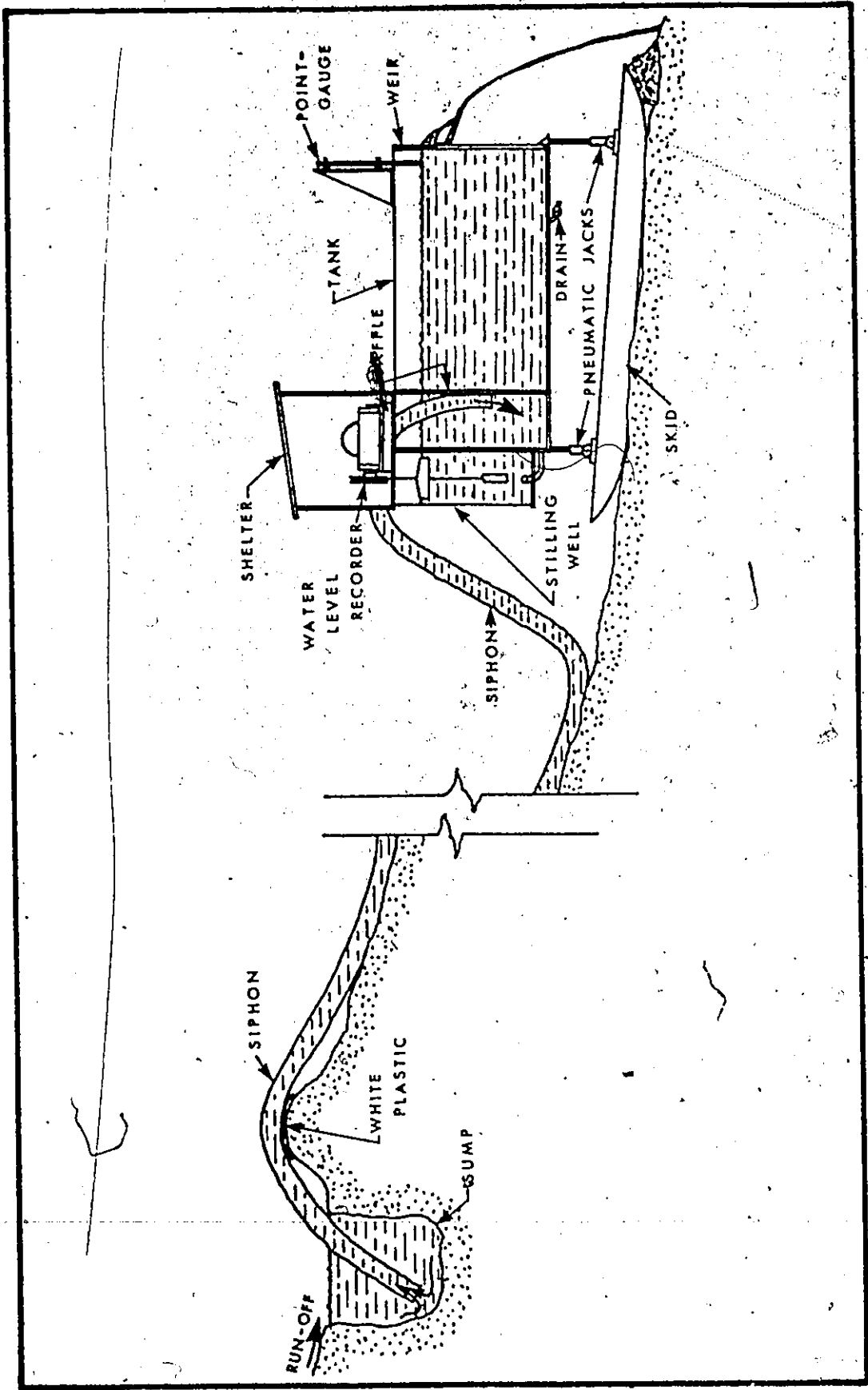
Figure A2.2. Schematic view of hydrological discharge measurement system (approximate scale 1:24).

off from the surrounding glacier surface through differential ablation around a boundary of white plastic. The tank is mounted on a set of skids so that it may be dragged over the glacier surface. Pneumatic jacks are used to adjust the attitude of the box to a level position.

A stilling well is mounted behind the tank. Water moves in and out of the well through a small diameter plastic tube, in response to water level changes in the tank. The water level is monitored by a recorder, which is housed in a shelter at the top of the stilling well. The effects of short-term inflow variations are smoothed out by a baffle.

2. System Calibration

The discharge equation was checked against direct field measurements of flow over the weir. This was done by collecting the water in a container. This discharge value was compared with the calculated value (Figure A2.3). Since good agreement was obtained, the discharge equation was accepted as being accurate.

The head reading on the water level recorder chart was calibrated against point-gauge readings taken near the V-notch (Figure A2.2) in thousandths of a foot. The two sets of readings, taken several times for each observation period, show good overall agreement (Figure A2.4). The main source of disagreement probably lies in point-gauge reading errors. These were sometimes difficult to make because of surface ripples which appeared during very windy conditions.
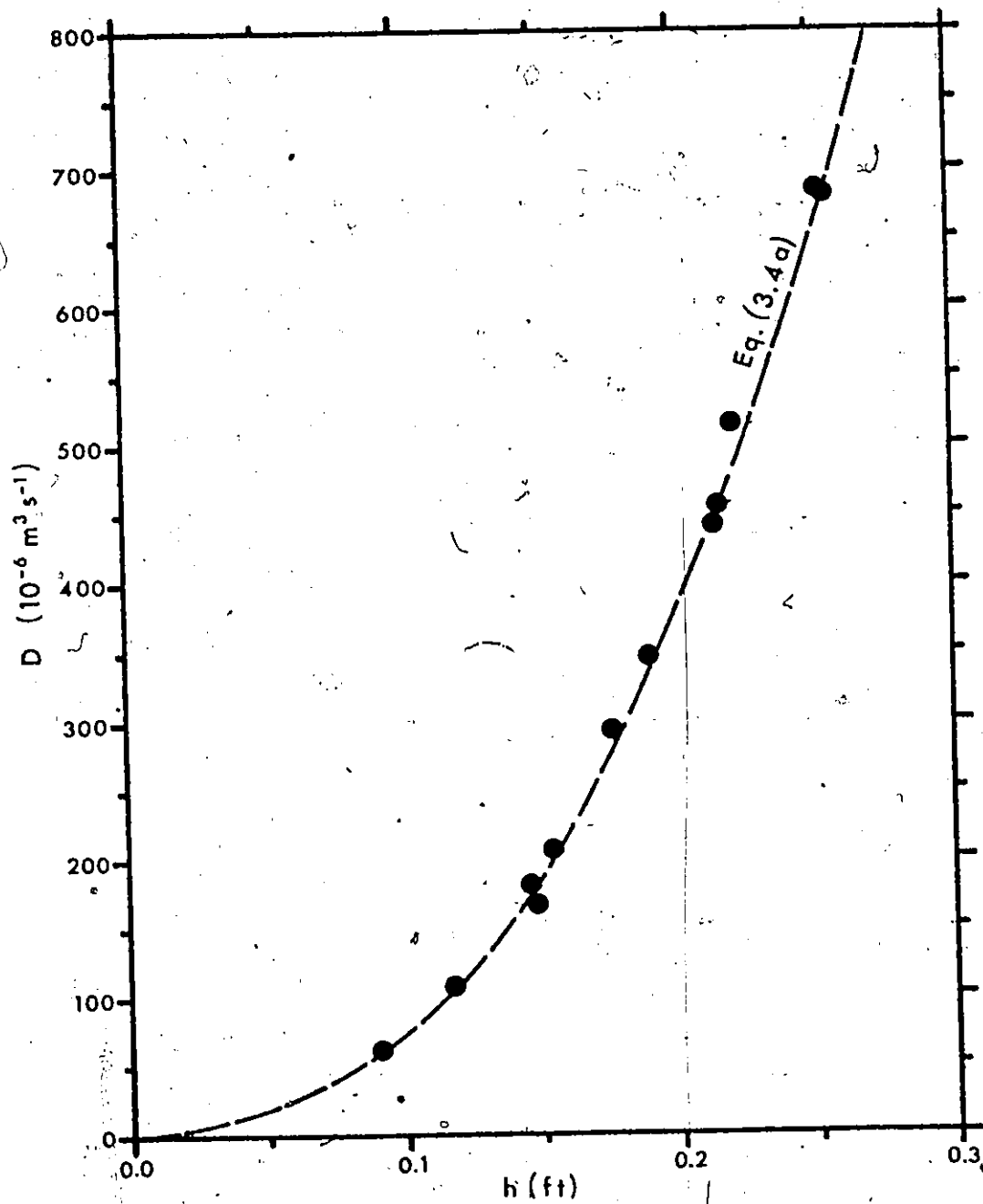
Figure A2.3. Comparison of direct discharge measurements (dots) with Eq. (3.4a).
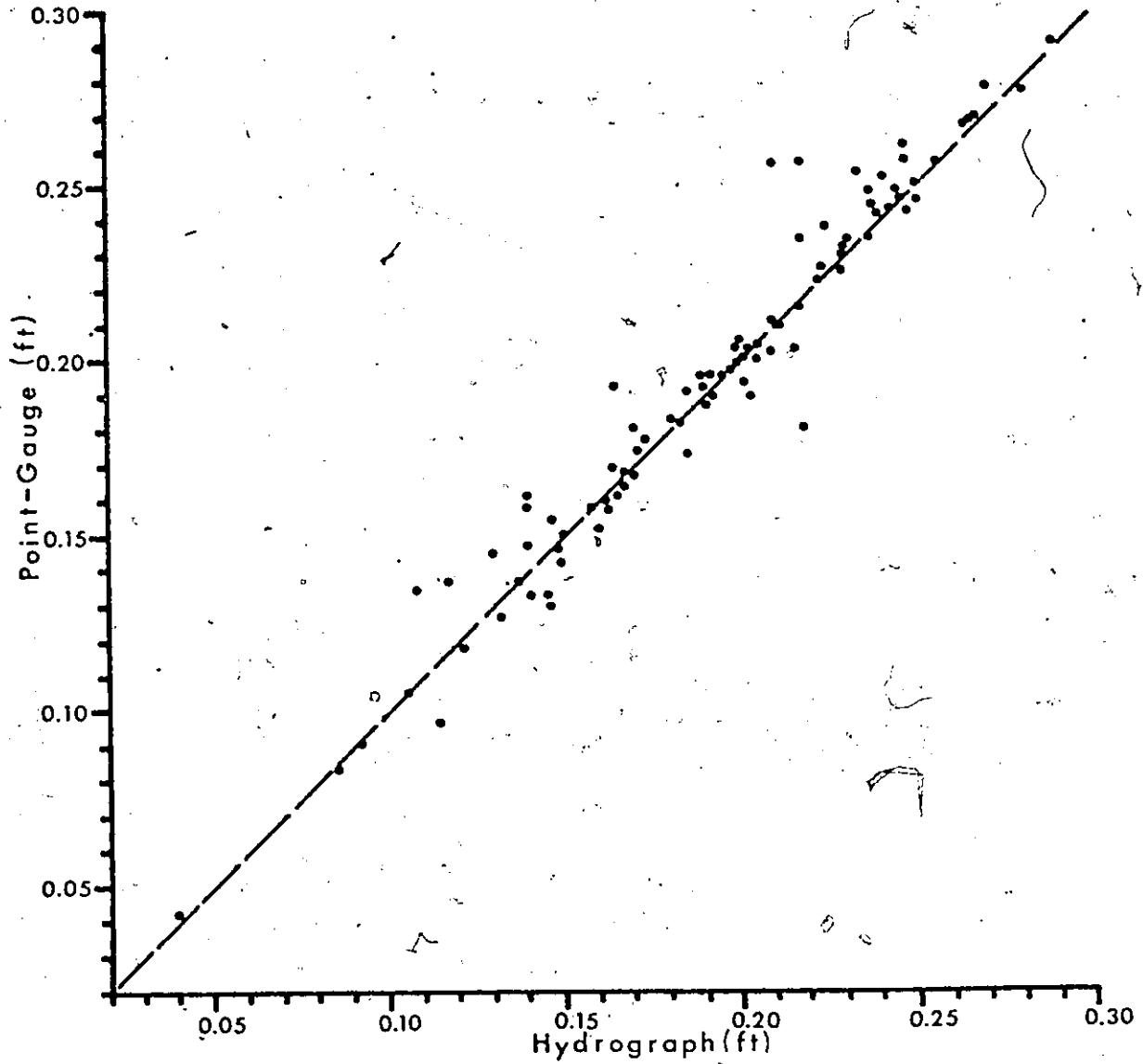
Figure A2.4.   Comparison of hydrograph and point-gauge measurements
of water level.

C. <u>Supplementary Anemometer and Thermopile Calibrations</u>

Correction factors for anemometer cup assemblies are listed in Table A2.1. Correction constants for thermopile thermometers are listed in Table A2.2.

The consistency of wind profile data, using correction factors established by the manufacturer, and by field intercomparisons, was checked by plotting 30 wind profiles which were sampled from all of the data. The samples were distributed throughout the observation period, and selection was confined to cases where all 12 anemometers functioned. Except for cup assemblies 1450, 1725, 1473 and 1606, smooth lines could be fitted through the data points in each sample.

Each of the four exceptional cup assemblies consistently over-estimated (1725) or underestimated (1450, 1473 and 1606) its corresponding value on the smooth line. Moreover, the relative magnitude of the deviation for any one of the four anemometers was approximately the same in each sample. These observations suggested that anemometer error was the most likely explanation for the exceptional results of the four cup assemblies, and their correction factors were adjusted according to the mean deviations observed.

TABLE A2.1

Correction Factors for Anemometer Cup Assemblies

Sensor	Correction Factor*	Height (m)
1567	1.0120	0.25
1326	0.9951	0.5
1450	0.9959	0.75
1434**	1.0000	1
1726	1.0000	1.5
1725	1.0084	2
1730	0.9977	2.5
1324	0.9985	3
1473	0.9848	3.5
1530	0.9948	4
1606	0.9870	5
1565	0.9970	6

* determined to $\pm$ 0.5%.

**used as a calibration standard.

TABLE A2.2

Correction Constants for Thermopile Thermometers

Sensor	Correction Constant (C)	Height (m)	Function
11	0.033	0.25	dry bulb
21	0.000	0.5	"
31	0.001	0.75	"
41	-0.008	1	"
51	0.000	1.5	"
61	-0.008	2	"
71	0.007	4	"
81	-0.001	6	"
12	-0.003	0.25	wet bulb
22	0.007	0.5	"
32	-0.019	0.75	"
42	-0.007	1	"
52	-0.019	1.5	"
62	0.053	2	"
81	-0.001	4	"

APPENDIX THREE

STATISTICAL TESTS

A. Test of Proportions

The test of proportions is applied to a set of N independent trials in which the outcome of each is either a success or a failure (Freund, 1962: p. 275). In this case success and failure are interpreted according to the direction of inequality between two quantities, A and B. Success occurs when $A < B$, failure when $A \geq B$.

The observed proportion of successes, S, is tested to see if it is significantly greater than 0.5, the value which would be expected if success occurred as frequently as failure. The probability distribution of S is binomial, but for $N > 100$ the normal probability distribution is used as an approximation, and a test statistic, z_s, is computed from

$$z_s = \frac{S - 0.5 N}{\sqrt{0.25 N}} \qquad (A3.1)$$

The test statistic is compared with a critical value of 1.65 at the 5% level. The value of S is taken to be significantly different from 0.5 if $z_s > 1.65$.

B. Skewness Test

Following Pearson and Hartley (1954: p. 61), the skewness of a sample containing N values of a particular quantity, X, is tested by

128

estimating the first three moments of the distribution of individual values, X_i,

$$m_1 = \sum_{i=1}^{N} \frac{X_i}{N} = \bar{X} \qquad (A3.2)$$

$$m_2 = \sum_{i=1}^{N} \frac{(X_i - X)^2}{N} \qquad (A3.3)$$

$$\text{and} \quad m_3 = \sum_{i=1}^{N} \frac{(X_i - X)^3}{N} \qquad (A3.4)$$

in which m_1, m_2 and m_3 are the moments about the mean, $\bar{X}$; and by computing the coefficient of skewness, $\sqrt{b_1}$:

$$\sqrt{b_1} = \frac{m_3}{m_2^{3/2}} \qquad (A3.5)$$

The value of $\sqrt{b_1}$ is compared with the critical value at the 5% level, which is obtained from Table 34.B of Pearson and Hartley (1954). This gives a critical value of 0.366 for the sample size used in Chapter Four ($N \cong 124$). The sample is considered to be normal if $|\sqrt{b_1}| \leq 0.366$.

RESULTS OF STABILITY ANALYSIS

This is a summary of the results of the investigation of Monin-Obukhov constants.

Date	Start	u_{1m} (m s^{-1})	θ_{1m} (C)	L (m)	$Ri_{0.5m}$	α_M	α_H
Aug. 12	1000	3.32	12.95	3.5	0.17	0.72	2.2
	1030	4.13	11.70	8.9	0.092	3.1	20
	1100	4.01	11.72	3.3	0.10	4.9	6.8
	1330	4.53	8.96	16	0.065	17	120
	1430	4.29	10.68	5.3	0.095	5.3	12
	1530	4.25	10.43	5.2	0.086	4.7	8.8
	1600	4.90	10.38	11	0.071	10	50
13	0830	4.20	9.55	48	0.064	69	1500
	1200	4.91	8.11	61	0.051	48	1200
	1700	5.18	9.50	6.2	0.061	5.6	6.6
	2100	5.53	7.81	6.5	0.050	6.9	6.1
14	0030	4.41	13.57	3.2	0.098	2.0	0.53
	0130	6.36	13.36	8.4	0.037	4.8	0.24
	0430	7.10	11.61	6.9	0.029	7.8	0.040
	0530	5.30	11.40	6.0	0.045	4.2	0.13
	0800	6.52	11.76	6.3	0.039	6.0	0.77

APPENDIX FOUR (cont'd.)

Date	Start	u_{1m} (m s^{-1})	θ_{1m} (C)	L (m)	$R1_{0.5m}$	σ_M	σ_H
Aug. 14	0830	6.65	12.16	10	0.033	5.3	0.99
	0930	8.59	12.16	17	0.019	12	5.4
	1130	7.82	11.98	15	0.023	7.8	2.0
	1330	6.73	11.15	9.0	0.029	7.6	0.94
	1530	4.73	10.08	6.2	0.064	3.0	2.5
	0700	3.72	7.74	1.9	0.10	2.5	0.18
16	1030	4.48	9.00	11	0.051	3.7	8.5
	1830	2.68	5.89	4.0	0.14	1.7	4.5
18	1100	3.55	9.24	17	0.065	14	100
19	1130	3.55	9.57	16	0.067	9.4	72
	1230	3.28	9.39	12	0.084	8.7	62
	1300	3.15	10.36	5.5	0.13	1.8	8.4
	1330	3.77	7.75	24	0.081	21	320
	1400	4.54	7.02	7.4	0.048	15	26
	1430	3.68	10.62	7.27	0.075	7.5	20
	1500	3.81	9.94	9.9	0.078	8.2	24
	1700	4.72	6.52	7.0	0.053	11	17
	1730	4.72	7.68	4.3	0.060	8.5	8.6
	1800	4.36	9.83	9.8	0.076	4.6	2.9

APPENDIX FOUR (cont'd.)

Date	Start	u_{1m} (m·s^{-1})	θ_{1m} (C)	L (m)	$Ri_{0.5m}$	α_M	α_H
Aug. 20	0700	6.21	11.13	22	0.028	10	31
	1000	6.22	10.70	14	0.031	8.1	10
	1100	6.36	11.37	9.8	0.031	7.1	1.9
	1130	6.71	10.59	13	0.025	9.7	5.6
	1200	5.48	11.38	12	0.042	7.7	16
	1230	4.15	10.48	5.7	0.075	4.8	8.0
	1300	3.41	10.20	1.8	0.11	2.8	0.90
	1330	3.79	8.99	5.8	0.093	6.5	17
	1400	4.08	10.52	6.8	0.075	6.7	16
	1430	3.97	9.83	9.8	0.075	7.6	32
	1500	4.29	10.58	13	0.064	9.9	53
	1530	4.42	10.60	7.5	0.061	6.8	12
	1600	4.08	11.58	5.9	0.090	3.3	7.9
	1630	4.65	10.65	7.7	0.061	6.2	12
	1730	5.54	10.71	2.9	0.053	5.3	0.85
	1900	5.11	9.88	4.4	0.064	3.9	1.3
	1930	4.69	9.90	2.1	0.080	3.6	0.79
	2000	5.52	10.25	4.5	0.050	5.4	1.3
	2030	5.78	10.56	4.4	0.048	5.0	0.38

APPENDIX FOUR (cont'd.)

Date	Start	u_{1m} (m·s^{-1})	θ_{1m} (C)	$\frac{L}{(m)}$	$Ri_{0.5m}$	α_M	α_H
Aug. 20	2130	6.26	10.46	6.2	0.046	4.5	0.71
	2200	6.31	10.21	4.9	0.041	7.2	2.1
21	0000	5.38	8.91	2.7	0.054	4.7	0.24
	0430	3.86	8.29	2.9	0.084	3.0	0.73
	0630	5.12	8.33	6.7	0.033	7.4	0.77
	0700	4.78	8.37	11	0.039	6.1	7.2
	1130	3.74	8.10	4.2	0.082	4.9	5.4
24	1500	4.14	7.21	3.6	0.059	4.7	1.1
	1530	4.16	7.39	2.6	0.067	4.8	1.5
	1630	3.71	7.89	4.1	0.087	5.2	6.8
	1700	3.91	7.01	3.2	0.089	4.9	4.5
	1730	4.12	9.45	4.5	0.058	3.9	0.67
	1800	5.33	8.93	7.5	0.037	5.5	0.28
	1900	4.23	8.13	3.9	0.067	3.6	0.85
25	1100	3.58	7.21	3.5	0.094	3.0	1.9
	1230	3.57	7.77	3.6	0.081	4.4	3.2
	1300	3.87	7.25	5.0	0.062	6.0	5.4
	1400	3.80	7.71	3.2	0.087	3.8	2.4

APPENDIX FOUR (cont'd.)

Date	Start	u_{1m} (m s^{-1})	θ_{1m} (C)	L (m)	$R1_{0.5m}$	α_M	α_H
Aug. 25	1430	3.72	7.01	4.3	0.088	5.8	8.9
	1530	3.66	9.40	2.8	0.13	1.2	0.16
	1600	3.66	8.76	2.7	0.11	2.8	1.9
	1630	3.98	7.79	2.4	0.089	2.6	0.05
	1700	3.84	7.97	2.2	0.10	2.8	0.79
	1730	3.99	8.10	2.5	0.087	3.9	1.9
	1800	3.94	7.48	3.1	0.090	3.0	1.3
28	1600	5.45	6.91	12	0.039	16	38
	1900	5.11	7.15	4.1	0.045	7.0	2.1
	1930	4.84	7.35	4.2	0.055	7.0	4.5
	2000	5.12	6.72	3.5	0.045	7.0	1.8
	2030	4.11	7.09	2.0	0.084	3.3	0.59
	2100	3.86	6.71	3.7	0.091	4.0	4.0
	2130	3.52	6.29	1.6	0.11	2.8	0.86
	2200	4.28	5.92	3.7	0.058	7.2	4.8
	2330	4.29	5.07	3.8	0.053	7.9	5.0
29	0000	4.43	4.69	3.1	0.046	7.4	2.2
	0100	4.51	4.74	4.6	0.043	8.0	3.3
	0130	4.59	4.68	3.1	0.043	7.7	2.3

APPENDIX FOUR (cont'd.)

Date	Start	u_{1m} (m s^{-1})	θ_{1m} (C)	L (m)	$Ri_{0.5m}$	α_M	α_H
Aug. 29	0230	3.57	5.41	4.3	0.078	3.7	2.7
	0300	3.04	5.51	5.8	0.12	2.5	10
	0330	3.53	5.17	8.6	0.091	0.60	8.6
	0400	3.69	5.30	4.3	0.070	16	5.7
	0500	2.60	5.41	3.4	0.22	1.2	6.4
	0600	3.44	4.97	4.9	0.074	5.7	7.1
	0630	2.90	5.09	2.5	0.11	3.4	3.1
	0700	3.17	5.24	5.3	0.12	0.45	2.6
	0800	2.70	6.25	2.4	0.18	0.96	0.92
	1130	6.01	5.96	15	0.023	11	7.3
	1200	5.03	7.20	6.9	0.040	6.8	3.0
	1230	5.50	7.10	9.0	0.032	7.0	1.7
	1300	5.58	4.31	18	0.019	18	19
	1330	6.22	4.55	19	0.017	19	14
	1400	5.95	5.07	14	0.022	14	11
	1430	5.66	5.61	5.5	0.027	20	0.57
	1530	6.05	6.65	7.7	0.030	7.7	0.62
	1700	6.12	6.24	6.4	0.030	8.6	1.2

APPENDIX FOUR (cont'd.)

Date	Start	u_{1m} (m s⁻¹)	θ_{1m} (C)	L (m)	$Ri_{0.5m}$	α_M	α_H
Aug. 29	1730	5.74	5.13	8.2	0.028	8.2	0.21
	1830	5.70	6.24	6.6	0.032	7.1	0.020
30	0800	3.99	5.90	5.5	0.058	4.3	2.3
	0830	3.40	7.23	3.1	0.12	2.6	2.9
	0900	4.94	6.78	11	0.039	4.6	4.2
	0930	4.47	6.29	18	0.038	4.0	22
	1000	5.10	6.83	6.5	0.037	7.5	2.1
	1030	5.18	7.03	7.9	0.036	8.4	5.1
	1100	6.18	6.45	24	0.020	11	19
	1200	5.52	4.99	24	0.022	8.8	17
Sept. 2	1600	3.14	2.30	12	0.033	6.9	6.3
	1700	3.63	2.30	10	0.032	5.8	0.85
4	1600	3.55	4.78	11	0.043	2.3	2.6
	1830	3.08	4.60	8.4	0.054	8.0	1.1
5	0700	5.75	6.86	21	0.018	1.3	0.48

APPENDIX FIVE

DATA SUMMARY

The summary of data collected in 1971 for this study is set out in the following condensed format:

Aug. 14 - 0830

387.0/572.0

5.55	10.62	4.06		0.25
6.05	11.39	4.14		0.50
6.39	11.83	4.46		0.75
6.65	12.16	4.58		1
7.00	12.51	4.79		1.5
7.27	12.86	4.59		2
7.52	*****	****		2.5
7.63	*****	****		3
7.79	*****	****		3.5
7.92	13.08	****		4
8.14	*****	****		5
8.34	12.87	****		6

First line: time of start. Second line: Q_* (W m^{-2})/D (10^{-6} m s^{-1}). The columns of data are (from left to right) u (m s^{-1}), θ (C), θ_w (C) and z (m). Heights are shown here for reference. Since they are common to all the measurements, they are omitted from the summary. Asterisks denote missing data. All values are half-hour means.

169

REFERENCES

Acheson, D.T., 1970: Response of cup and propeller rotors and wind direction vanes to turbulent wind fields. *Meteor. Monogr.*, 11, 252-262.

Adkins, C.J., 1958: The summer climate in the accumulation area of the Salmon Glacier. *J. Glaciol.*, 3, 195-206.

Angus, D.E., 1963: *The Influence of Meteorological and Soil Factors on the Rate of Evapotranspiration of a Crop.* Ph.D. Thesis, Univ. of California, Davis, 128 pp.

Ball, F.K., 1960: Winds on the ice slopes of Antarctica. in *Antarctic Meteorology*, Proc. Symp., Melbourne, 1959, Pergamon, Oxford.

Bernstein, A.B., 1967: A note on the use of cup anemometers in wind profile experiments. *J. Appl. Meteor.*, 6, 280-286.

Binkowski, F.S., 1975: On the empirical relationship between the Richardson number and the Monin-Obukhov stability parameter. *Atmos. Env.*, 9, 453-454.

Bradley, E.F., 1968a: A micrometeorological study of velocity profiles and surface drag in the region modified by a change in surface roughness. *Quart. J. R. Meteor. Soc.*, 94, 361-379.

Bradley, E.F., 1968b: A shearing stress meter for micrometeorological studies. *Quart. J. R. Meteor. Soc.*, 94, 380-387.

Bradley, E.F., 1972: The influence of thermal stability on a drag coefficient measured close to the ground. *Agr. Meteor.*, 9, 183-190.

British Standards Institution, 1961: Draft British Standard Method of Measurement of Liquid Flow in Open Channels, Part 2, Notches, Weirs and Flumes. AB (INE) 5390, British Standards Institution, 53 pp.

Businger, J.A., 1955: On the structure of the atmospheric surface layer. J. Meteor., 12, 553-561.

Businger, J.A., J.C. Wyngaard, Y. Izumi and E.F. Bradley, 1971: Flux-profile relationships in the atmospheric surface layer. J. Atmos. Sci., 28, 181-189.

Calder, K.L., 1966: Concerning the similarity theory of A.S. Monin and A.M. Obukhov for the turbulent structure of the thermally stratified layer of the atmosphere. Quart. J. R. Meteor. Soc., 92, 141-146.

Carl, D.M., T.C. Tarbell and H.A. Panofsky, 1973: Profiles of wind and temperature from towers over homogeneous terrain. J. Atmos. Sci., 30, 788-794.

Chamberlain, A.C., 1968: Transport of gases to and from surfaces with bluff and wave-like roughness elements. Quart. J. R. Meteor. Soc., 94, 318-332.

Cook, N.H. and E. Rabinowicz, 1963: Physical Measurement and Analysis. Addison-Wesley, Reading, Mass., 312 pp.

Crawford, T.V., 1965: Moisture transfer in free and forced convection. Quart. J. R. Meteor. Soc., 91, 18-27.

Dalrymple, P.C., H.H. Lettau and S. Wollaston, 1963: South Pole Micro-meteorology Program. Report No. 20, Inst. Polar Studies, Ohio State Univ., Columbus, 94 pp.

Davar, K.S. 1970: Peak flow - snowmelt events. in Handbook on the Principles of Hydrology, NRC Canada, Ottawa.

Deacon, E.L. and W.C. Swinbank, 1958: Comparison between momentum and water vapour transfer. pp. 38-41 in UNESCO Arid Zone Research, 2, Proc. Canberra Symp.

Deacon, E.L. and E.K. Webb, 1962: Small-scale interactions. pp. 43-87 in The Sea, 1, Wiley (Interscience), New York.

Defant, F., 1951: Local winds. pp. 655-672 in Compendium of Meteorology, Amer. Meteor. Soc., Boston.

Derikx, L., 1971: The heat balance and associated runoff from an experimental site on the glacier tongue. Conference Paper, Int. Assoc. Sci. Hydrol., Moscow.

DeWalle, D.R. and L.H. Parmelle, 1974: Application of error analysis to surface temperature determination by radiation budget techniques. J. Appl. Meteor., 13, 430-434.

Dilley, A.C., 1968: On the computer calculation of vapour pressure and specific humidity gradients. J. Appl. Meteor., 7, 717-719.

Durst, C.S., 1933: The breakdown of steep wind gradients in inversions. Quart. J. R. Meteor. Soc., 59, 131-136.

Dyer, A.J., 1967: The turbulent transport of heat and water vapour in an unstable atmosphere. Quart. J. R. Meteor. Soc., 93, 501-508.

Dyer, A.J. and B.B. Hicks, 1970: Flux-gradient relationships in the constant flux layer. Quart. J. R. Meteor. Soc., 96, 715-731.

Dyer, A.J. and B.B. Hicks, 1972: The spatial variability of eddy fluxes in the constant flux layer. Quart. J. R. Meteor. Soc., 98, 206-212.

Dyer, A.J.; 1974: A review of flux-profile relationships. <u>Boundary Layer Meteor.</u>, 7, 363-372.

Elliott, W.P. 1960: An hypothesis for the diabatic mixing length. <u>J. Meteor.</u>, 17, 680-681.

Ellison, T.H., 1957: Turbulent transport of heat and momentum from an infinite rough plane. <u>J. Fluid Mech.</u>, 2, 456-466.

Fogel, C.M., 1962: <u>Introduction to Engineering Computations.</u> Scranton, Int. Textbooks Co., 210 pp.

Föhn, P.M.B., 1973: Short-term snowmelt and ablation derived from heat and mass balance measurements. <u>J. Glaciol.</u>, 12, 275-290.

Fuchs, M. and C.B. Tanner, 1965: Radiation shields for air temperature thermometers. <u>J. Appl. Meteor.</u>, 4, 544-547.

Fuchs, M. and C.B. Tanner, 1970: Error analysis of Bowen ratios measured by differential psychrometry. <u>Agr. Meteor.</u>, 7, 329-334.

Funk, J.P., 1962: A net radiometer designed for optimum sensitivity and a ribbon thermopile used in a miniturized version. <u>J. Geophys. Res.</u>, 67, 2753-2760.

Garratt, J.R. and B.B. Hicks, 1973: Momentum, heat and water vapour transfer to and from natural and artificial surfaces. <u>Quart. J. R. Meteor. Soc.</u>, 99, 680-687.

Grainger, M.E. and H. Lister, 1966: Wind speed, stability and eddy viscosity over melting ice surfaces. <u>J. Glaciol.</u>, 6, 101-128.

Gray, D.M. and J.M. Wigham, 1970: Peak flow - rainfall events. In <u>Handbook on the Principles of Hydrology</u>, NRC Canada, Ottawa.

Harbeck, G.E., 1967: A note concerning the eddy transfer coefficients of momentum and water vapour under near-adiabatic conditions. Water Resour. Res., 3, 201-202.

Haugen, D.A., J.C. Kaimal and E.F. Bradley, 1971: An experimental study of Reynolds stress and heat flux in the atmospheric surface layer. Quart. J. R. Meteor. Soc., 97, 168-170.

Havens, J.M., F. Müller and G.C. Wilmot, 1965: Comparative meteorological survey and a short-term heat balance study of the White Glacier, Canadian Arctic Archipelago - summer 1962. Meteorology, No. 4, Axel Hieberg Island Res. Rep., McGill Univ., Montreal, 68 pp.

Hicks, B.B. and H.C. Martin, 1972: Atmospheric turbulent fluxes over snow. Boundary Layer Meteor., 2, 496-502.

Högström, U., 1967: Turbulent water vapour transfer at different stability conditions. Phys. Fluids, Supp., 10, 247-254.

Högström, U., 1974: A field study of the turbulent fluxes of heat, water vapour and momentum at a 'typical' agricultural site. Quart. J. R. Meteor. Soc., 100, 624-639.

Hölmgren, B., 1971: Climate and energy exchange on a sub-polar ice cap in summer. Medd. Meteor. Inst., Uppsala Univ., 109, 43 pp.

Holzman, B., 1943: The influence of stability on evaporation. Ann. N.Y. Acad. Sci., 44, 13-18.

Hubley, R.C., 1957: An analysis of surface energy during the ablation season on Lemom Creek Glacier, Alaska. Trans. Amer. Geophys. Union, 38, 68-85.

Hyson, P., 1972: Cup anemometer response to fluctuating wind speeds. J. Appl. Meteor., 11, 843-848.

Kaimal, J.C. and Y. Izumi, 1965: Vertical velocity fluctuations in a nocturnal low-level jet. J. Appl. Meteor., 4, 576-584.

Krumbein, W.C. and F.A. Graybill, 1965: An Introduction to Statistical Models in Geology, McGraw-Hill, Toronto, 475 pp.

La Casinière, A.C. de, 1974: Heat exchange over a melting snow surface. J. Glaciol., 13, 55-72.

LaChapelle, E., 1959: Annual mass and energy exchange on the Blue Glacier. J. Geophys. Res., 64, 443-449.

Langleben, M.P., 1968: Albedo measurements of an Arctic ice cover from high towers. J. Glaciol., 7, 289-297.

Langleben, M.P., 1969: Albedo and degree of puddling of a melting cover of sea ice. J. Glaciol., 8, 407-412.

Langleben, M.P., 1972: A study of the roughness parameters of sea ice from wind profiles. J. Geophys. Res., 77, 5935-5944.

Latimer, J.R., 1972: Radiation measurement. Int. Field Year for the Great Lakes, Tech. Manual Ser., 2, 53 pp.

Lieth, C.E., 1973: The standard error of time-average estimates of climatic means. J. Appl. Meteor., 12, 1066-1069.

Lettau, H.H., 1949: Isotropic and non-isotropic turbulence in the atmospheric surface layer. Geophys. Res. Papers, 1, 86 pp.

Lettau, H.H., 1962: Notes on theoretical models of profile structure in the diabatic surface layer. In Studies of the Three-Dimensional Structure of the Planetary Boundary Layer, Dept. of Meteor., Univ. of Wisconsin, Final Report, Contract DA-36-039-SC-80282.

Lettau, H.H., 1966: A case study of katabatic flow on the South Polar
Plateau. Studies in Antarctic Meteorology, 9, Antarctic Res.
Ser., Amer. Geophys. Union.

Liljequist, G.H., 1955: Energy exchange of an Antarctic snowfield.
Norwegian-British-Swedish Antarctic Expedition, 1949-52,
Scientific Results, 2, Norsk Polarinstitutt, Öslo, 298 pp.

List, R.J., 1966: Smithsonian Meteorological Tables. Smithsonian
Institution, Washington.

Lourence, F.J. and W.O. Pruitt, 1969: A psychrometer system for micro-
meteorology profile determination. J. Appl. Meteor., 8,
492-498.

Lumley, J.L. and H.A. Panofsky, 1964: The Structure of Atmospheric
Turbulence. Interscience, New York, 239 pp.

MacCready, P.B., 1966: Mean wind speed measurements in turbulence.
J. Appl. Meteor., 5, 219-225.

MacCready, P.B., 1970: Theoretical considerations in instrument design.
Meteor. Monogr., 11, 202-210.

McVehil, G.E., 1964: Wind and temperature profiles near the ground in
stable stratification. Quart. J. R. Meteor. Soc., 90, 136-146.

Monin, A.S. and A.M. Obukhov, 1954: Basic laws of turbulent mixing in
the ground layer of the atmosphere. Tr. Geofiz. Inst. Akad.
Nauk SSSR, 24, 163-187 (Amer. Meteor. Soc. Translation, AFCRC
Contract 19 (604) - 1936).

Monteith, J.L., 1973: Principles of Environmental Physics. Edward-
Arnold, London, 241 pp.

Müller, F., 1962: Zonation in the accumulation area of the glaciers of
Axel Heiberg Island, N.W.T., Canada. J. Glaciol., 4, 302-310.

Müller, F. and C.M. Keeler, 1969: Errors in short-term ablation measure-
ments on melting ice surfaces. J. Glaciol., 8, 91-105.

Obukhov, A.M., 1946: Turbulence in an atmosphere with a non-uniform
temperature. Tr. Geofiz. Inst. Akad. Nauk SSSR, 15, (English
translation, Boundary Layer Meteor., 2, 7-29, 1971).

Okamoto, M. and E.K. Webb, 1970: The temperature fluctuations in stable
stratification. Quart. J. R. Meteor. Soc., 96, 591-600.

Oke, T.R., 1970: Turbulent transport near the ground in stable conditions.
J. Appl. Meteor., 9, 778-786.

Orlanski, I., B.B. Ross and L.J. Polinsky, 1974: Diurnal variation of the
planetary boundary layer in a meso-scale model. J. Atmos. Sci.,
31, 965-989.

Owen, P.R. and W.R. Thompson, 1963: Heat transfer across rough surfaces.
J. Fluid Mech., 15, 321-334.

Panofsky, H.A., 1961: An alternative derivation of the diabatic wind
profile. Quart. J. R. Meteor. Soc., 87, 109-110.

Paterson, W.S.B., 1969: The Physics of Glaciers. Pergamon, London,
250 pp.

Paterson, W.S.B., 1971: Temperature measurements in Athabasca Glacier,
Alberta, Canada. J. Glaciol., 10, 339-350.

Pearson, E.S. and H.O. Hartley, 1954: Tables for Statisticians and
Biometricians, 1, Cambridge Univ. Press.

Portman, D.J., F.C. Elder, E. Ryznar and V.E. Noble, 1962: Some optical properties of turbulence in stratified flow near the ground. J. Geophys. Res., 67, 3223-3235.

Priestley, C.H.B., 1959: Turbulent Transfer in the Lower Atmosphere. Univ. of Chicago Press, 130 pp.

Pruitt, W.O., D.L. Morgan and F.J. Lourence, 1973: Momentum and mass transfers in the surface boundary layer. Quart. J. R. Meteor. Soc., 99, 370-386.

Reifsnyder, W., 1967: Radiation geometry in the measurement and interpretation of the radiation balance. Agr. Meteor., 4, 255-265.

Richardson, L.F., 1920: The supply of energy to and from atmospheric eddies. Proc. R. Soc. London, A97, 354-373.

Rider, N.E. and G.D. Robinson, 1951: A study of the transport of heat and water vapour above a surface of short grass. Quart. J. R. Meteor. Soc., 77, 375-401.

Rider, N.E., 1954: Eddy diffusion of momentum, water vapour and heat near the ground. Phil. Trans. R. Soc. London, A246, 481-501.

Sedgewick, J.K., 1966: Geomorphology and Mass Budget of Peyto Glacier, Alberta. M. Sc. Thesis, McMaster Univ., Hamilton, 165 pp.

Sellers, W.D., 1962: A simplified derivation of the diabatic wind profile. J. Atmos. Sci., 19, 180-181.

Sheppard, P.A., 1958: Transfer across the earth's surface and to the air above. Quart. J. R. Meteor. Soc., 84, 205-224.

Sheppard, P.A., D.T. Tribble and J.R. Garratt, 1972: Studies of turbulence in the surface layer over water (Lough Neagh). Part I.

Instrumentation, programme, profiles. Quart. J. R. Meteor. Soc., 98, 627-641.

Stenborg, T., 1970: Delay of runoff from a glacier basin. Geogr. Annaler, A52, 1-30.

Stewart, R.W., 1959: The problem of diffusion in a stratified fluid. Adv. Geophys., 6, 303-311.

Suomi, V.E. and C.B. Tanner, 1958: Evapotranspiration estimates from heat budget measurements over a field crop. Trans. Amer. Geophys. Union, 39, 298-304.

Sutton, O.G., 1953: Micrometeorology. McGraw-Hill, London, 333 pp.

Sverdrup, H.U., 1936: The eddy conductivity of the air over a smooth snow field: results of the Norwegian-Swedish Spitsbergen Expedition in 1934. Geophys. Pub., 11, 69 pp.

Sverdrup, H.U., 1951: Evaporation from the oceans. Compendium of Meteorology, 1071-1081, Waverly Press.

Swinbank, W.C., 1964: The exponential wind profile. Quart. J. R. Meteor. Soc., 90, 119-135.

Swinbank, W.C. and A.J. Dyer, 1967: An experimental study in micro-meteorology. Quart. J. R. Meteor. Soc., 93, 494-500.

Swinbank, W.C., 1968: A comparison between the predictions of dimensional analysis for the constant-flux layer and observations in unstable conditions. Quart. J. R. Meteor. Soc., 94, 460-467.

Tanner, C.B., 1963: Basic instrumentation and measurements for plant environment and micrometeorology. Soils Bull., 6, Univ. of Wisconsin.

Taylor, G.I., 1927: Turbulence. Quart. J. R. Meteor. Soc., 53, 201-211.

Taylor, R.J., 1960: Similarity theory in the relation between fluxes and gradients in the lower atmosphere. Quart. J. R. Meteor. Soc., 86, 67-78.

Thom, A.S., 1972: Momentum, mass and heat exchange of vegetation. Quart. J. R. Meteor. Soc., 98, 124-134.

Thornthwaite, C.W., W.J. Superior, J.R. Mather and F.K. Hare, 1961: The measurement of vertical winds and momentum flux. Pub. Clim., 14, C.W. Thornthwaite Assoc., Centerton, N.J..

Untersteiner, N. and F.I. Badgley, 1965: The roughness parameters of sea ice. J. Geophys. Res., 70, 4573-4577.

Wallén, C.C., 1948: Glacial meteorological investigations on the Kårsa Glacier in Swedish Lappland, 1942-48. Geogr. Annaler, 30, 451-572.

Webb, E.K., 1965: Aerial microclimate. Meteor. Monogr., 6, 27-58.

Webb, E.K., 1970: Profile relationships: the log-linear range, and extension to strong stability. Quart. J. R. Meteor. Soc., 96, 67-90.

Weller, G.E., 1967: Radiation fluxes over an Antarctic ice surface, Mawson, 1961-62. ANARE Sci. Rep., A4 (96), 106 pp.

Weller, G.E., 1968: The heat budget and heat transfer processes in Antarctic plateau ice and sea ice. ANARE Sci. Rep., A4 (102), 155 pp.

Wendler, G.A. and N.A. Streten, 1969: A short-term heat-balance study on a coast range glacier. Pure Appl. Geophys., 77, 68-77,

Wendler, G.A. and N. Ishikawa, 1973: Experimental study of the amount of
ice melt using three different methods: a contribution to the
International Hydrological Decade. J. Glaciol., 12, 399-410.

Wesley, M.L., G.W. Thurtell and C.B. Tanner, 1970: Eddy correlation
measurements of sensible heat flux near the earth's surface.
J. Appl. Meteor., 9, 45-50.

Wexler, A., 1970: Measurement of humidity in the free atmsophere near the
surface of the earth. Meteor. Monogr., 11, 262-281.

Yamamoto, G., 1959: Theory of turbulent transfer in non-neutral conditions.
J. Meteor. Soc. Japan, 2, 60-70.